International Atomic Energy Agency

INDC(BLR)-008
Distr. G

INDC INTERNATIONAL NUCLEAR DATA COMMITTEE

EVALUATION OF NEUTRON DATA FOR AMERICIUM-242g

V.M. Maslov, E.Sh. Sukhovitskij, Yu.V. Porodzinskij,
G.B. Morogovskij

Radiation Physics & Chemistry Problems Institute
220109, Minsk-Sosny, Belarus

June 1997

IAEA NUCLEAR DATA SECTION, WAGRAMERSTRASSE 5, A-1400 VIENNA

Reproduced by the IAEA in Austria
June 1997

INDC(BLR)-008
Distr. G

EVALUATION OF NEUTRON DATA FOR AMERICIUM-242g

V.M. Maslov, E.Sh. Sukhovitskij, Yu.V. Porodzinskij,
G.B. Morogovskij

Radiation Physics & Chemistry Problems Institute
220109, Minsk-Sosny, Belarus

Abstract

The evaluation of neutron data for ^{242g}Am is made in the energy region from 10^{-5} eV up to 20 MeV. The results of the evaluation are compiled in the ENDF/B-VI format.

This work is performed under the Project Agreement CIS-03-95 with the International Science and Technology Center (Moscow). The Financing Party for the Project is Japan. The evaluation was requested by Y. Kikuchi (JAERI).

Date of Manuscript: March 7, 1997

Contents

1 Introduction

The advanced nuclear fuel cycle studies request the nuclear data of transplutonium isotopes[1]. The neutron data for americium isotopes are especially important in this respect. Recently we have evaluated the data for ^{242m}Am nuclide [2]. In this work the evaluation of ^{242g}Am neutron data is performed. Neutron capture on ^{241}Am produces ^{242}Am nuclides in metastable (m) and short-lived (g) ground states. Rather high difference of target spin values of $J^{\pi}_{m} = 5^{-}$ and $J^{\pi}_{g} = 1^{-}$ may influence neutron-nucleus interaction. The curium and americium isotopes data evaluated within International Science and Technology Center (Moscow) Project "Evaluation of Actinide Nuclear Data"[2, 3, 4, 5, 6, 7], were requested by the former General Manager of Japan Nuclear data Center Dr. Y. Kikuchi. The quantities evaluated are resolved and unresolved resonance parameters, total, elastic and inelastic scattering, fission, capture, (n,2n) and (n,3n) reaction cross sections, angular and energy distributions of secondary neutrons, including partial (n,xn) and (n,xnf) reaction spectra, fission spectra and number of neutrons per fission. The incident neutron energy range covered is from 10^{-5} eV up to 20 MeV. The evaluated quantities are compared with ENDF/B-VI [8] and JENDL-3 [9] evaluations.

2 Resolved resonance region

There are almost no measurements in the resolved resonance region. Only thermal fission cross section was measured by Street et al. [10], Higgins et al. [11], Bak et al. [12], Ihle et al. [13] and Thompson et al. [14]. Upper limit of fission resonance integral is predicted by Bak et al. [12].

2.1 Previous evaluations of resolved resonance parameters

The evaluated resonance parameters of ENDF/B-VI are given for 81 equidistant resonances up to 101.2 eV with equal partial widths Γ°_{n}, Γ_{γ} and Γ_{f}. The value of reduced neutron width for negative resonance is ~50 times greater than that of positive resonances. In JENDL-3 evaluation the resonance parameters are missing, instead the partial cross section shape of $1/\sqrt{E}$ was assumed below 0.225 eV, above this energy point optical and statistical models were used.

Thermal fission σ_{f} cross sections of ENDF/B-VI and JENDL-3.2 are rather compatible, while capture cross sections σ_{γ} are drastically discrepant.

Rather high estimate of thermal capture cross section in JENDL-3.2 evaluation is due to assumption of about equal thermal total cross section values for ^{242g}Am and ^{242m}Am targets. In ENDF/B-VI thermal fission cross section σ_f value is a weighted average of data values by Street et al.[10], Higgins et al. [11], Bak et al.[12], Ihle et al.[13] and Thompson et al. [14].

2.2 Measured data fitting

2.2.1 Thermal cross sections

The following measured data on thermal cross section are available:

1) value for σ_f = 2000 b by Street et al.[10];
2) value for σ_f = 2950 b by Higgins et al.[11];
3) value for σ_f = 3500 b by Thompson et al.[14];
4) value for σ_f = 2100 b by Bak et al.[12];
5) value for σ_f = 2100 b by Ihle et al.[13];
6) value for $\sigma\gamma$ = 4500 b by Thompson et al.[14];

2.2.2 Resolved resonance parameters

Evaluated resolved resonance parameters of ^{242g}Am are statistically sampled based on average resonance parameters $\langle\Gamma_f\rangle$, $\langle\Gamma_n^o\rangle$, $\langle\Gamma_\gamma\rangle$ and $\langle D_{obs}\rangle$ of ^{242m}Am. Average fission width $\langle\Gamma_f\rangle$ is calculated with double-humped fission barrier parameters and transition state structure fixed for ^{242m}Am+n interaction [2]. Neutron $s-$wave strength function S_0 was calculated with coupled channel optical potential adopted for metastable state ^{242m}Am (5^-) [2] and coupling scheme relevant for ^{242g}Am (1^-) ground state. We generated two samples of resonances with spin values $J_i^\pi = J_g^\pi \pm 1/2$, J_1^π =$1/2^-$and J_2^π =$3/2^-$. Reduced neutron width values follow χ^2-distribution with degrees of freedom number ν_n =1, S_0 =1.364×10^{-4} $(\mathrm{eV})^{-1/2}$. Fission width values for resonances with $J_1 = 1/2^-$and $J_2 = 3/2^-$ follow χ^2-distribution with degrees of freedom number $\nu_{f1} = 3$ and $\nu_{f2} = 4$, respectively,$\langle\Gamma_{f1}\rangle$ =0.240 eV, $\langle\Gamma_{f2}\rangle$ =0.547 eV. Neutron resonance spacings for each spin value were supposed to follow Wigner distribution, while $\langle D_{J_1}\rangle$ =2.572 eV, $\langle D_{J_2}\rangle$ =1.331 eV. Root mean square error of sampling was less than 10%.

Resonance parameter sample was chosen to fit thermal fission cross section. We employed the value of thermal cross sections σ_f = 2100 b, defined by weighted averaging of available data. Evaluated fission resonance integral equals I_f = 997.812 barns. That is much higher than upper limit estimate of $I_f \leq$ 300 barns by Bak et al. [12], anyway this value is of the same order of magnitude as other measurements of fission resonance integrals for odd-odd actinide targets (^{238}Np, ^{236}Np, etc.) [15], [16]. Comparison of current and other evaluated thermal cross sections and resonance integrals is presented in Table 2.1.

The multi-level Breit-Wigner formalism is employed. This is almost totally correct procedure, since due to high number of fission channels there is almost no resonance-resonance interference, just as in case of ^{242m}Am target nuclide.

2.2.3 Resonance parameter analysis

We have got 122 resonance parameters up to 100 eV. The average resonance parameters, thermal cross sections and resonance integrals are presented in Table 2.1. Figures 2.1- 2.4 demonstrate the comparison of present and previous evaluations of fission and capture cross sections below 100 eV.

Table 2.1

	ENDF/B-VI	JENDL-3	This evaluation
$\langle\Gamma_n^o\rangle$, meV	0.319		0.2604
$\langle\Gamma_f\rangle$, eV	0.487		0.424
$\langle\Gamma_\gamma\rangle$, meV	51.13	50.00	50.00
$\langle D\rangle$, eV	1.261	0.45	0.8635
R, fermi	9.009	9.540	9.420
S_0x10^{4}eV$^{-1/2}$	1.284		1.371
σ_t , barn	2549.76	7611.44	2319.73
σ_γ , barn	252.08	5500.0	218.32
σ_f , barn	2268.73	2100.0	2093.23
σ_n , barn	28.95	11.44	7.6638
g_γ	0.99308	1.0015	1.05047
g_f	0.99308	1.00067	1.05357
I_γ , barn	72.13	390.63	187.006
I_f , barn	622.27	1258.55	997.812

The estimate of fission resonance integral I_f in ENDF/B-VI is ~1.5 times lower than our estimate. That is due to rather high spacing ($\sim 5\langle D\rangle$) between negative and first positive resonance, assumed in ENDF/B-VI evaluation. Large Γ_n^0 value of negative resonance increases appreciably $\langle\Gamma_n^0\rangle$ value on ENDF/B-VI evaluation. The specific feature of ^{242m}Am odd-odd target is large symmetric 0.178-eV resonance, which defines high thermal fission cross section ($\sim$ 6400 barns) value and small, if any, influence of negative resonances on neutron cross sections. For ^{242g}Am target neutron resonance spacing estimate $\langle D_{obs}^g\rangle \sim 3\langle D_{obs}^m\rangle$, so the probability of occurrence of strong resonance below 2 eV might be lower. Assumption of equidistant resolved resonances with non-fluctuating widths in ENDF/B-VI evaluation is unnecessarily strong. That will lead to overestimate of capture and underestimate

of elastic and fission cross sections, averaged over resonance region as compared with statistical resonance sample, the average width value being the same.

The average resonance parameters, thermal total σ_t, capture σ_γ, fission σ_f and scattering σ_n cross sections, $g_\gamma-$, and g_f-factors, as well as resonance integrals $I\gamma$ and I_f values are calculated with codes PSYCHE and INTER [17]. In case of present evaluation the multi-level Breit-Wigner formalism was used, while for ENDF/B-VI evaluation single-level formula was employed.

3 Unresolved resonance region

3.1 Review

Unresolved resonance region of ^{242g}Am is supposed to be from 0.1 keV up to 44.2838 keV. The lower energy is the end-point of resolved resonance region, the upper energy is the threshold energy of the first excited level, giving notable inelastic scattering. We suppose $s-$, $p-$ and $d-$wave neutron-nucleus interactions to be effective.

3.2 The s-, p- and d-wave average resonance parameter evaluation

Average resonance parameters in unresolved resonance region for ^{242g}Am are derived using estimates of average resonance parameters for ^{242m}Am. The influence of target nucleus ground state differences is taken into account.

3.2.1 Neutron width

Average neutron width is calculated as follows

$$\langle \Gamma_n^{lJ} \rangle = S_l \langle D_J \rangle E_n^{1/2} P_l,$$

where P_l is the transmission factor for the lth partial wave, which was calculated within black nucleus model. The p-wave neutron strength function $S_1 = 2.046\times10^{-4}$ $(\mathrm{eV})^{-1/2}$ was calculated with the optical model, using the deformed optical potential, described below. According to the results of optical model calculations S_0 was assumed to decrease linearly from S_0=1.363×10^{-4} $(\mathrm{eV})^{-1/2}$ to the value of S_0=$1.267\times10^{-4}(\mathrm{eV})^{-1/2}$ for neutron energy of 44.2838keV. The d-wave neutron strength function was taken from optical model calculations: $S_2 = 1.924\times10^{-4}$ $(\mathrm{eV})^{-1/2}$.Since the d-wave contribution is rather small, the impact of any reasonable approximation on calculated values is negligible.

3.2.2 Neutron resonance spacing

Neutron resonance spacing $\langle D_J \rangle$ was calculated with the phenomenological model [18], which takes into account the shell, pairing and collective effects. The main parameter of the model $\tilde{a}$ was normalized to the neutron resonance spacing of ^{242g}Am $\langle D_{obs} \rangle$ =0.877 eV (for details see below).

3.2.3 Fission width

Fission widths are calculated within a double-humped fission barrier model. We constructed transition spectra by supposing the triaxiality of inner saddle and mass asymmetry at outer saddle. Energy and angular momentum dependence of fission width is defined by the transition state spectra at inner and outer barrier humps , which was fixed for n+ ^{242m}Am interaction (for details see below). The calculated fission widths are $\langle \Gamma_f^{1/2^-} \rangle = 0.240$ eV and $\langle \Gamma_f^{3/2^-} \rangle = 0.547$ eV.

3.2.4 Radiative capture width

Energy and angular momentum dependences of radiative capture width are calculated within a two-cascade γ-emission model with allowance for the (n,γf) and (n,γn) reaction competition to the (n,$\gamma\gamma$) reaction. In this energy region (n,$\gamma\gamma$) reaction appears to be a radiative capture reaction. The radiative capture width was normalized to the value of $\langle \Gamma_\gamma \rangle$ =50.0 meV (for details see Chapter IV).

3.3 Cross section evaluation in the region 0.1-44.2838 keV

3.3.1 Fission and capture cross sections energy dependence

There is no data on fission and capture cross sections of ^{242g}Am, the evaluation is based on calculated values.

3.3.2 Comparison of current and JENDL-3 and ENDF/B-VI evaluated data

Present evaluated fission cross section is consistent with JENDL-3, while fission cross section of ENDF/B-VI is ~2 times lower and covers energy region only up to 11 keV. Figure 3.1 shows the comparison of evaluated fission cross sections σ_f. The discrepancies are noticed also when comparing capture cross sections (see Fig. 3.2). Present evaluated capture cross section σ_γ is in agreement with JENDL-3, which is ~25% higher at lower energy edge and almost coincides at higher boundary of unresolved resonance region.

Comparisons of the evaluated fission and capture cross-sections for metastable ^{242m}Am and ground ^{242g}Am states are given on Figs. 3.3 and 3.4. Data by Browne et al.[20] for ^{242m}Am neutron-induced fission were chosen as the most reliable. Statistical model calculations reproduce the overall trend

of data by Browne et al. [20]. Measured fission data exhibit prominent structure below incident neutron energy of 1 keV (see Fig. 3.3), which can not be reproduced varying average fission width value, since the degrees of freedom number for fission width distribution $\nu_f \sim 10$, consistent with the fission barrier transition states structure. (For details see Chapter IV). Structure present in data by Browne et al. [20] was fitted by adjusting S_0 strength function values in the chosen energy intervals up to 1 keV. That is the main reason of the fission and capture cross sections dicrepancies for ^{242m}Am and ^{242g}Am target nuclides. Above ~1 keV average resonance parameters fit the measured data for ^{242m}Am target nuclide. Comparison of the evaluated fission and capture cross-sections is given in Table 3.1.

Table 3.1 Comparison of the valuated fission and capture cross-sections

Energy, keV	σ_f, b			$\sigma\gamma, b$		
	present	JENDL-3	B-VI	present	JENDL-3	B-VI
0.10	45.54	44.05	44.10	9.40	12.38	4.90
0.15	37.05	35.93	22.53	7.61	9.95	3.99
0.25	28.55	27.82	17.51	5.83	7.55	3.09
0.40	22.44	22.02	13.70	4.55	5.83	2.40
0.70	16.85	16.67	10.24	3.38	4.23	1.78
1.00	14.03	13.98	8.53	2.80	3.46	1.47
1.50	11.41	11.45	6.92	2.26	2.80	1.18
2.50	8.82	8.95	5.33	1.73	2.08	0.88
4.00	6.99	7.18	4.21	1.36	1.59	0.66
7.00	5.38	5.60	3.20	1.04	1.18	0.43
10.0	4.60	4.84	2.74	0.89	0.98	0.30
15.0	3.92	4.16	0.0	0.76	0.82	0.0
25.0	3.31	3.55	0.0	0.64	0.68	0.0
40.	2.93	3.18	0.0	0.56	0.58	0.0
44.2638	2.87	3.12	0.0	0.54	0.56	0.0

3.3.3 Drawbacks of ENDF/B-VI format and associated inconsistencies in neutron cross sections

Within ENDF/B-VI format number degrees of freedom for fission width distributions must not exceed the value of 4, while structure of fission barriers predicts greater number degrees of freedom value for most spin and parity compound states. This results in ~7% underestimate of fission cross section and overestimate of capture cross section at the higher edge of unresolved

resonance region, as compared with calculations involving correct number of degrees of freedom for fission width distributions.

4 Fast neutron cross sections

There is no measured neutron data for short-lived ground state ^{242g}Am target nuclide in fast neutron energy region, i.e. above ~44 keV. We will calculate fission cross section using the optical potential, level density and fission barrier parameters fixed by ^{242m}Am target nuclide fission cross section fit. There is a systematic discrepancy in fission data for ^{242m}Am up to 20 MeV. Basically, the most extensive data sets by Dabbs et al. [21] and Browne et al. [20] agree both in energy calibration and overall shape, while the latter data average appear to be ~18% lower. Above emissive fission threshold there is a striking shape difference. Fission data fit by Browne et al. [20] would be used as a constraint for (n,n'), (n,γ), $(n,2n)$ and $(n,3n)$ reaction cross sections calculation for ^{242g}Am target nuclide. The average resonance fission width will be calculated within double-humped fission barrier model.

The evaluation of ^{242g}Am data is very much similar to the ^{242m}Am data evaluation [2], however we wish this report to be a self-contained one, so in some cases it just repeats relevant items of previous publication [2].

4.1 Optical potential

The deformed optical potential found previously for n+^{242m}Am interaction is employed. The starting values for the potential parameters were those for n+^{238}U interaction [22]. The isotopic dependences of real and imaginary parts of the potential were calculated using the optical potential parameter systematics [23]. We modified the original potential geometry parameters [22] to fit total cross section and differential scattering data for N-odd and -even targets above 10 MeV. This procedure of parameter fitting is well tested in case of and ^{233}U, ^{239}Pu, ^{235}U, ^{232}Th and ^{238}U targets. Four levels of the ground state rotational band (J^π = 1$^-$,3$^-$,5$^-$,7$^-$) are coupled. The potential parameters are as follows:

$$V_R = 46.10 - 0.3E, MeV, r_R = 1.26\ fm, a_R = 0.615\ fm$$
$$W_D = \begin{cases} 3.53 + 0.4E, MeV, & E \leq 10 MeV, r_D = 1.24\ fm, a_D = 0.5\ fm \\ 7.56\ MeV, & E > 10\ MeV \end{cases}$$
$$V_{SO} = 6.2\ MeV, r_{SO} = 1.12\ fm, a_{SO} = 0.47\ fm, \beta_2 = 0.206, \beta_4 = 0.092$$

The s-, p-, and d-wave strength functions and potential scattering cross section, calculated with this potential parameters in a coupled channel approach at incident neutron energy of 40 eV are:

$$S_0 = 1.363 \times 10^{-4}(\text{eV})^{-1/2} \quad , \quad R' = 9.42 \text{ fm}$$

and at 42.2838 keV are:

$$S_0 = 1.267 \times 10^{-4}(\text{eV})^{-1/2} \quad S_1 = 2.046 \times 10^{-4}(\text{eV})^{-1/2} \quad S_2 = 1.924 \times 10^{-4}(\text{eV})^{-1/2}$$

Differences of optical cross sections for ^{242m}Am+n and ^{242g}Am+n interactions are attributed to the different coupling scheme. The ^{242g}Am+n reaction cross sections, calculated with deformed optical potential and spherical optical potential, which is used in JENDL-3 evaluation, are compared on Fig. 4.1. The significant differences below 1 MeV and above 10 MeV would be manifested in inelastic scattering cross section and $(n, 3n)$ cross section. The total cross sections appear to be rather similar (see Fig. 4.2), while elastic scattering cross section are rather different below ~5 MeV and above ~15 MeV (see Fig. 4.3).

4.2 Fission cross section

4.2.1 Status of the experimental data

A small number of measurements are available for ^{242m}Am fission cross section, unfortunately most of them are discrepant with each other either in shape and absolute values. There is no measured for unstable nuclide ^{242g}Am.

4.2.2 Statistical model calculation of fission cross section

Basically, we choose to fit data by Browne et al. [20] in describing measured data base for ^{242m}Am neutron-induced fission cross section. That means the lower cross section level in the first plateau region and at lower energies as compared with data by Dabbs et al. [21]. We will follow the trend of data by Browne et al. [20] and Fursov et al. [25] up to ~7.8 MeV. The comparison of calculated fission cross sections for ^{242g}Am and ^{242m}Am with measured data for ^{242m}Am target nuclide is shown on Figs. 4.4, 4.5 and 4.6. The statistical theory calculation of fission cross section was accomplished within the double-humped fission barrier model. The approach employed in code STAT is described in more details elsewhere [26, 27, 44]. Basically the differences that should be accounted for are spin value of the ground state and excitation energy difference as compared with excited metastable state. The procedure of calculating fission transmission coefficients is briefly described below.

4.2.3 Fission transmission coefficient, level density and transition state spectrum

The different behavior of level densities of fissioning odd-even and residual odd-odd nuclei at low excitation energies should be taken into account [29]. The one-quasiparticle neutron states of odd-even ^{243}Am fissioning nuclide, lying below the three-quasiparticle states excitation threshold define the shape of ^{242g}Am(n,f) fission cross section below incident neutron energy of ~1 MeV. Specifically, the step-like shape of fission cross section around 0.1 - 0.4 MeV. At higher incident neutron energies three-quasiparticle states could be excited in fissioning nucleus ^{243}Am at deformations of inner fission barrier hump. They define the fission cross section shape around 1 - 2.5 MeV incident neutron energy.

We construct the discrete transition state spectra up to 200 keV, using one-quasiparticle states of Bolsterli et al. [30] (see Table 4.1). At higher excitation energies the continuous level densities are used. Each one-quasiparticle state is assumed to have a rotational band built on it with a rotational constant, dependent upon the respective saddle deformation. These levels comprise the discrete transition spectra at both saddles. The discrete transition spectra, as well as continuous level contribution to the fission transmission coefficient are dependent upon the order of symmetry for ^{243}Am fissioning nucleus at inner and outer saddles. Due to the axial asymmetry at the inner saddle [31] we additionally assume $(2J+1)$ rotational levels for each J value. The negative parity bands $K^{\pi} = 1/2^{-}$,$3/2^{-}$, $5/2^{-}$ ... at outer saddle are assumed to be doubly degenerate due to mass asymmetry [31]. With transition state spectra thus defined (see Table 4.1) the fission barrier parameters were obtained (see Table 4.2) by fitting the ^{242m}Am neutron-induced fission cross section data. The transition state spectra probed by n+^{242g}Am compound nuclide is rather different as compared with n+^{242m}Am compound nuclide. Anyway, this result in differing cross section levels below ~10 keV incident neutron energies. The fission widths $\Gamma_f^{1/2^-} \sim 0.240$ eV and $\Gamma_f^{3/2^-} \sim 0.547$ eV are calculated at incident neutron energy of 0.040 keV. These values give average fission width $\langle\Gamma_f\rangle =$ 0.424 eV, which is consistent with estimate, obtained for unresolved resonance region. At higher energies, e.g. above ~ 300 keV and up to emissive fission threshold the differences of fission cross section values are due to reaction cross section. Coupled channel potential calculations depend on the coupling scheme which are rather different for n+^{242g}Am and n+^{242m}Am interactions.

The generalized pairing model provides the means of taking into account the discrete character of few-quasiparticle excitations. It was shown to be important in case of even-odd fissioning and even-even residual nuclei in ^{244}Cm(n,f) and ^{246}Cm(n,f) reactions [29, 32]. The quasi-resonance structure,

appearing above fission threshold in neutron-induced fission cross section is interpreted. The discrete character of few-quasiparticle excitations is virtually unimportant in case of odd-odd ^{242}Am residual nuclide. We will model the discrete few-quasiparticle excitation effects in level density of odd-even ^{243}Am fissioning nuclide in the following approximate way [32]. The level density of axially symmetric fissioning nucleus is calculated in constant temperature approximation, i.e. $\rho(U) = T_f^{-1} \exp((U - U_o)/T_f)$. The respective parameters, nuclear temperature T_f and excitation energy shift U_o are defined at the matching energy $U_c = 3.6$ MeV. At excitation energies above U_c the continuum part of the transition state spectrum is represented with the phenomenological model [18], which takes into account pairing, shell and collective effects at saddle deformations. The asymptotic value of the main parameter of the level density for fissioning nucleus ^{243}Am is assumed to be the same, as that of ^{243}Am compound nuclide. After that the effects of non-axiality and mass asymmetry are included. The detailed procedure of calculating fission transmission coefficient is described elsewhere [26, 27, 44]. The respective parameters: shell correction at saddles δW, pairing correlation function Δ, quadrupole deformation ε,and momentum of inertia at zero temperature $F_0/\hbar^2$ are given in Table 4.3.

The threshold energies for the excitations of few-quasiparticle states are calculated within generalized pairing model [18] using closed-form equations by Fu [33]. The procedure is described in more detail elsewhere [34]. In case of odd-even nuclei the nuclear level density $\rho(U)$ up to the three-quasiparticle excitation threshold is virtually independent on the excitation energy, since the intrinsic state density is constant. In this excitation energy region we will model the level density as $\rho(U) = T_f^{-1} \exp((\Delta_f - U_o)/T_f)$. Above the three-quasiparticle states excitation threshold the constant temperature model is used, since the intrinsic state density here is a smooth function of excitation energy. For excitation energies below five-quasiparticle and above three-quasiparticle states excitation threshold the level density is slightly increased, as compared with constant temperature model approximation: $\rho(U) = T_f^{-1} \exp((U - U_o + \delta)/T_f), \delta$ =0.1 MeV. The one- and three-quasiparticle states level density of odd-even fissioning nucleus ^{243}Am defines the fission cross section shape at incident neutron energies below ~3 MeV. Above ~3 MeV incident neutron energy fission cross section the pre-equilibrium emission of secondary neutron is important. The parameters used for calculation of residual nuclide ^{242}Am level density for neutron emission competition are described below.

The parameters used for calculation of residual nuclide ^{242}Am level density for neutron emission competition are described below.

Below incident neutron energy of 0.320 MeV the neutron cross sections are calculated within Hauser-Feshbach approach with a width fluctuation

correction taken into account. For width fluctuation correction calculation only Porter-Thomas fluctuations are taken into account. Effective number of degrees of freedom for fission channel is defined at the higher (inner) saddle as $\nu_f^{J\pi} = T_f^{J\pi}/T_{f\,max}^{J\pi}$, where $T_{f\,max}^{J\pi}$ is the maximum value of the fission transmission coefficient $T_f^{J\pi}$. Above incident neutron energy of 0.273 MeV the Tepel et al. [35] approach is employed. The calculations are made with code STAT [36].

4.2.4 Fission cross section above emissive fission threshold

The first chance fission cross section of ^{242g}Am(n,f) reaction above the emissive fission threshold is fixed with the level density and fission barrier parameters systematics [26] (see Tables 4.2, 4.3) and secondary neutron spectra parameterization (see Fig. 4.7). A consistent description of a complete set of measured data on (n,f), (n,2n) and (n,3n) for ^{238}U and ^{235}U targets was accomplished with the secondary neutron spectra parameterization [37], which is used here.

Fission cross section is calculated with the statistical code STAPRE [38] (see Fig.4.6). Near the emissive fission threshold the pre-equilibrium emission of first neutron is rather important due to high neutron binding energy of ^{243}Am compound nuclide. The fission barrier parameters of ^{242}Am nuclide, fissioning in (n,nf) reaction are defined by fitting [19] data on ^{241}Am neutron-induced fission in the first plateau region (see Fig. 4.7). The resulted fission barrier parameters of ^{242}Am does not allow fitting ^{242m}Am(n,f) data by Browne et al. [20] well above emissive fission threshold. This discrepancy is unavoidable within present model approach without appreciable variation of model parameters. To fit the data by Browne et al. [20] first-chance fission cross section should be increased appreciably by softening the first emitted neutron spectra. However, we do not think this procedure justified in this particular case, since the discrepancy of the same kind we encounter [39] in case of ^{245}Cm(n,f) data by White et al. [40], measured in the same environment. The peculiar feature is that the calculated fission cross section shape is similar to that of data by Dabbs et al. [21]. The calculated fission cross section around (n,2nf) reaction threshold neutron energy is roughly consistent with data by Fomushkin et al. [24] at 14.8 MeV. On the other hand, the ^{243}Am compound nuclide fission barrier parameters describe the measured data on neutron-induced fission cross section of ^{243}Am target above emissive fission threshold [41] (see Fig.4.8).

The calculated fission cross section is different from JENDL-3 and ENDF/B-VI evaluated curves above (n,nf) reaction threshold (see Fig. 4.9). The reaction cross sections for neutron interaction with ^{242g}Am and ^{242m}Am are somewhat different. That is most pronounced in first chance cross section near emissive fission threshold (see Fig. 4.6).

Table 4.1

Transition spectra band-heads of ^{243}Am

inner saddle		outer saddle	
K^π	E_{K^π}, MeV	K^π	E_{K^π}, MeV
$3/2^-$	0.0	$5/2^+$	0.0
$5/2^+$	0.140	$5/2^-$	0.0
$7/2^-$	0.180	$3/2^+$	0.08
$5/2^-$	0.180	$3/2^-$	0.08
		$1/2^+$	0.04
		$1/2^-$	0.04
		$1/2^+$	0.05
		$1/2^-$	0.05

Table 4.2

Fission barrier parameters

Nucleus	Barrier	Barrier height, MeV	Curvature, MeV
^{243}Am	inner	6.4	0.8
^{243}Am	outer	4.85	0.5
^{242}Am	inner	6.315	0.6
^{242}Am	outer	5.775	0.4
^{241}Am	inner	6.000	0.8
^{241}Am	outer	5.350	0.5
^{240}Am	inner	6.100	0.6
^{240}Am	outer	6.000	0.4
^{239}Am	inner	6.000	0.8
^{239}Am	outer	5.400	0.6

Table 4.3

Level density parameters of ^{243}Am fissioning nucleus and residual nucleus ^{242}Am

Parameter	inner saddle	outer saddle	neutron channel
δW, MeV	2.5	0.6	-2.487
$\triangle$, MeV	$\triangle_0$	$\triangle_0$	$\triangle_0$
ε	0.6	0.8	0.24
$F_0/\hbar^2$, MeV^{-1}	100	200	73

4.3 Inelastic scattering cross section

The inelastic scattering cross section is calculated with the statistical codes STAT [36] and STAPRE [38]. The discrete level excitation (compound and direct), continuum excitation and pre-equilibrium emission contribute to the inelastic scattering cross section.

4.3.1 Levels of ^{242}Am

The low-lying levels of scheme of Nuclear Data Sheets [42] appears incomplete at rather low excitation energy (see Fig. 4.10). The experimental data on odd-odd ^{242}Am nuclide energy levels are supplemented by the results of the intrinsic level modelling by Sood et al. [43]. The still unobserved doublet of two-quasiparticle band heads $J = 6^-$ ($K^\pi = 6^-$) and $J = 1^-$ ($K^\pi = 1^-$) is predicted, the Gallagher-Moszkovski splitting energy being ~80 keV. Assuming $E^J_{K^\pi} = A[J(J+1) - K(K+1)]$, A =5.5 keV, we model a rotational level sequence.

4.3.2 ^{242}Am level density

The continuum level density below excitation energy U_c = 2.4 MeV is calculated with the constant temperature model

$$\rho(U) = T^{-1} \exp((U - U_o)/T),$$

here, energy shift U_0 = -1.6452 MeV, nuclear temperature T = 0.39241 MeV are the constant temperature model parameters. The cumulative number of observed levels is compared with constant temperature approximation on Fig.4.10. At higher excitation energies the phenomenological model [18] is used. The main model parameter $\tilde{a}$ for ^{242}Am residual nucleus is obtained by fitting the evaluated neutron resonance spacing of ^{241}Am target nuclide $\langle D_{obs} \rangle$ = 0.505 eV.

4.3.3 Compound inelastic scattering

The residual nucleus ^{242}Am level density modelling, adopted in present work changes the inelastic scattering cross section below 5 MeV as compared with previous evaluation of JENDL-3 (see Figs. 4.11 - 4.22). The discrete level excitation functions of present work and JENDL-3 evaluation are rather different. We assume that missing of levels in odd-odd nuclide ^{242}Am occurs at rather low excitation energy of ~0.320 MeV. That is the main reason of discrepancy with JENDL-3 evaluation, where discrete levels are used up to ~0.7 MeV. Above ~1.5 MeV incident neutron energy the discrepancies are due to direct excitation of the ground state band $K^\pi = 0^-$ levels $J^\pi = 3^-$, $J^\pi = 5^-$and $J^\pi = 7^-$. Above 1 MeV incident neutron energy inelastic

scattering to the continuum gives a major contribution to the total inelastic scattering cross section (see Fig. 4.11). However, the continuum inelastic scattering contributions of JENDL-3 evaluation seems to be distorted. Above 5 MeV incident neutron energy pre-equilibrium emission and direct inelastic scattering are the two reaction mechanisms which define inelastic scattering cross section (see Fig. 4.11). The pre-equilibrium model parameters were tested by the statistical model description of ^{238}U+n interaction secondary neutron spectra and consistent description of fission and (n,xn) reaction data for major actinides [37]. Steep increase of continuum inelastic scattering cross section of ENDF/B-VI above 15 MeV (see Fig. 4.12) can not be interpreted in physical terms, possibly that is due some normalization error. The shape of continuum inelastic scattering cross section of JENDL-3 around 20 MeV possibly is due to reaction cross section shape, since there is no pre-equilibrium emission contribution in JENDL-3 evaluation.

4.3.4 Direct inelastic scattering

The direct inelastic scattering mechanism changes the shape of ground state band head K^{π} =0^{-} rotational levels $J^{\pi} = 3^{-}$, $J^{\pi} = 5^{-}$and $J^{\pi} = 7^{-}$ excitation cross sections above 1 MeV incident neutron energy (see Figs. 4.15, 4.18 and 4.21). The most striking evidence is found in case of $J^{\pi} = 7^{-}$ level, where compound mechanism contribution is virtually negligible. This mechanism defines partly the hard-energy tail in total inelastic scattering cross section (see Fig. 4.11). The calculations were accomplished with the code COUPLE [23].

4.3.5 ^{243}Am level density

The level density of odd-even compound nuclide ^{243}Am one needs to calculate radiative capture width and (n,γn') reaction contribution to the compound inelastic scattering cross section. The continuum level density below excitation energy U_c = 3.6 MeV is calculated with the constant temperature model, the constant temperature model parameters are: energy shift U_0 = -0.98278 MeV, nuclear temperature T = 0.39984 MeV. The cumulative number of observed levels is compared with constant temperature approximation on Fig. 4.23. At higher excitation energies the phenomenological model [18] is used. The main model parameter $\tilde{a}$ for ^{243}Am residual nucleus is obtained by fitting the evaluated neutron resonance spacing of ^{242m}Am target nuclide $\langle D_{obs} \rangle$ = 0.271 eV, the metastable state excitation energy is taken into account. To calculate the neutron resonance spacing for ^{242g}Am target nuclide $\langle D_{obs} \rangle$ = 0.877 eV, we employed the $\tilde{a}$ -parameter value obtained by fitting ^{242m}Am metastable nuclide resonance spacing.

Table 4.4
Level scheme of ^{242}Am

$E^J_{K^\pi}$, MeV	J	π	K	band	$E^J_{K^\pi}$, MeV	J	π	K	band
0.0000	1	–	0	A	0.24200	2	-	1	D*
0.04410	0	-	0	A	0.24410	3	-	3	E
0.04863	5	-	5	B	0.26300	6	-	0	A
0.05290	3	-	0	A	0.26310	7	-	0	A
0.07580	2	-	0	A	0.27010	2	+		
0.11400	6	-	5	B	0.27500	3	-	1	D*
0.14000	6	-	6	C*	0.28330	3	+		
0.14800	5	-	0	A	0.28840	4	-	3	E
0.14990	4	-	0	A	0.29180	2	-	2	F
0.19000	7	-	5	B	0.30500	8	-	6	C*
0.19760	3	-			0.30690	3	-		
0.21700	7	-	6	C*	0.31900	4	-	1	D*
0.22000	1	-	1	D*					
0.2305	2	+							

*)added

4.4 Radiative capture cross section

The radiative capture cross section is calculated within a statistical approach up to 5 MeV. Radiative capture strength function equals $S_{\gamma 0} = 234.76$, this is rather different from the $S_{\gamma 0} = 759.72$ estimate for n+^{242m}Am interaction. This difference contributes to the discrepancy of neutron capture cross sections for ^{242g}Am and ^{242m}Am targets. At higher incident neutron energies we assume radiative capture cross section to be constant. The radiative capture width was calculated with (n,γf) and (n,γn') reactions competition against "true" capture reaction (n,$\gamma\gamma$). Notwithstanding rather high fission threshold for ^{243}Am compound nuclide the competition of (n,γf) reaction is still stronger than that of (n,γn') reaction. The influence of (n,γn') and (n,γf) reaction competition on radiative capture cross section is illustrated on Fig. 4.24 by sharp decrease of capture cross section above 1 MeV incident neutron energy, as compared with (n,γx) reaction cross section.

4.5 Cross sections of (n,2n) and (n,3n) reactions

The current and previous evaluated (n,2n) and (n,3n) cross sections are rather different. The magnitude of (n,2n) cross section below the (n,2nf)

reaction threshold is defined by (n,nf) and (n,2n) reaction competition. To calculate the (n,2n) reaction cross section we use an approach, developed for the description of ^{238}U(n,2n) reaction cross section[37]. The present and previous evaluated fission cross sections are rather different, as well as reaction cross sections above 10 MeV incident neutron energy (see Fig. 4.1). The present and previous evaluations are compared in Fig. 4.25. There is no hard-energy tail in (n,2n) reaction cross sections of ENDF/B-VI, JENDL-3 and JEF-2 evaluations. In case of (n,3n) reaction the difference in reaction cross section above 11 MeV (see Fig. 4.1) contributes essentially to the discrepancy with JENDL-3 evaluation, shown on Fig. 4.26.

4.6 Energy distributions of secondary neutrons

Neutron energy distributions for ^{242g}Am were calculated with the parameters fixed for ^{242m}Am target nuclide. The differences in calculated spectra are due to slightly different contribution of pre-equilibrium emission. Different coupling schemes used in optical calculations for ^{242m}Am and ^{242g}Am lead to differences in compound and first chance fission cross sections. To calculate neutron energy distributions of (n,xnγ) and (n,xnf), x=1, 2, 3 reactions we use a simple Weisscopf-Ewing evaporation model[44] taking into account fission,and gamma competition to neutron emission for appearing A+1, A, A-1, A-2 -mass nuclei. The pre-equilibrium emission of first neutron is included.

4.6.1 Model calculations of (n,nx) reaction spectra

The first neutron spectra for the (n,nx) reaction is the sum of evaporated and pre-equilibrium emitted neutron contributions. The pre-equilibrium emission contribution is calculated with a parameter systematics tested in case of n+^{238}U and n+^{235}U interactions [26, 37]. Fission and neutron competition and pre-equilibrium emission of first neutron is tested to be consistent with adopted in Chapter IV and give (n,nf), (n,2f), (n,3nf), (n,2n), (n,3n) and (n,nγ) cross-sections close to calculated above. The pre-equilibrium neutron emission contribution in case of ^{242g}Am target nucleus is notable for rather low neutron incident energies (see Chapter IV). We have calculated the 1st, 2nd and 3d neutron spectra for the (n,nγ), (n,2n) and (n,3n), where applicable. According to the ENDF/B-VI format we included the secondary neutron spectra in the following way. The calculated spectra were summed up and tabular spectra for the (n,nγ), (n,2n) and (n,3n) reactions were obtained. To clarify the competition of neutron, γ-emission and fission in case of (n,nx) and (n,2nx) reactions we have chosen the following presentation of spectra. Figure 5.1 shows the spectra of 1st neutron of the reaction (n,nx) and its partial contributions of (n,nγ), (n,2n), (n,nf) (n,2nf) and (n,3n) re-

actions. Figure 5.2 shows the spectra of 2nd neutron of the reaction (n,2nx) and its partial contributions of (n,2nγ), (n,3n) and (n,2nf) reactions. The neutron spectra shown on Figs. 5.1-5.2 are normalized to the contributions of appropriate cross-sections in (n,nx) and (n,2nx) respectively. The incident neutron energy is 14 MeV.

Table 5.1 Average energies of secondary neutron spectra

E_n, MeV	1^{st} neutron average energy, MeV									
	(n, n')			(n, 2n)			(n, n'f)	(n, 3n)		(n, 2n'f)
	pres.	J - 3	B-6	pres.	B-6	J - 3	pres.	pres.	J - 3	pres.
2.0	0.55	0.58	0.40							
8.0	4.04	1.14.	1.22	1.17	0.70	1.14	0.82			
14.0	10.1	1.49	1.58	4.11	1.23	1.50	2.69	0.63	1.49	1.05
20.0	16.1	1.77	1.86	10.5	1.58	1.78	4.11	2.94	1.78	3.37

E_n, MeV	2^{nd}neutron average energy, MeV						3d neutron	
	(n, 2n)			(n, 3n)		(n, 2n'f)		
	pres.	B-6	J - 3	pres.	J - 3	pres.	pres.	J - 3
8.0	0.34	1.22	0.70					
14.0	0.82	1.47	1.04	0.52	1.08	0.73	0.18	0.70
20.0	0.77	1.86	1.41	1.17	1.41	1.17	0.66	0.90

The inclusion of pre-equilibrium emission changes significantly the average energies of emitted neutron spectra. That is shown in Table 5.1, where the average secondary neutron energies for current, JENDL-3 and ENDF/B-VI evaluations are compared. The most significant is the change of neutron spectra of (n,nγ) reaction. Figures 5.3-5.7 demonstrate the discrepancies of secondary neutron spectra in current and JENDL-3 evaluations.

The 1st neutron spectra of (n,nf) reaction also becomes harder and that influences prompt fission neutron spectra. On the other hand, the spectra of 2nd and 3d neutrons become softer.

4.7 Prompt fission neutron spectra

Prompt fission neutron spectra were calculated within the framework of Madland-Nix model [45] in the same manner as it was done for ^{242m}Am neutron induced fission and is described elsewhere [2].

4.7.1 Prompt fission neutron spectra evaluation

Below emissive fission threshold prompt fission neutron spectra are calculated with the parameters given in Table 5.2. Figure 5.8 shows the compari-

son of calculated thermal prompt fission neutron spectrum with maxwellian spectra of JENDL-3 ($T = 1.38$ MeV). Average energy of fission spectrum equals 2.15 MeV, it is compatible with evaluated value of JENDL-3, however the spectra shapes are significantly different. Figure 5.9 demonstrates the discrepancies of our calculation with JENDL-3 evaluation. The discrepancies are due to incident neutron energy independent maxwellian fission spectrum representation in JENDL-3 as well as emissive fission contribution in present evaluation.

Above emissive fission threshold the fission neutron spectra $N(E)$ is the superposition of emissive fission spectra, i.e.

$$N(E) = (\frac{\sigma_{nf}}{\sigma_{nF}}\nu_1 N_1(E) + \frac{\sigma_{nn'f}}{\sigma_{nF}}\left[\Phi_{nn'f}(E) + \nu_2 N_2(E)\right]$$

$$+\frac{\sigma_{n2nf}}{\sigma_{nF}}\left[\Phi^1_{n2nf}(E) + \Phi^2_{n2nf}(E) + \nu_3 N_3(E)\right])/$$

$$\left[\frac{\sigma_{nf}}{\sigma_{nF}}\nu_1 + \frac{\sigma_{nn'f}}{\sigma_{nF}}(1+\nu_2) + \frac{\sigma_{n2nf}}{\sigma_{nF}}(2+\nu_3)\right],$$

where σ_{nF}, σ_{nf}, $\sigma_{nn'f}$, σ_{n2nf} are the total and i-th chance fission cross sections (i = 1,2,3); $\Phi_{nn'f}$, Φ^1_{n2nf}, and Φ^2_{n2nf} are emitted neutron spectra: for (n,nf) reaction, 1st and 2nd neutrons of (n,2nf) reaction, respectively; ν_i and N_i are multiplicity and prompt neutron spectra for the i-th fissioning nucleus. The pre-equilibrium emission of the first neutron is included, the secondary neutron spectra for emissive fission $\Phi^i_{n,xnf}$ are calculated with Weisscopf-Ewing evaporation model [44].

The influence of pre-equilibrium pre-fission neutrons on prompt fission neutron multiplicity ν_i and prompt neutron spectra N_i predictions as well as $N(E)$ and $\nu(E)$, is illustrated in Table 5.3 and Fig. 5.10. In Table 5.3 $\langle E_i \rangle$ denotes average prompt fission neutron energy of i-th fissioning nucleus, $\langle E \rangle$ is the average fission neutron energy, $\langle E_{n'f} \rangle$, $\langle E_{2nf} \rangle^1$ and $\langle E_{2nf} \rangle^2$ are the average energies of neutrons, emitted in (n,nf) and 1st and 2nd neutrons emitted in (n,2nf) reactions, respectively. Figures 5.11-5.13 show the partial contributions of i-th chance fission to the total fission neutron spectrum at incident neutron energies of 8, 14 and 20 MeV.

Table 5.2

Parameters of the Madland-Nix model

Fissioning nucleus	A_L fragm.	A_H fragm.	$\langle E_R \rangle$, MeV	$\langle TKE \rangle$, MeV	B_n, MeV
^{243}Am	^{103}Nb	^{140}Xe	204.651	182.20-0.08E_n	6.367
^{242}Am	^{102}Nb	^{140}Xe	204.963	183.02-0.08E_n	5.538
^{241}Am	^{101}Nb	^{140}Xe	204.353	183.26-0.08E_n	6.641

5 Number of neutrons per fission

The number of prompt fission neutrons for ^{242g}Am was adopted to be the same as for the ^{242m}Am [2]. The evaluation of $\nu_p(E)$ for ^{242m}Am is based on calculation within Madland-Nix model, fitted to the data of Howe et al. [46]in the energy range up to 5 MeV. The calculated value of $d\nu_p/dE = 0.145$ MeV^{-1}in the first plateau region is consistently lower than $d\nu_p/dE = 0.128$ MeV^{-1}, estimated by Howe et al. [46] in a linear least-squares data fit up to 30 MeV. That is essentially the same kind of discrepancy, that we have encountered in case of $\nu_p(E)$ data by Howe et al. [47] for ^{245}Cm(n,f) reaction, measured in the same environment. The calculated $d\nu_p/dE = 0.133$ MeV^{-1} was considerably higher than $d\nu_p/dE = 0.08\pm0.015$, MeV^{-1}, estimated by Howe et al. [47]. However, calculated energy slope $\nu_p(E)$ was supported by recent data by Khokhlov et al. [48]. To increase the $d\nu_p/dE$ within Madland-Nix model calculation even further, as systematics by Howerton [49] predicts (see ENDF/B-VI evaluation on Fig. 6.1), one should assume rather low value of $\langle TKE \rangle$ for ^{243}Am compound system. The comparison of $\nu_p(E)$ with measured data and JENDL-3 evaluation is shown in Fig. 6.1. The Madland-Nix model calculations predict non-linear decrease of $\nu_p(E)$ above emissive fission threshold. The influence of pre-equilibrium pre-fission neutrons manifests in additional appreciable decrease of $d\nu_p/dE$ above 12 MeV.

The delayed number of neutrons per fission ν_d and decay constants for six groups of delayed neutrons are taken from Brady and England [50]. Specifically, $\nu_d = 0.0078$ for incident neutron energies up to 4 MeV and $\nu_d = 0.0043$ for $E_n \geq 7$ MeV.

6 Angular distributions of secondary neutrons

The angular distributions of elastically scattered neutrons and those for neutrons, scattered on two levels of ground state band are calculated with the coupled channel method. The isotropic compound scattering contribution is taken into account by renormalizing l-th Legendre polynomial coefficients A_l^{cc}, calculated with coupled channels:

$$A_l = A_l^{cc}\sigma_{dir}/(\sigma_{dir}+\sigma_{comp}),$$

where σ_{dir} and σ_{comp} are the scattering cross section direct and compound contributions, respectively. For the other contributing reactions angular distributions of secondary neutrons are assumed isotropic.

Table 5.3 Comparison of Madland-Nix and present approach

Quantity	E_n = 8 MeV		E_n = 14 MeV		E_n = 20 MeV	
	M-N model [45]	Present	M-N model [45]	Present	M-N model [45]	Present
$\langle E_1 \rangle$	2.350	2.350	2.478	2.478	2.598	2.598
ν_1	4.430	4.430	5.269	5.269	6.085	6.085
$\langle E_{n'f} \rangle$	1.176	0.821	1.543	2.688	1.834	4.106
$\langle E_2 \rangle$	2.180	2.189	2.316	2.289	2.442	2.393
ν_2	3.329	3.381	4.146	3.982	4.949	4.632
$\langle E_{2nf} \rangle^1$	-	-	1.543	1.048	1.834	3.365
$\langle E_{2nf} \rangle^2$	-	-	1.098	0.729	1.472	1.167
$\langle E_3 \rangle$	-	-	2.152	2.174	2.284	2.255
ν_3	-	-	3.105	3.232	3.880	3.704
$\langle E \rangle$	2.278	2.264	2.318	2.387	2.558	2.615
ν	4.411	4.421	5.211	5.155	5.992	5.807

7 Conclusions

The evaluated neutron data file for ^{242g}Am is compiled in ENDF/B-VI format and sent to the International Science and Technology Center (Moscow), Japan Nuclear Data Center at Japan Atomic Energy Research Institute and Nuclear Data Section of International Atomic Energy Agency (Austria).

Numerous discrepancies of experimental data coupled with possibility of some new data becoming available (for example, thermal fission cross section might be measured) may urge some revision of data file. Present version of ^{242g}Am data file may be revised before March of 1998, the expiration date of Project CIS-03-95.

References

[1]Nakagawa T., Kikuchi Y., Proc. of the Int. Conf. on Nuclear Data and Technology, Gatlinburg, Tenn., USA, 9-13 May, 1994, Dickens J.K. (Editor), 709, ANS Inc., 1994.

[2]Maslov V.M., Porodzinskij Yu.V., Sukhovitskij E.Sh., Morogovskij G.B., INDC(BLR)-7, 1997.

[3]Maslov V.M., Porodzinskij Yu.V., Sukhovitskij E.Sh., Klepatskij A.B., Morogovskij G.B., INDC(BLR)-2, 1995.

[4]Maslov V.M., Porodzinskij Yu.V., Sukhovitskij E.Sh., Klepatskij A.B., Morogovskij G.B., INDC(BLR)-3, 1996.

[5]Maslov V.M., Porodzinskij Yu.V., Sukhovitskij E.Sh., Klepatskij A.B., Morogovskij G.B., INDC(BLR)-4, 1996.

[6]Maslov V.M., Porodzinskij Yu.V., Sukhovitskij E.Sh., Klepatskij A.B., Morogovskij G.B., INDC(BLR)-5, 1996.

[7]Maslov V.M., Porodzinskij Yu.V., Sukhovitskij E.Sh., Klepatskij A.B., Morogovskij G.B., INDC(BLR)-6, 1996.

[8]C.L. Dunford, Nuclear Data for Science and Technology, Proc. Int. Conf. Julich, 1991,788. Springer-Verlag,1992, Berlin.

[9]Japanese Evaluated Data Library, Version 3, JAERI 1319, 1990.

[10]Street K., Jr., Ghiorso A., Thompson S.G., Phys. Rev., 85, 135 (1952).

[11]Higgins G.H., Crane W.W. Phys. Rev., 94, 735 (1954).

[12]Bak M.A., Krivobatskij A.S., Petrzhak K.A., et al. Sov. At. Energy, 23, 1059 (1967).

[13]Ihle H., Michael H., Neubert A. et al., J. Inorg. Nucl. Chem., 34, 2427 (1972).

[14]Thompson S.G., Muga M., Proc. Second International Conf. on the Peaceful Uses of Atomic Energy, Geneva, September, 1-13, 1958, p. 331.

[15]Abramovich S. et al., Proc. XIII Meeting on Physics of Nuclear Fission, Obninsk, 1995, Ed. B. Kuzminov, p. 303.

[16]Danon Y, Moore M.S., Koehler P.E., et al., Nucl. Sci. Eng. 124, 482 (1996).

[17]Dunford C.L.: "ENDF Utility Codes Release 6.9", IAEA-NDS-29 (1993).

[18]Ignatjuk A.V., Istekov K.K., Smirenkin G.N. Sov. J. Nucl. Phys. 29, 450 (1979).

[19]Maslov V.M., Porodzinskij Yu.V., Sukhovitskij E.Sh., Klepatskij A.B., Morogovskij G.B., INDC(BLR)-5, 1996.

[20]Browne J.C., White R.M., Howe R.E. et al. Phys. Rev. 29, 2188 (1984).

[21]Dabbs J.W. , Bemis C.E., Raman S., et al., Nucl. Sci. Engng. 84, 1 (1983).

[22]Haouat, Lachkar J., Lagrange Ch., et al., Nucl.Sci. Engng. 81, 491 (1982).

[23]Klepatskij A.B., Sukhovitskij E.Sh., private communication.

[24]Fomushkin E.F., Novoselov G.F., Vinogradov Yu.I., et al. Yad. Fyz.., 33, 620 (1981).

[25]Fursov B.I., Samylin B.F., Smirenkin G.N., Polynov V.N., Nuclear Data for Science and Technology, Proc. of the Int. Conf., Gatlinburg, Tennessee, USA, May 9-13, 1994, v.I, p. 269.

[26]Ignatjuk A.V., Maslov V.M., Proc. Int. Symp. Nuclear Data Evaluation Methodology, Brookhaven,USA, October 12-16, 1992, p.440, World Scientific, 1993.

[27]Maslov V.M. and Y. Kikuchi JAERI-Research, 1996.

[28]Maslov V.M. Sov. J. At. Energy 64, 478 (1988).

[29]Maslov V.M., Proc. Int. Seminar on Interactions of Neutrons with Nuclei, Dubna, Russia, April, 27-30, 1996.

[30]Bolsterli M., Fiset E.O., Nix J.R., Norton J.L. Phys.Rev., C 5, 1050 (1972).

[31]Howard W.M., Moller P. Atomic Data and Nuclear Data Tables,25, 219 (1980).

[32]Maslov V.M., Porodzinskij Yu.V., Sukhovitskij E.Sh., Klepatskij A.B., Morogovskij G.B., INDC(BLR)-4, 1996.

[33]Fu C. Nucl. Sci. Engng. 86, 344 (1984).

[34]Maslov V.M. Zeit. Phys. A, Hadrons & Nuclei, 347, 211 (1994).

[35]Tepel J.W., Hoffman H.M., Weidenmuller H.A. Phys. Lett. 49, 1 (1974).

[36]Klepatskij A.B., Maslov V.M., Sukhovitskij E.Sh., private communication.

[37]Ignatjuk A.V., Maslov V.M., Pashchenko A.B. Sov. J. Nucl. Phys. 47, 224 (1988).

[38]Uhl M. and Strohmaier B., Report IRK - 76/10 (Vienna,1976).

[39]Maslov V.M., Porodzinskij Yu.V., Sukhovitskij E.Sh., Klepatskij A.B., Morogovskij G.B., INDC(BLR)-3, 1996.

[40]White R.M., Browne J.C., in: Nuclear Data for Science and Technology (North-Holland, 1983), p.281.

[41]Maslov V.M., Porodzinskij Yu.V., Sukhovitskij E.Sh., Klepatskij A.B., Morogovskij G.B., INDC(BLR)-6, 1996.

[42]ENSDF, 1995.

[43]Sood P.C., Singh R.N. Nucl. Phys. A373, 519 (1982).

[44]Maslov V.M., Porodzinskij Yu.V.,Sukhovitskij E.Sh., Proc. Int. Conf. on Neutron Physics, 14-18 Sept., Kiev, USSR, V.1, p.413, 1988.

[45]Madland D.G., Nix J.R., Nucl. Sci. Engng. 81, 213 (1982).

[46]Howe R.E., Browne J.C., Dougan R.J., Dupzyk R.J., Landrum J.H. Nucl. Sci. Eng. 77,454 (1981).

[47]Howe R.E., White R.M., Browne J.C., Landrum J.H., Dougan R.J., Lougheed R.W., Dupzyk R.J., Nucl. Phys., A407, 193 (1983).

[48]Khokhlov Yu.A. et al., Nuclear Data for Science and Technology, Proc. of the Int. Conf., Gatlinburg, Tennessee, USA, May 9-13, 1994, v.I, p. 272.

[49]Howerton R.J. Nucl. Sci. Engng., 62, 438 (1977).

[50]Brady M.C. and England T.R., Nucl.Sci. Engng. 103, 129 (1989).

8 Figure captions

Fig. 2.1 Fission cross section of ^{242g}Am in the energy region below 1 eV.
Fig. 2.2 Fission cross section of ^{242g}Am in the energy region below 100 eV.
Fig. 2.3 Capture cross section of ^{242g}Am in the energy region below 1 eV.
Fig. 2.4 Capture cross section of ^{242g}Am in the energy region below 100 eV.
Fig. 3.1 Fission cross section of ^{242g}Am in unresolved resonance region.
Fig. 3.2 Capture cross section of ^{242g}Am in unresolved resonance region.
Fig. 3.3 Comparison of fission cross sections of ^{242g}Am and ^{242m}Am in unresolved resonance region.
Fig. 3.4 Comparison of capture cross sections of ^{242g}Am and ^{242m}Am in unresolved resonance region.
Fig. 4.1 Compound reaction cross section of ^{242g}Am.
Fig. 4.2 Total cross section of ^{242g}Am.
Fig. 4.3 Elastic scattering cross section of ^{242g}Am.
Fig. 4.4 Fission cross section of ^{242g}Am.
Fig. 4.5 Fission cross section of ^{242g}Am.
Fig. 4.6 Fission cross section of ^{242g}Am.
Fig. 4.7 Fission cross section of ^{241}Am.
Fig. 4.8 Fission cross section of ^{243}Am.
Fig. 4.9 Fission cross section of ^{242g}Am.
Fig. 4.10 Cumulative number of levels of ^{242}Am.
Fig. 4.11 Inelastic scattering cross section of ^{242g}Am.
Fig. 4.12 Continuum inelastic scattering cross section of ^{242g}Am.
Fig. 4.13 Cross section of ^{242g}Am: 0.0441 MeV, 0^- level excitation.
Fig. 4.14 Cross section of ^{242g}Am: 0.04863 MeV, 5^- level excitation.
Fig. 4.15 Cross section of ^{242g}Am: 0.0529 MeV, 3^- level excitation.
Fig. 4.16Cross section of ^{242g}Am: 0.0758 MeV, 2^- level excitation.
Fig. 4.17 Cross section of ^{242g}Am: 0.114 MeV, 6^- level excitation.
Fig. 4.18 Cross section of ^{242g}Am: 0.148 MeV, 5^- level excitation.
Fig. 4.19 Cross section of ^{242g}Am: 0.1499 MeV, 4^- level excitation.
Fig. 4.20 Cross section of ^{242g}Am: 0.190 MeV, 7^- level excitation.
Fig. 4.21 Cross section of ^{242g}Am: 0.263 MeV, 7^- level excitation.
Fig. 4.22 Cross section of ^{242g}Am: 0.2631 MeV, 6^- level excitation.
Fig. 4.23 Cumulative number of levels of ^{243}Am.
Fig. 4.24 Radiative capture cross section of ^{242g}Am.
Fig. 4.25 ^{242g}Am(n,2n) reaction cross section.
Fig. 4.26 ^{242g}Am(n,3n) reaction cross section.
Fig. 5.1 Components of first neutron spectrum of ^{242g}Am for incident neutron energy 14 MeV.

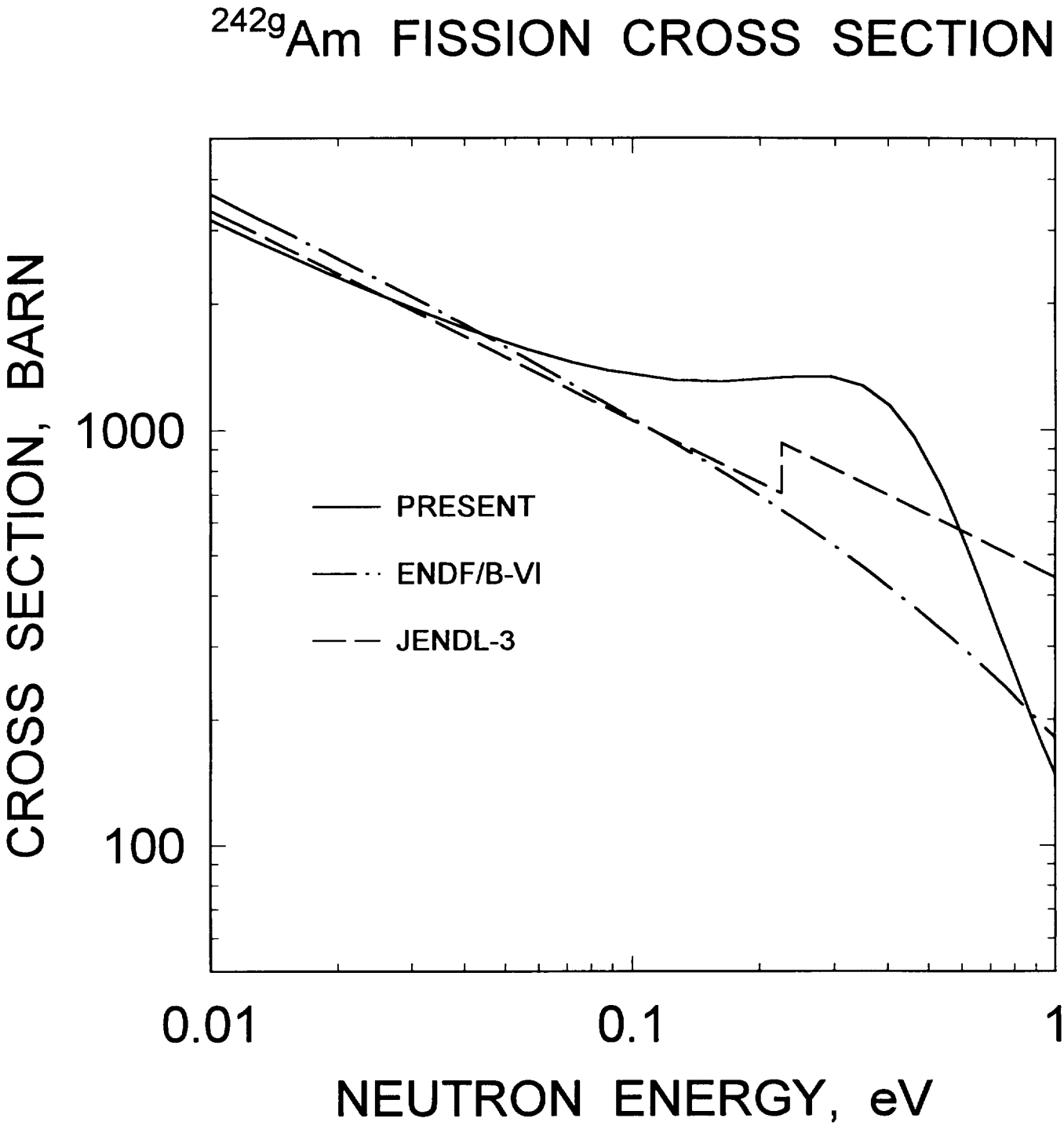
^{242g}Am FISSION CROSS SECTION
CROSS SECTION, BARN
1000
100
PRESENT
ENDF/B-VI
JENDL-3
0.01
0.1
1
NEUTRON ENERGY, eV

FIG.2.1

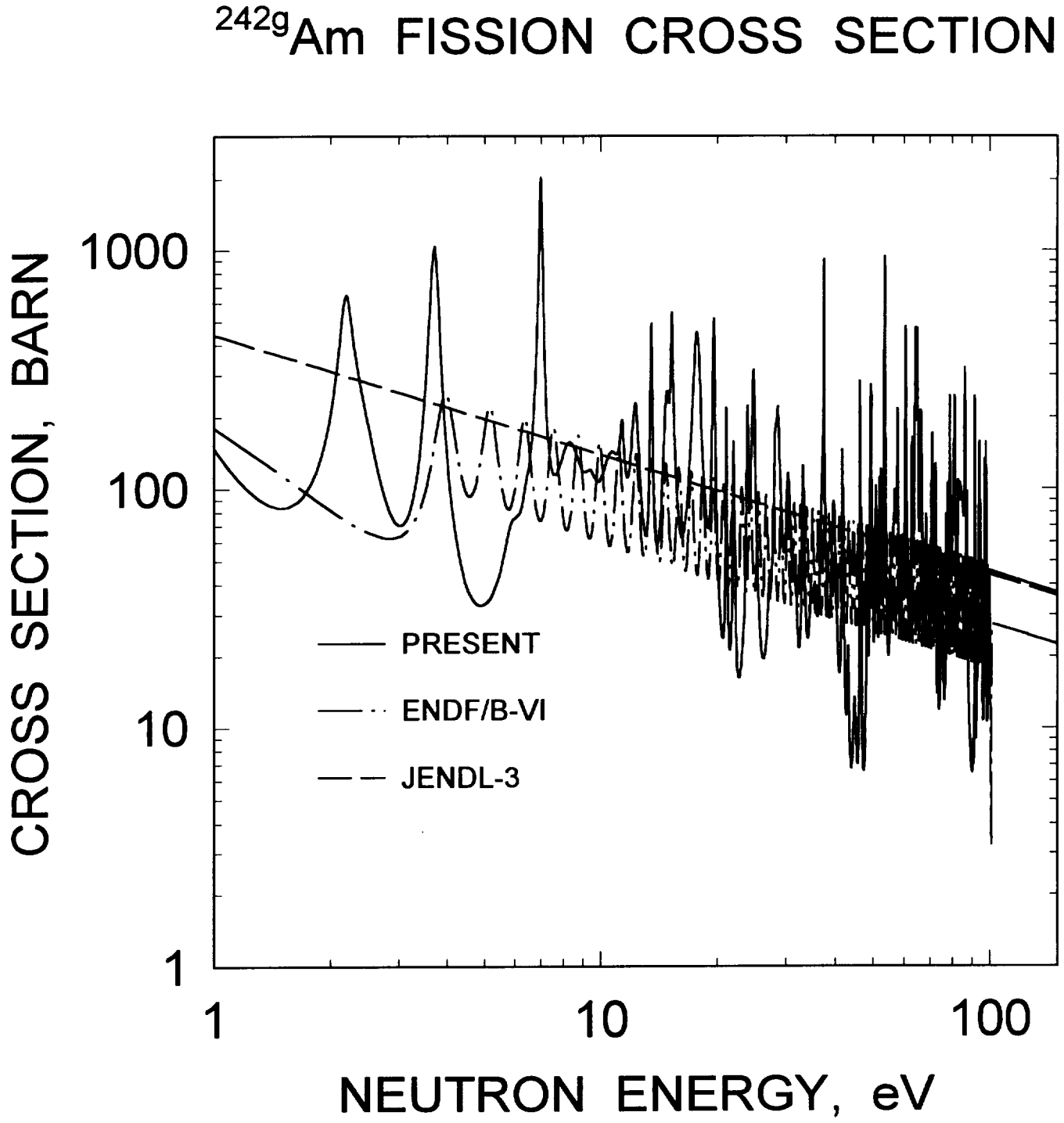
^{242g}Am FISSION CROSS SECTION
CROSS SECTION, BARN
1000
100
10
1
1
10
100
NEUTRON ENERGY, eV
PRESENT
ENDF/B-VI
JENDL-3

FIG.2.2

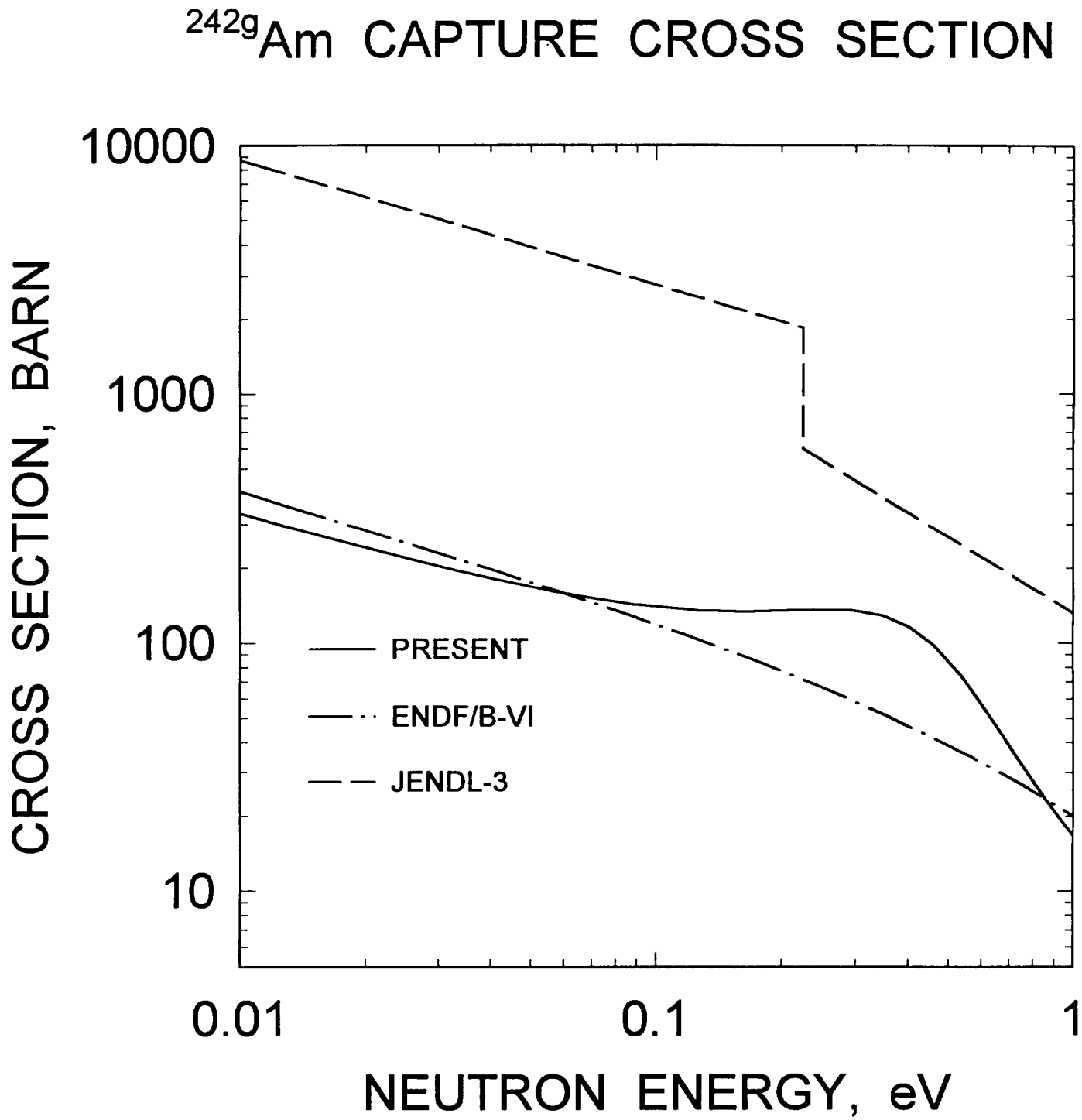
^{242g}Am CAPTURE CROSS SECTION
10000
1000
100
10
CROSS SECTION, BARN
PRESENT
ENDF/B-VI
JENDL-3
0.01
0.1
1
NEUTRON ENERGY, eV

FIG.2.3

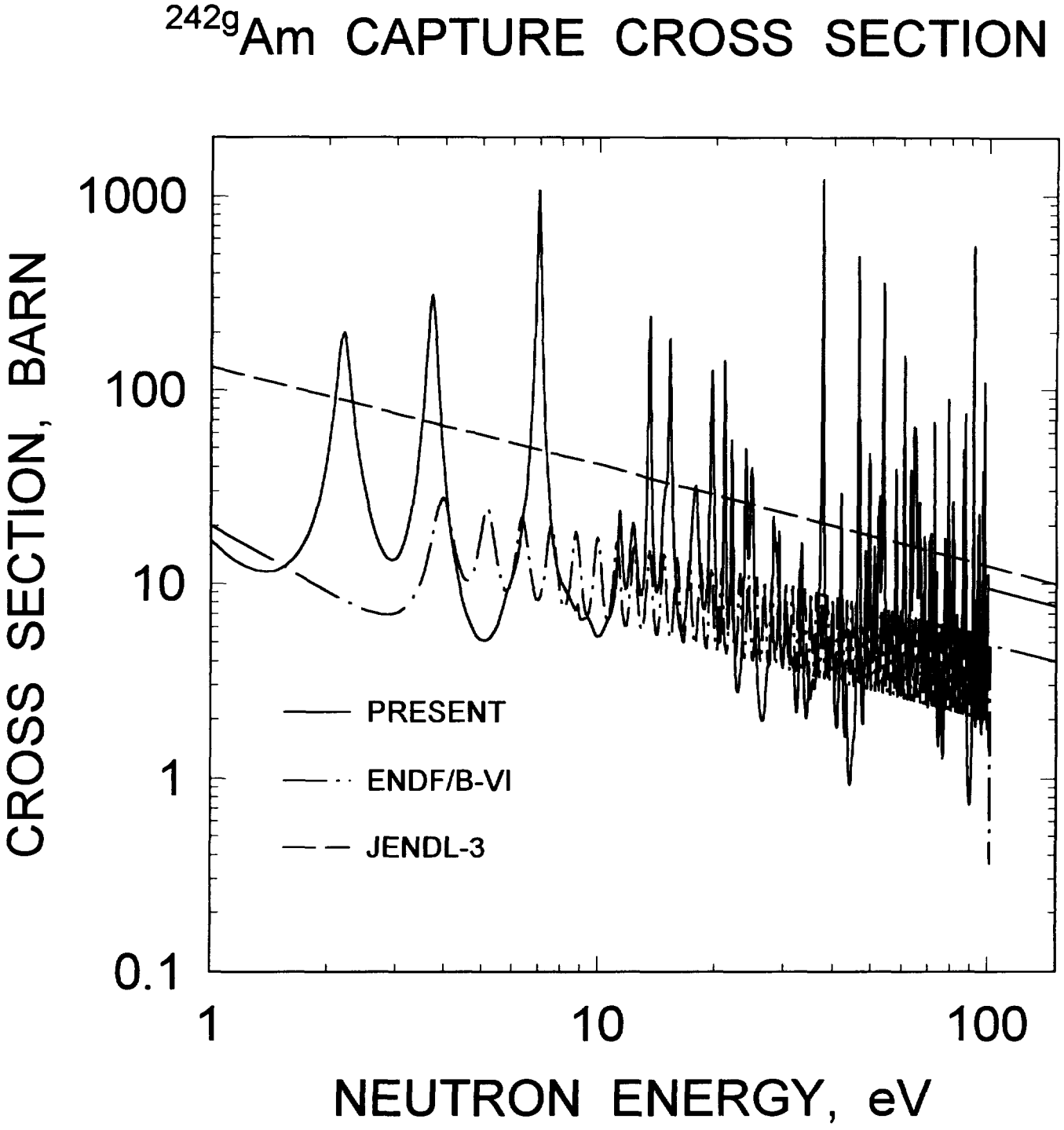
^{242g}Am CAPTURE CROSS SECTION
CROSS SECTION, BARN
1000
100
10
1
0.1
1
10
100
NEUTRON ENERGY, eV
PRESENT
ENDF/B-VI
JENDL-3

FIG.2.4

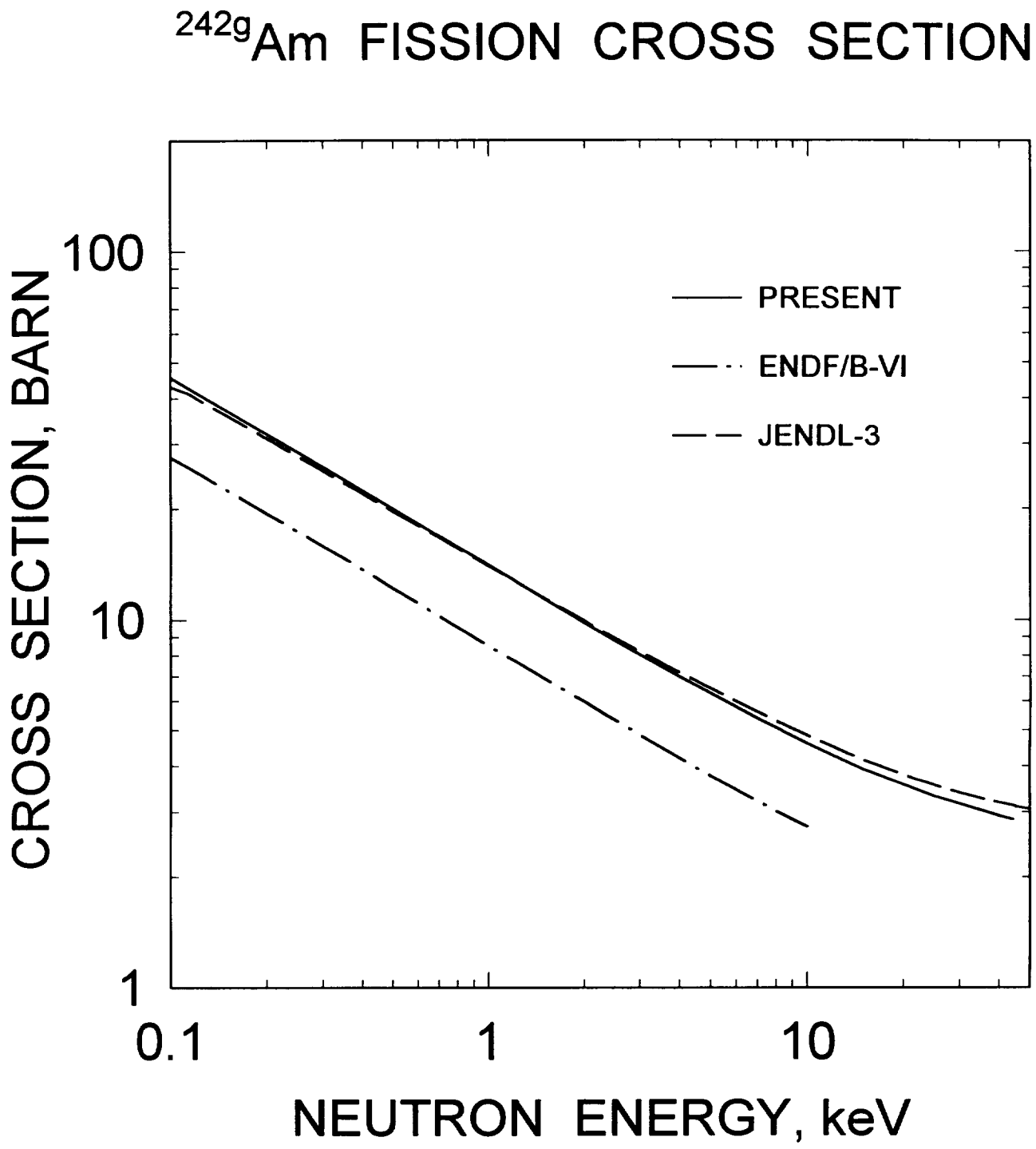
^{242g}Am FISSION CROSS SECTION
CROSS SECTION, BARN
100
10
1
0.1
1
10
NEUTRON ENERGY, keV
PRESENT
ENDF/B-VI
JENDL-3

FIG.3.1

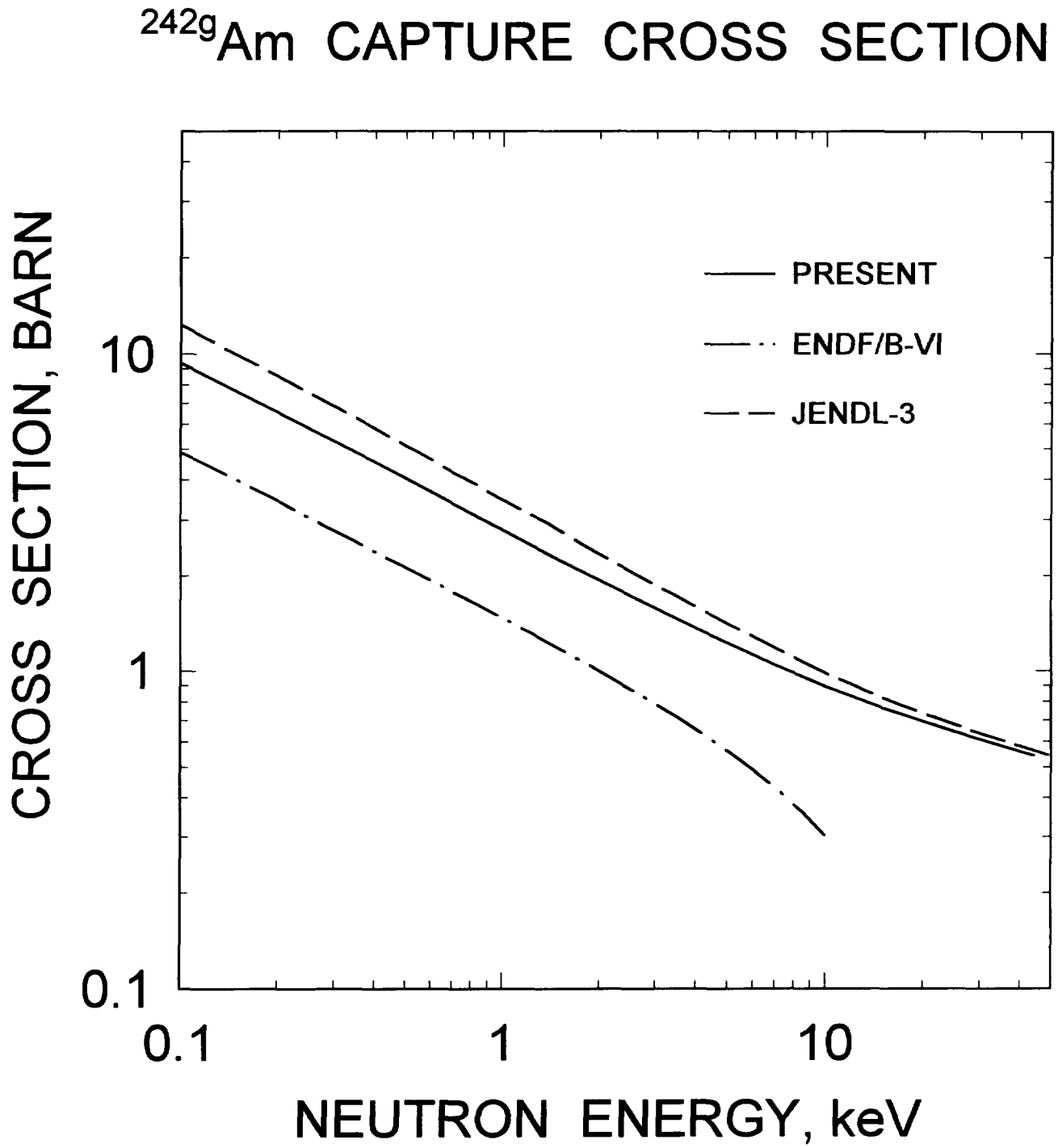
^{242g}Am CAPTURE CROSS SECTION
CROSS SECTION, BARN
10
1
0.1
0.1
1
10
NEUTRON ENERGY, keV
PRESENT
ENDF/B-VI
JENDL-3

FIG.3.2

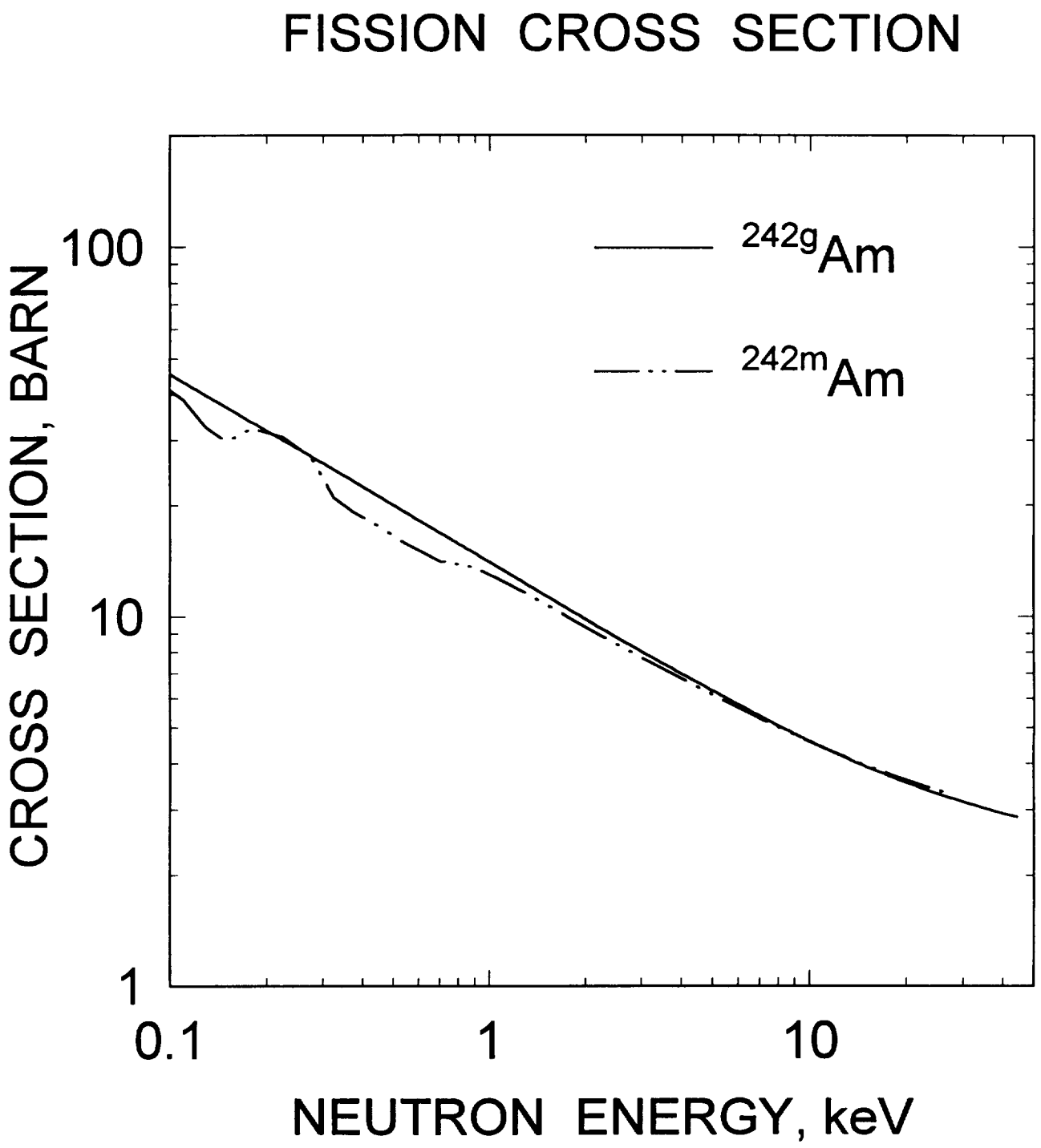
FISSION CROSS SECTION
CROSS SECTION, BARN
100
10
1
0.1
1
10
NEUTRON ENERGY, keV
242g Am
242m Am

FIG.3.3

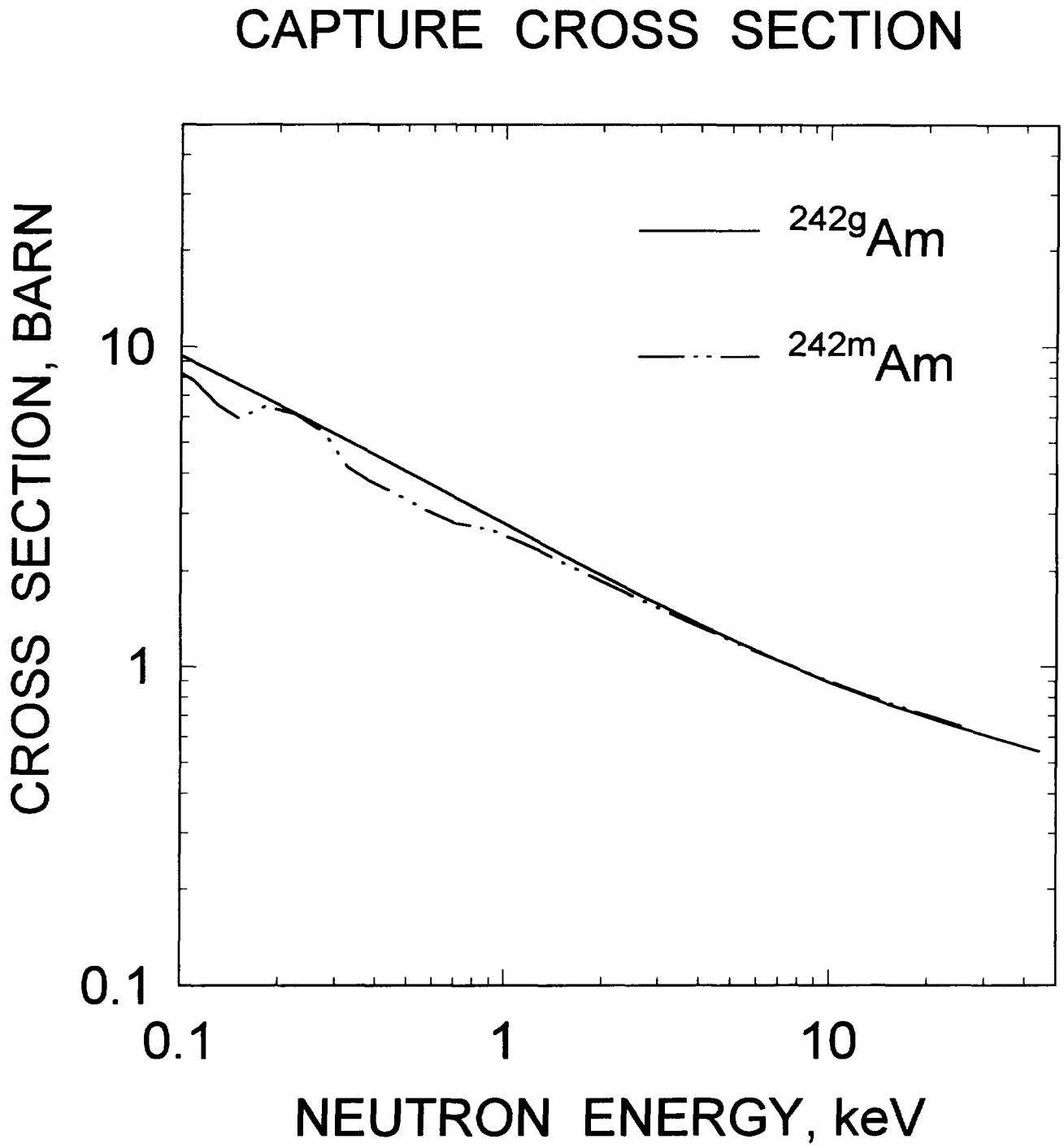
CAPTURE CROSS SECTION
CROSS SECTION, BARN
10
1
0.1
0.1
1
10
NEUTRON ENERGY, keV
242g Am
242m Am

FIG.3.4

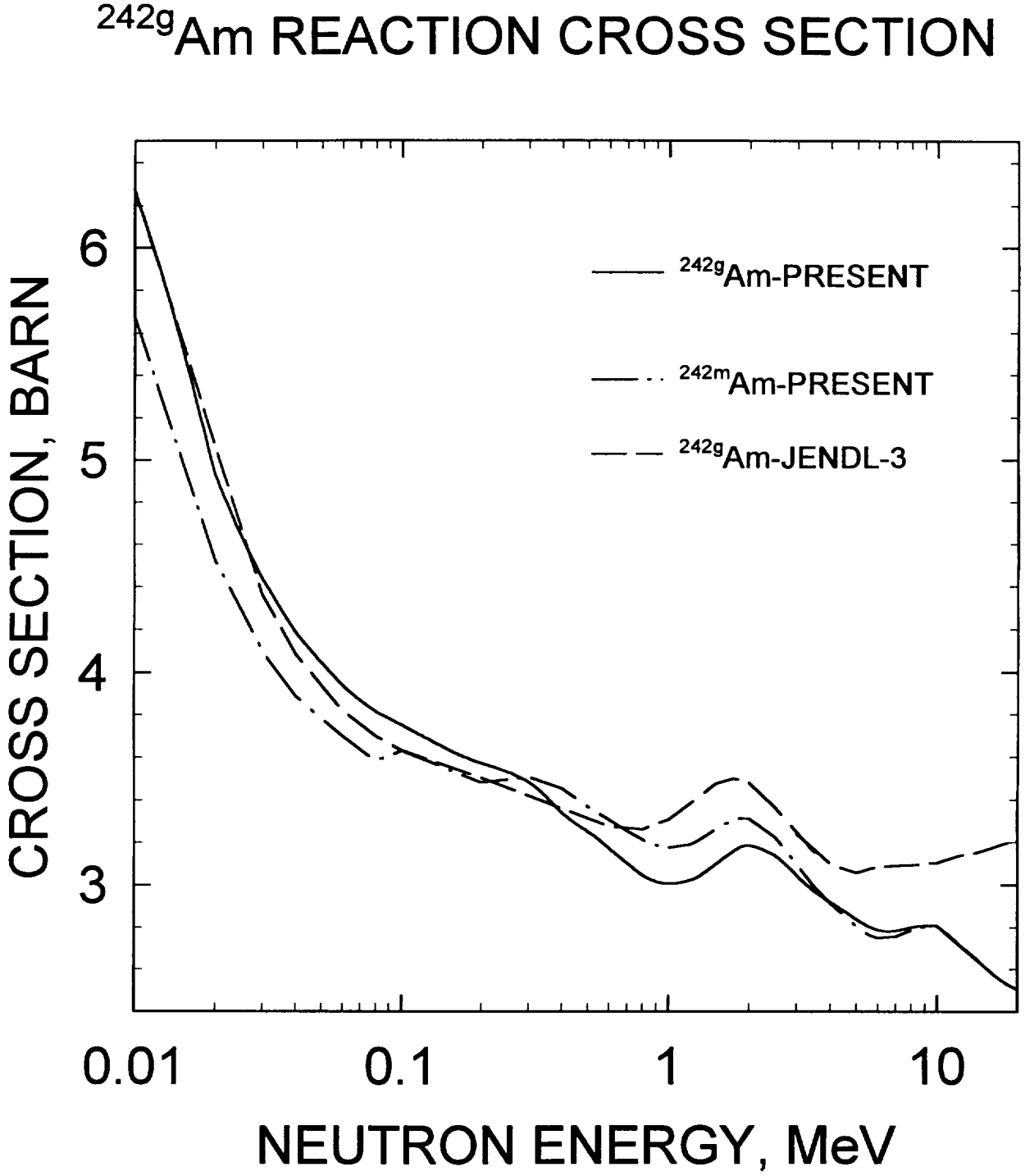
^{242g}Am REACTION CROSS SECTION
CROSS SECTION, BARN
6
5
4
3
0.01
0.1
1
10
NEUTRON ENERGY, MeV
^{242g}Am-PRESENT
^{242m}Am-PRESENT
^{242g}Am-JENDL-3

FIG.4.1

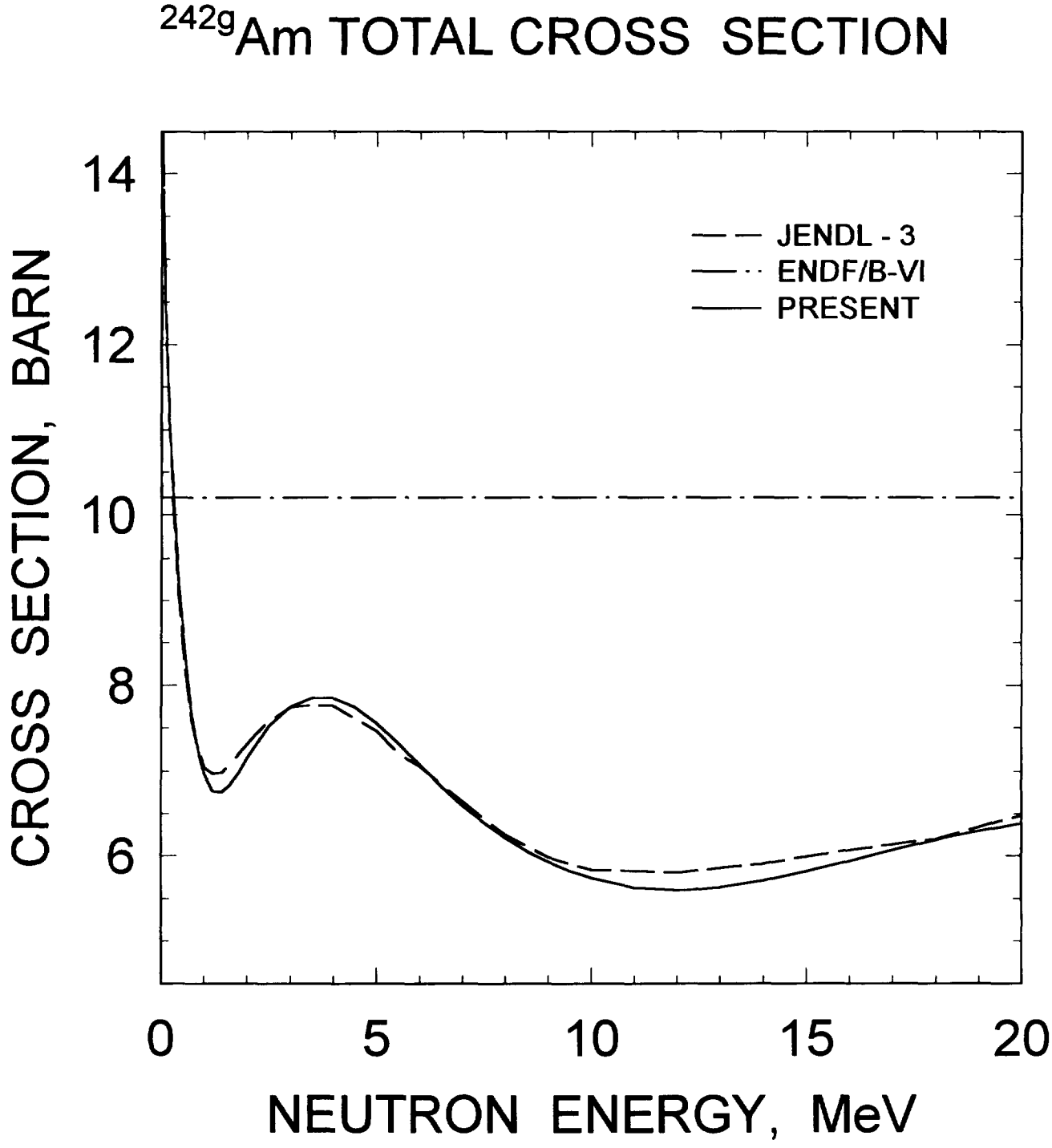
^{242g}Am TOTAL CROSS SECTION
CROSS SECTION, BARN
14
12
10
8
6
0
5
10
15
20
NEUTRON ENERGY, MeV
JENDL - 3
ENDF/B-VI
PRESENT

FIG. 4.2

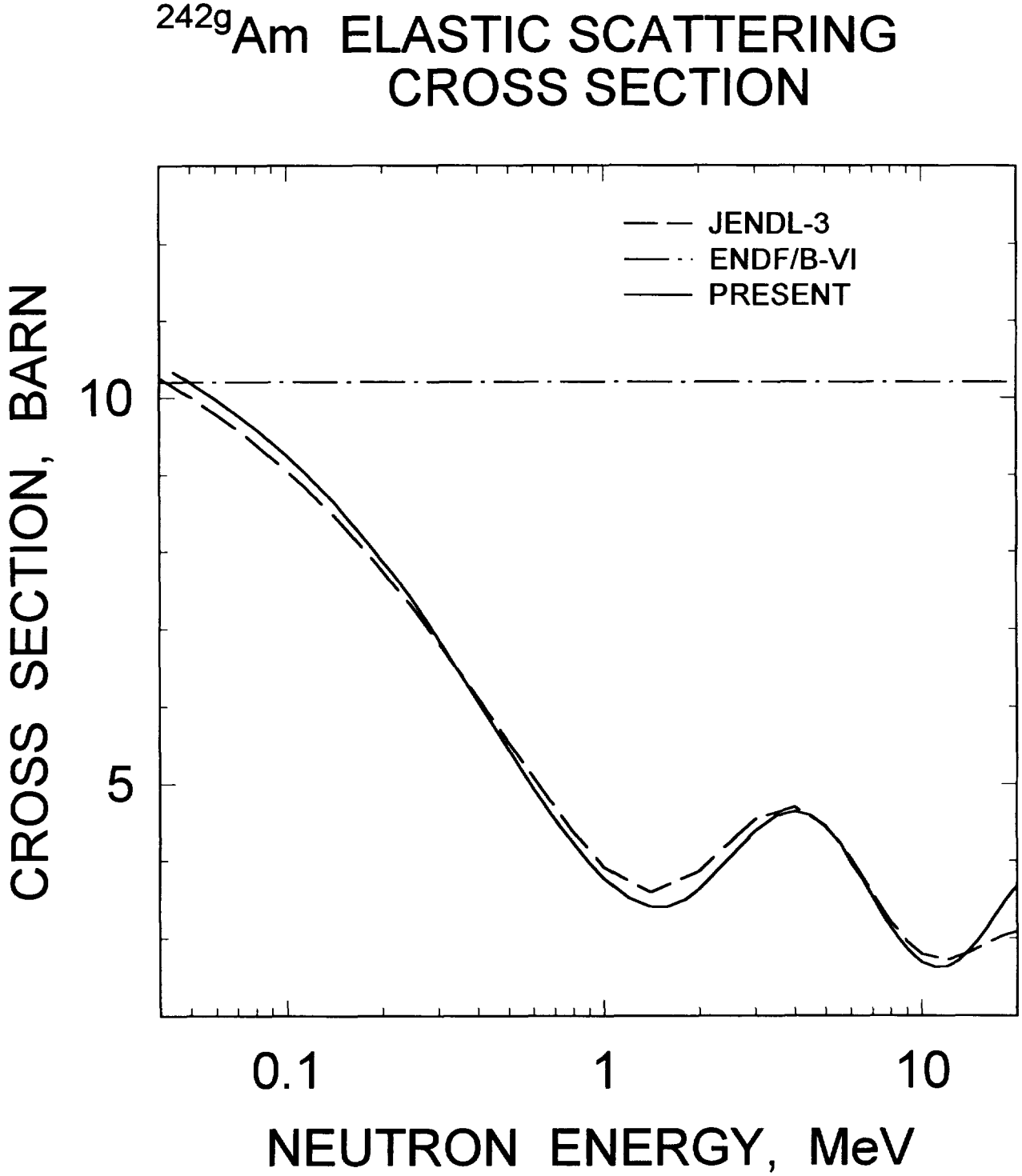
^{242g}Am ELASTIC SCATTERING CROSS SECTION
JENDL-3
ENDF/B-VI
PRESENT
CROSS SECTION, BARN
10
5
0.1
1
10
NEUTRON ENERGY, MeV

FIG. 4.3

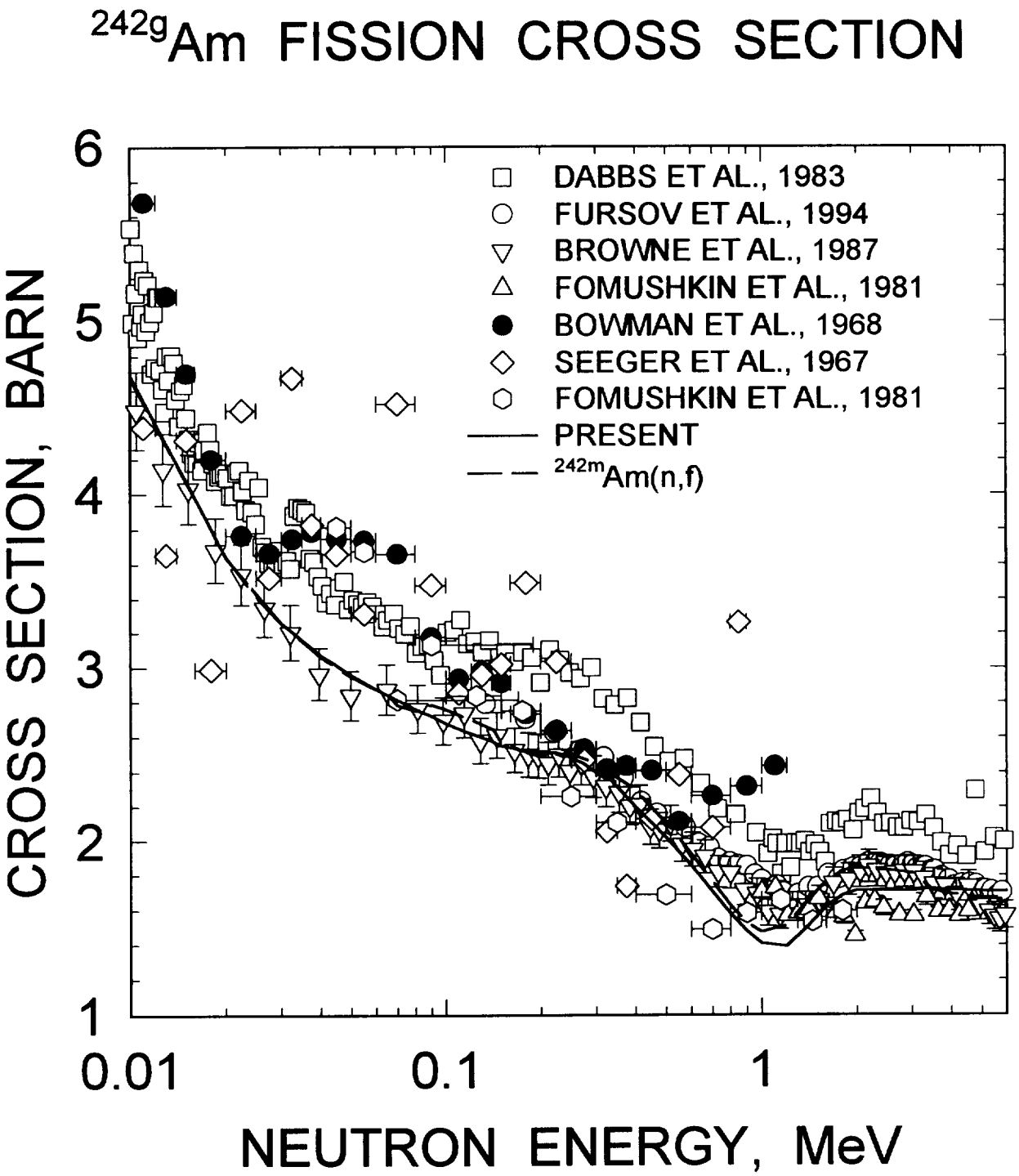
^{242g}Am FISSION CROSS SECTION
CROSS SECTION, BARN
NEUTRON ENERGY, MeV
6
5
4
3
2
1
0.01
0.1
1
DABBS ET AL., 1983
FURSOV ET AL., 1994
BROWNE ET AL., 1987
FOMUSHKIN ET AL., 1981
BOWMAN ET AL., 1968
SEEGER ET AL., 1967
FOMUSHKIN ET AL., 1981
PRESENT
^{242m}Am(n,f)

FIG. 4.4

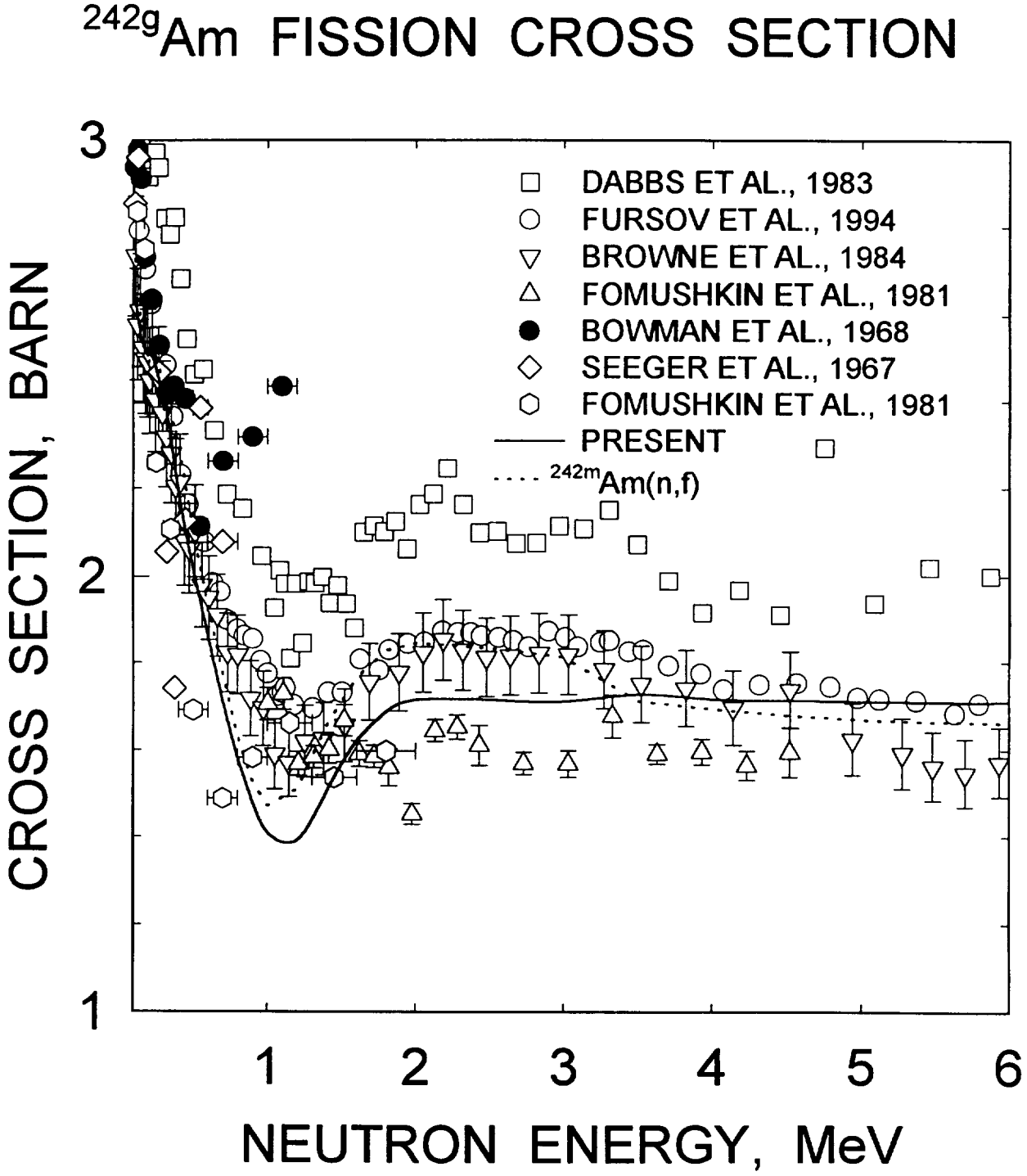
^{242g}Am FISSION CROSS SECTION
CROSS SECTION, BARN
NEUTRON ENERGY, MeV
DABBS ET AL., 1983
FURSOV ET AL., 1994
BROWNE ET AL., 1984
FOMUSHKIN ET AL., 1981
BOWMAN ET AL., 1968
SEEGER ET AL., 1967
FOMUSHKIN ET AL., 1981
PRESENT
^{242m}Am(n,f)
1
2
3
1
2
3
4
5
6

FIG. 4.5

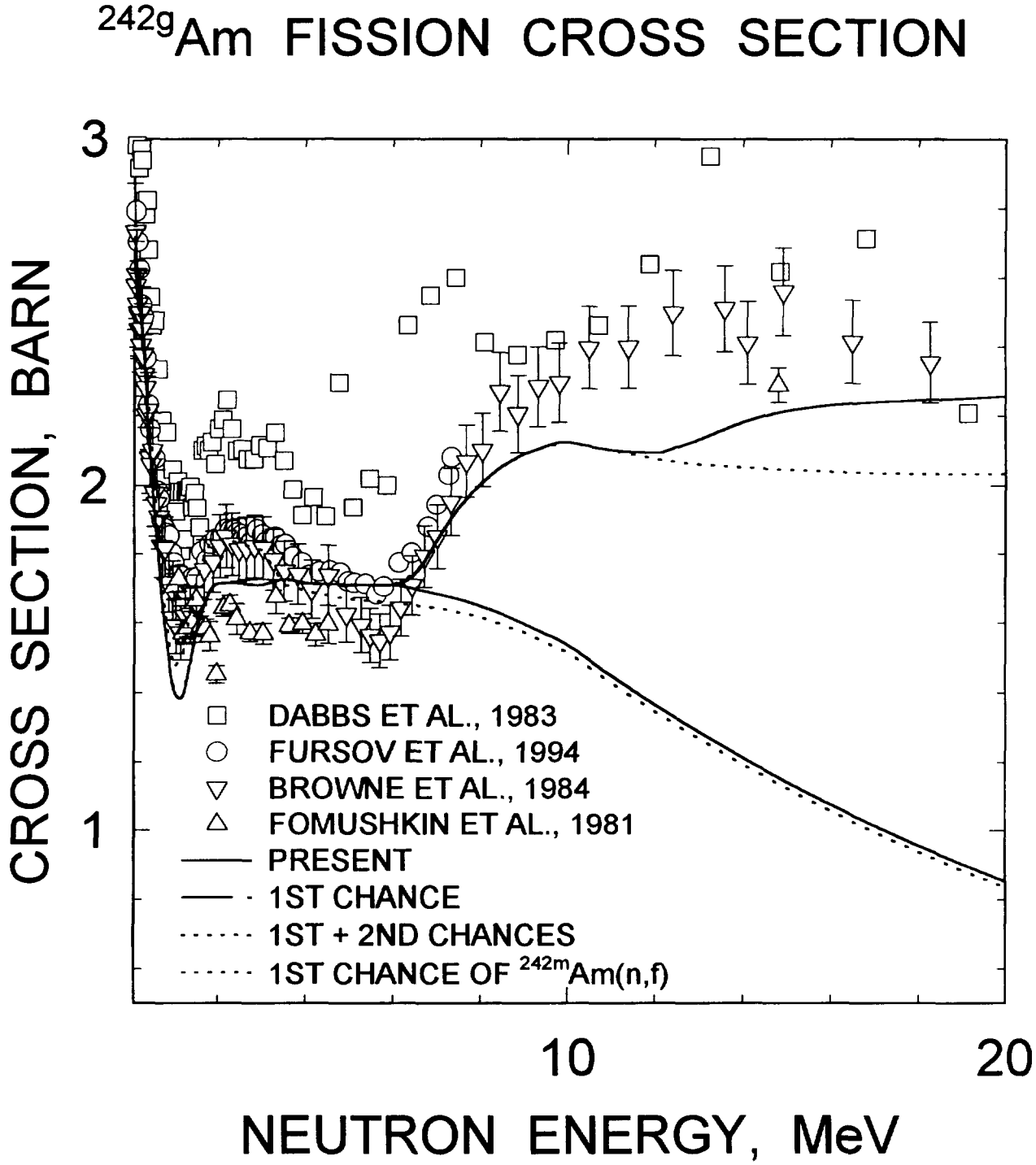
242gAm FISSION CROSS SECTION
CROSS SECTION, BARN
3
2
1
10
20
NEUTRON ENERGY, MeV
DABBS ET AL., 1983
FURSOV ET AL., 1994
BROWNE ET AL., 1984
FOMUSHKIN ET AL., 1981
PRESENT
1ST CHANCE
1ST + 2ND CHANCES
1ST CHANCE OF 242mAm(n,f)

FIG. 4.6

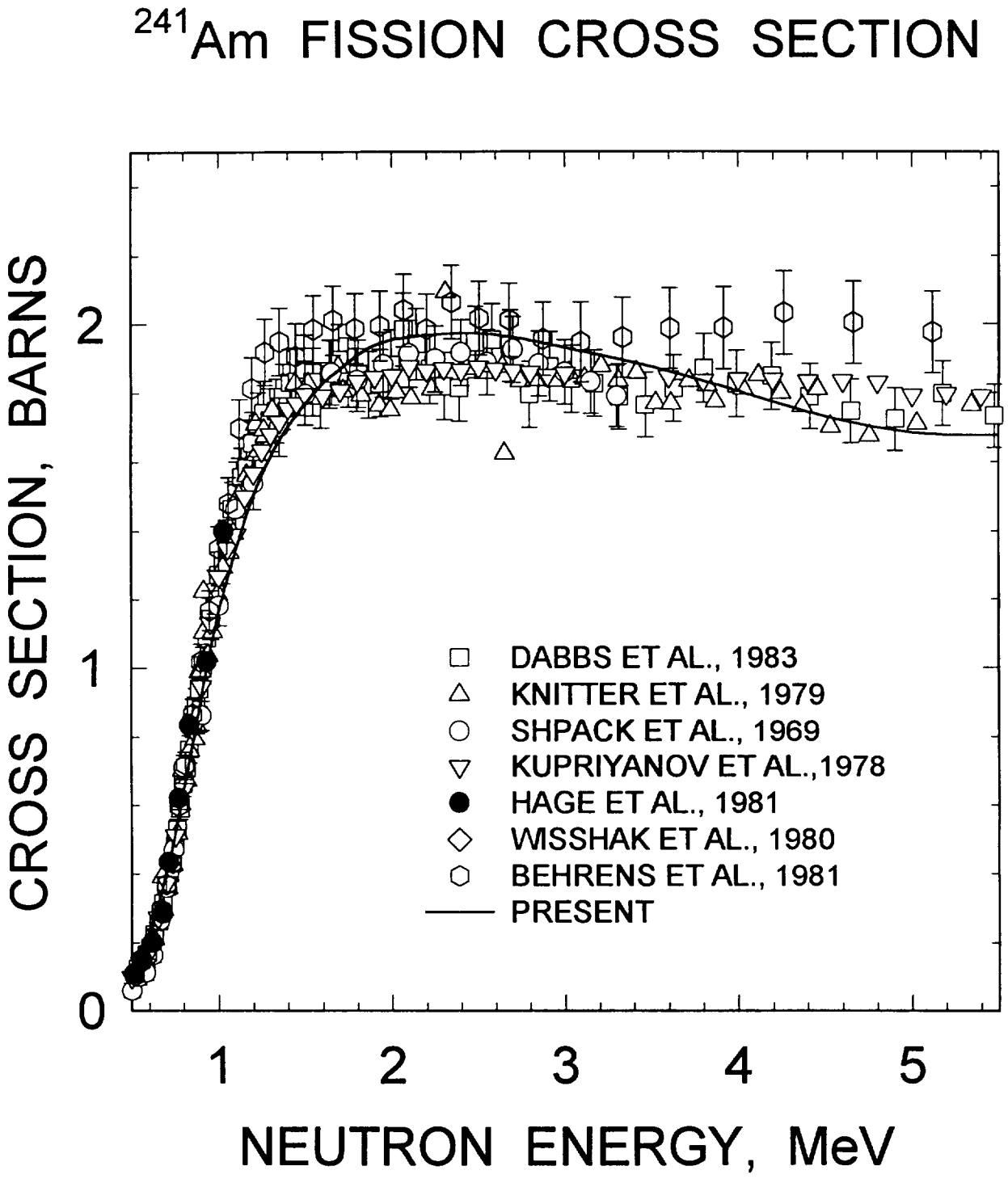
^{241}Am FISSION CROSS SECTION
CROSS SECTION, BARNS
0
1
2
1
2
3
4
5
NEUTRON ENERGY, MeV
DABBS ET AL., 1983
KNITTER ET AL., 1979
SHPACK ET AL., 1969
KUPRIYANOV ET AL.,1978
HAGE ET AL., 1981
WISSHAK ET AL., 1980
BEHRENS ET AL., 1981
PRESENT

FIG. 4.7

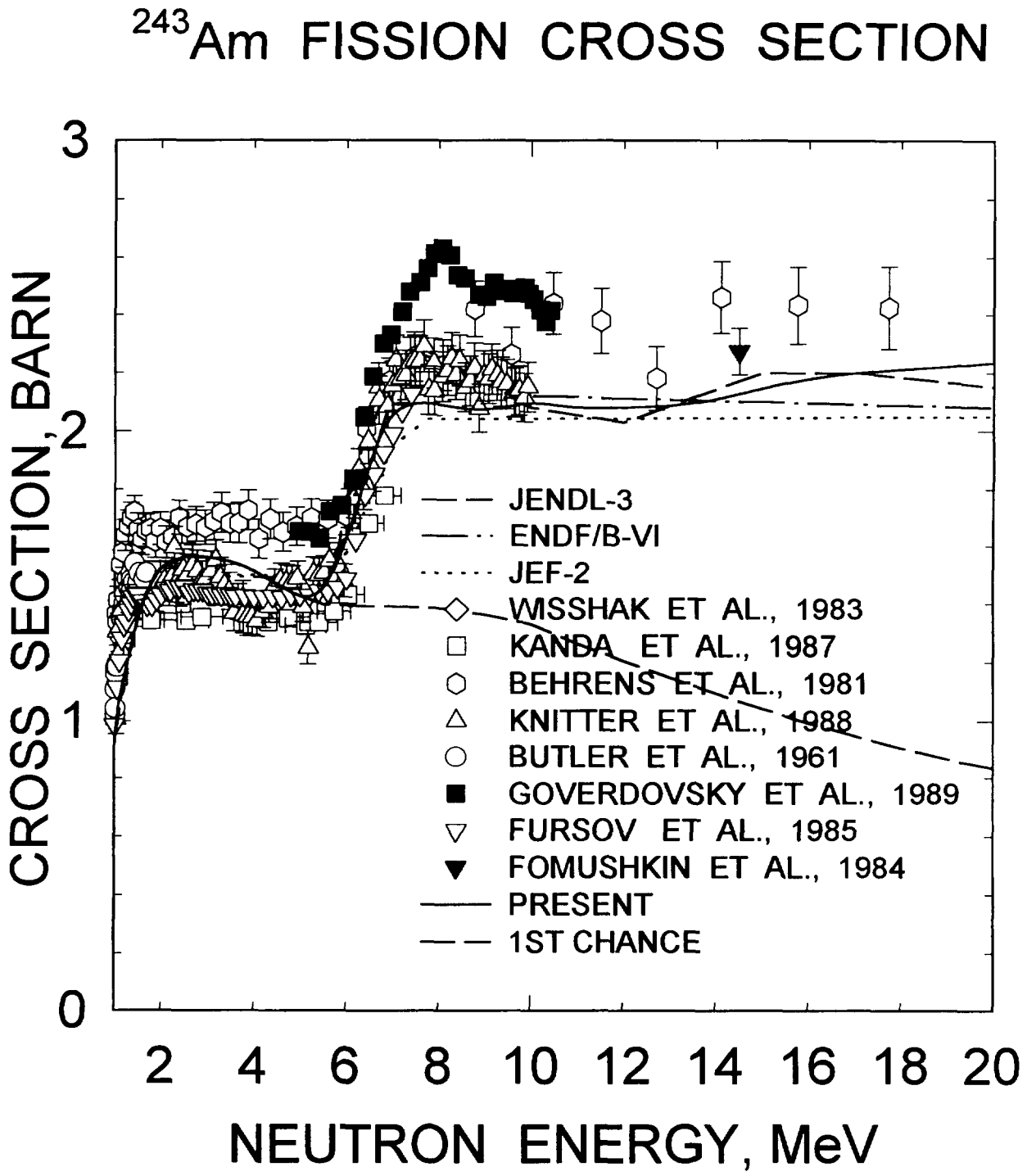
^{243}Am FISSION CROSS SECTION
CROSS SECTION, BARN
NEUTRON ENERGY, MeV
0
1
2
3
2
4
6
8
10
12
14
16
18
20
JENDL-3
ENDF/B-VI
JEF-2
WISSHAK ET AL., 1983
KANDA ET AL., 1987
BEHRENS ET AL., 1981
KNITTER ET AL., 1988
BUTLER ET AL., 1961
GOVERDOVSKY ET AL., 1989
FURSOV ET AL., 1985
FOMUSHKIN ET AL., 1984
PRESENT
1ST CHANCE

FIG.4.8

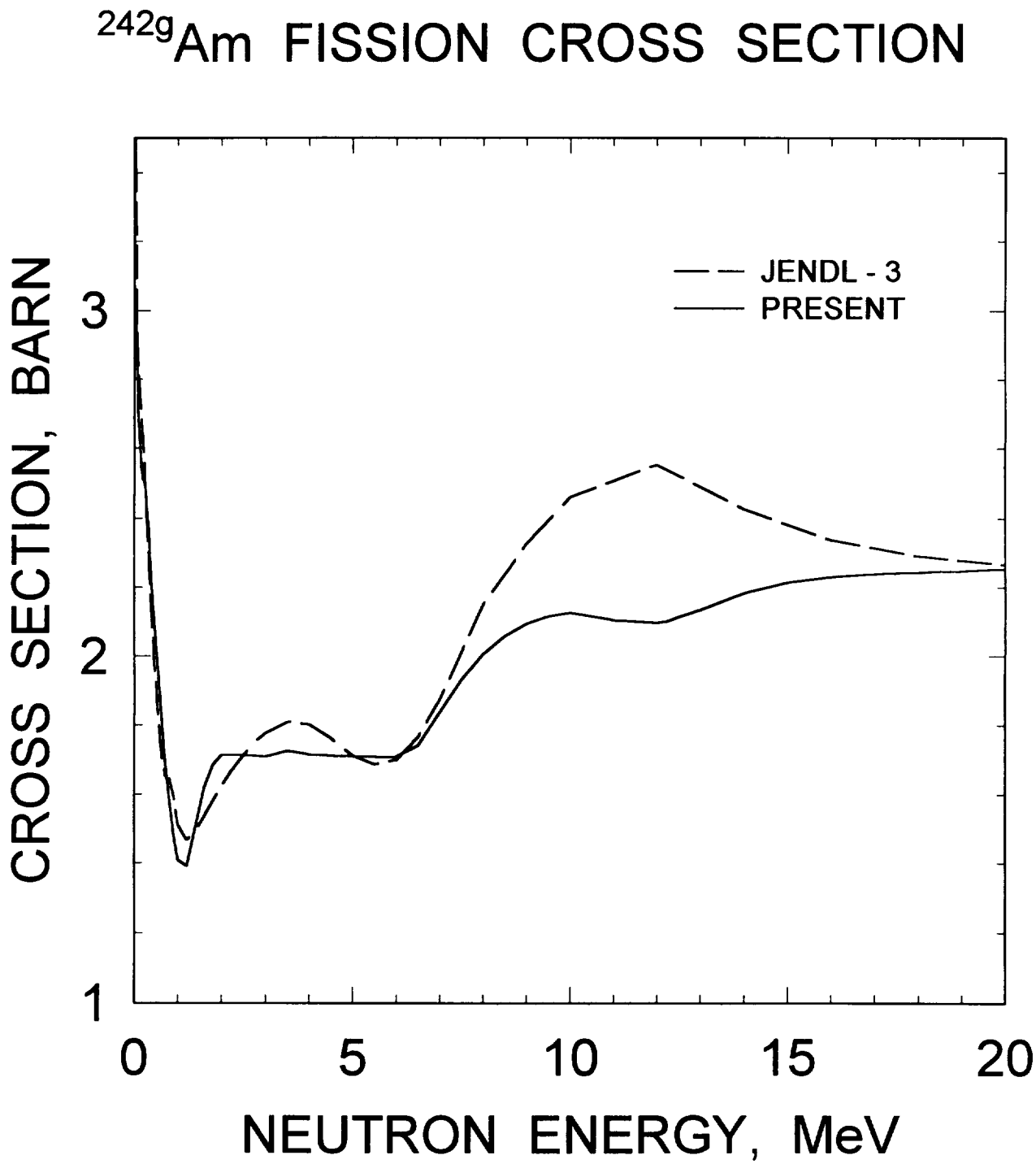
^{242g}Am FISSION CROSS SECTION
JENDL - 3
PRESENT
CROSS SECTION, BARN
1
2
3
0
5
10
15
20
NEUTRON ENERGY, MeV

FIG. 4.9

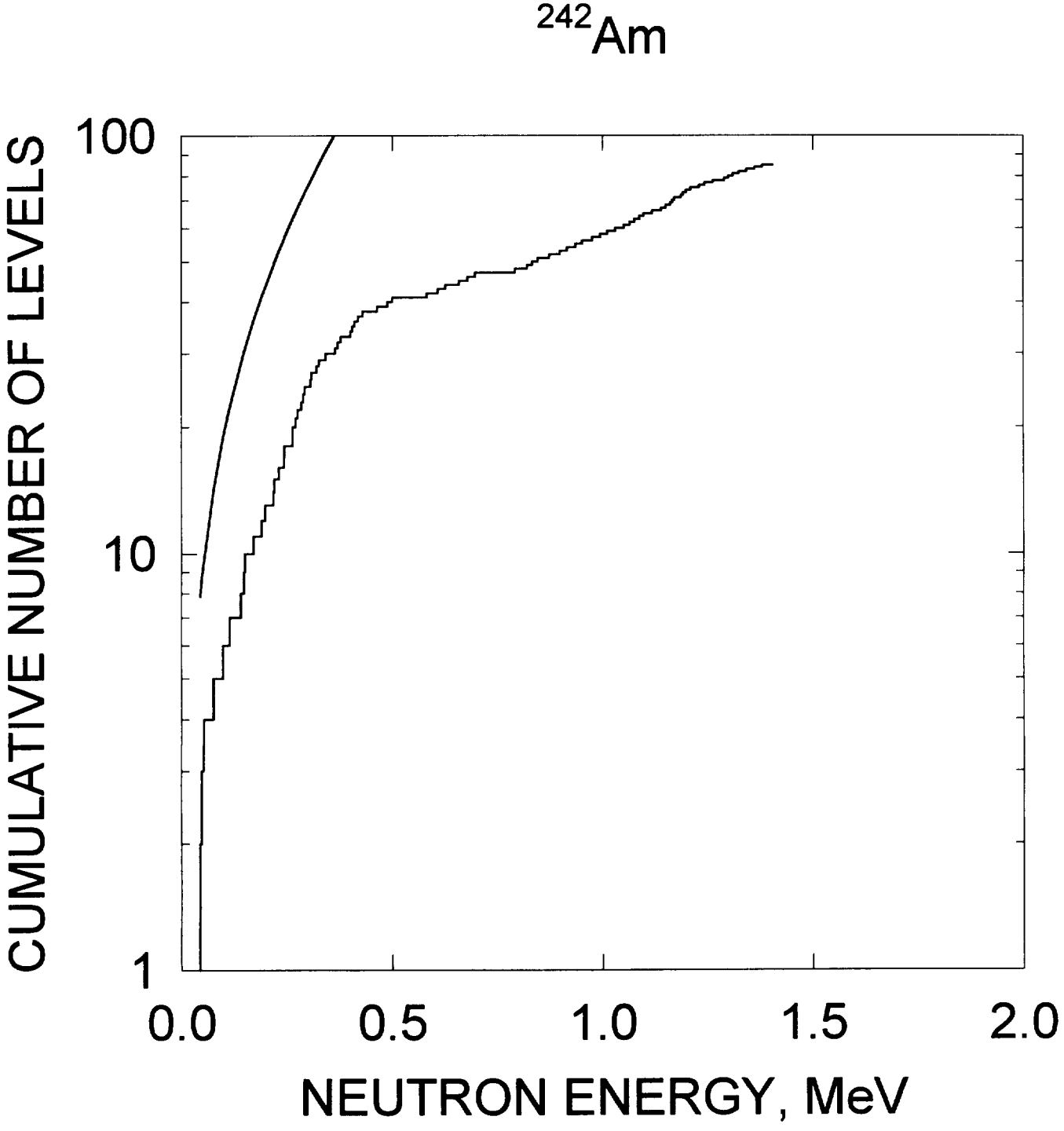
^{242}Am
CUMULATIVE NUMBER OF LEVELS
100
10
1
0.0
0.5
1.0
1.5
2.0
NEUTRON ENERGY, MeV

FIG. 4.10

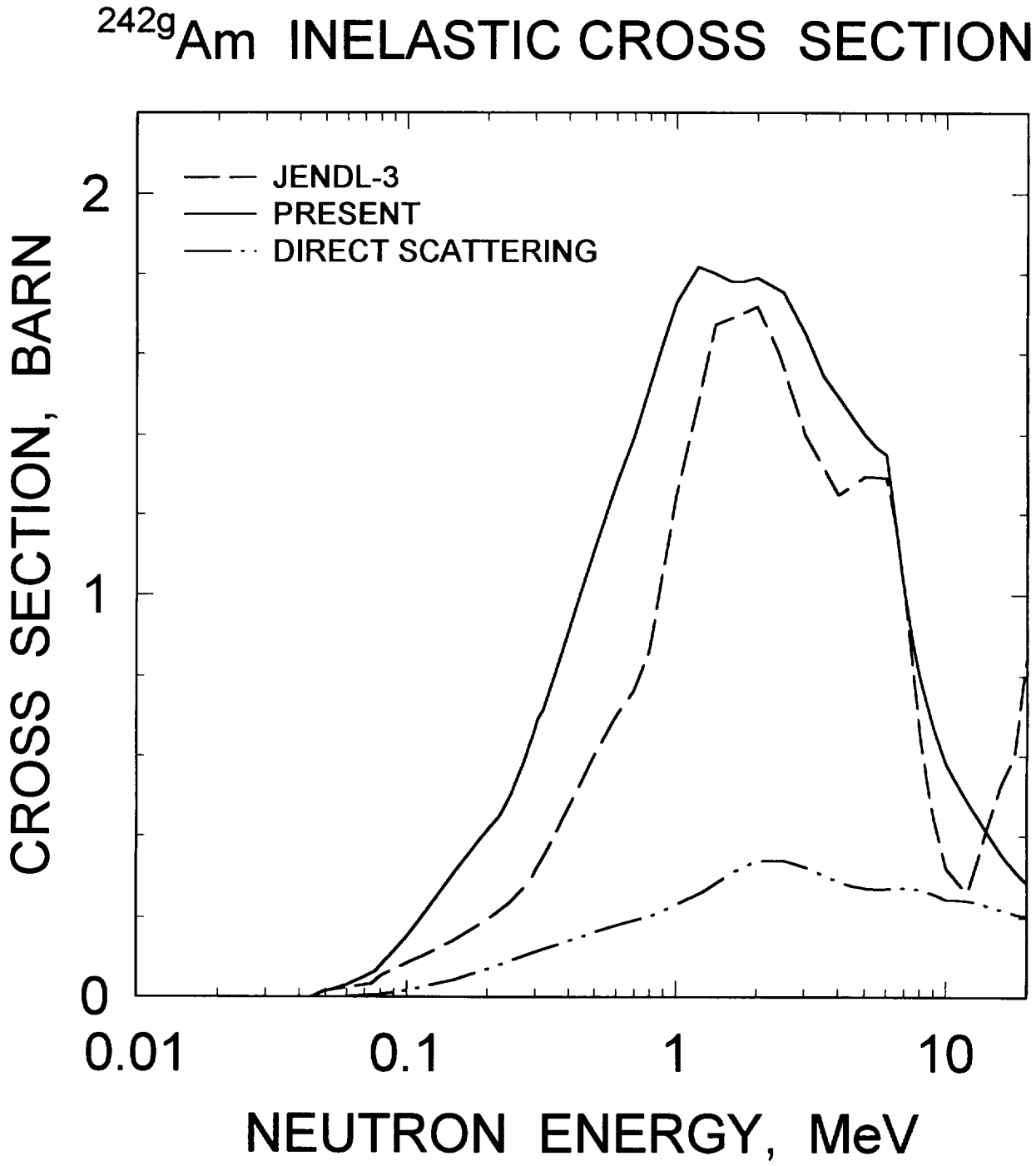
^{242g}Am INELASTIC CROSS SECTION
JENDL-3
PRESENT
DIRECT SCATTERING
CROSS SECTION, BARN
0
1
2
0.01
0.1
1
10
NEUTRON ENERGY, MeV

FIG. 4.11

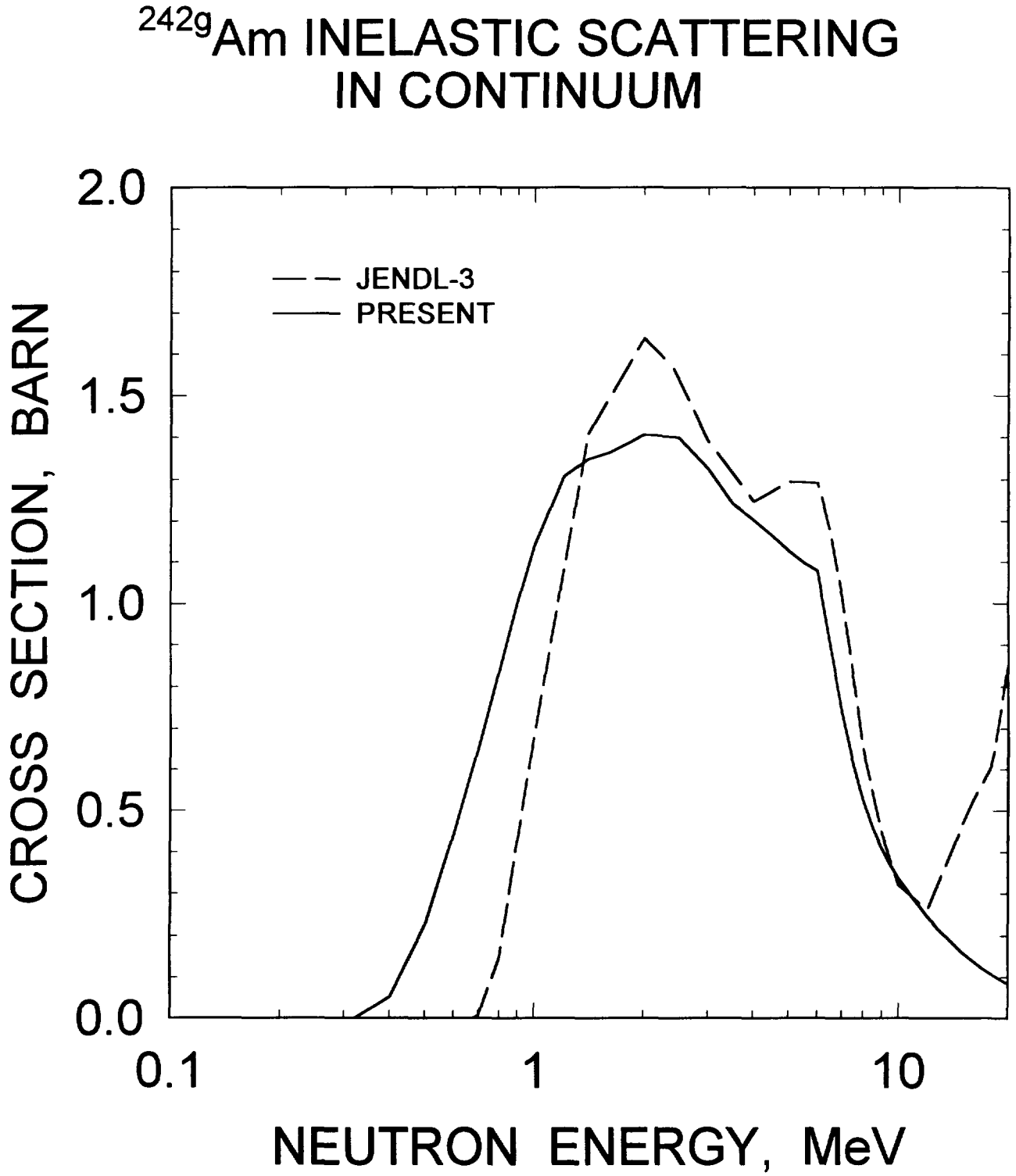
^{242g}Am INELASTIC SCATTERING
IN CONTINUUM
JENDL-3
PRESENT
CROSS SECTION, BARN
2.0
1.5
1.0
0.5
0.0
0.1
1
10
NEUTRON ENERGY, MeV

FIG. 4.12

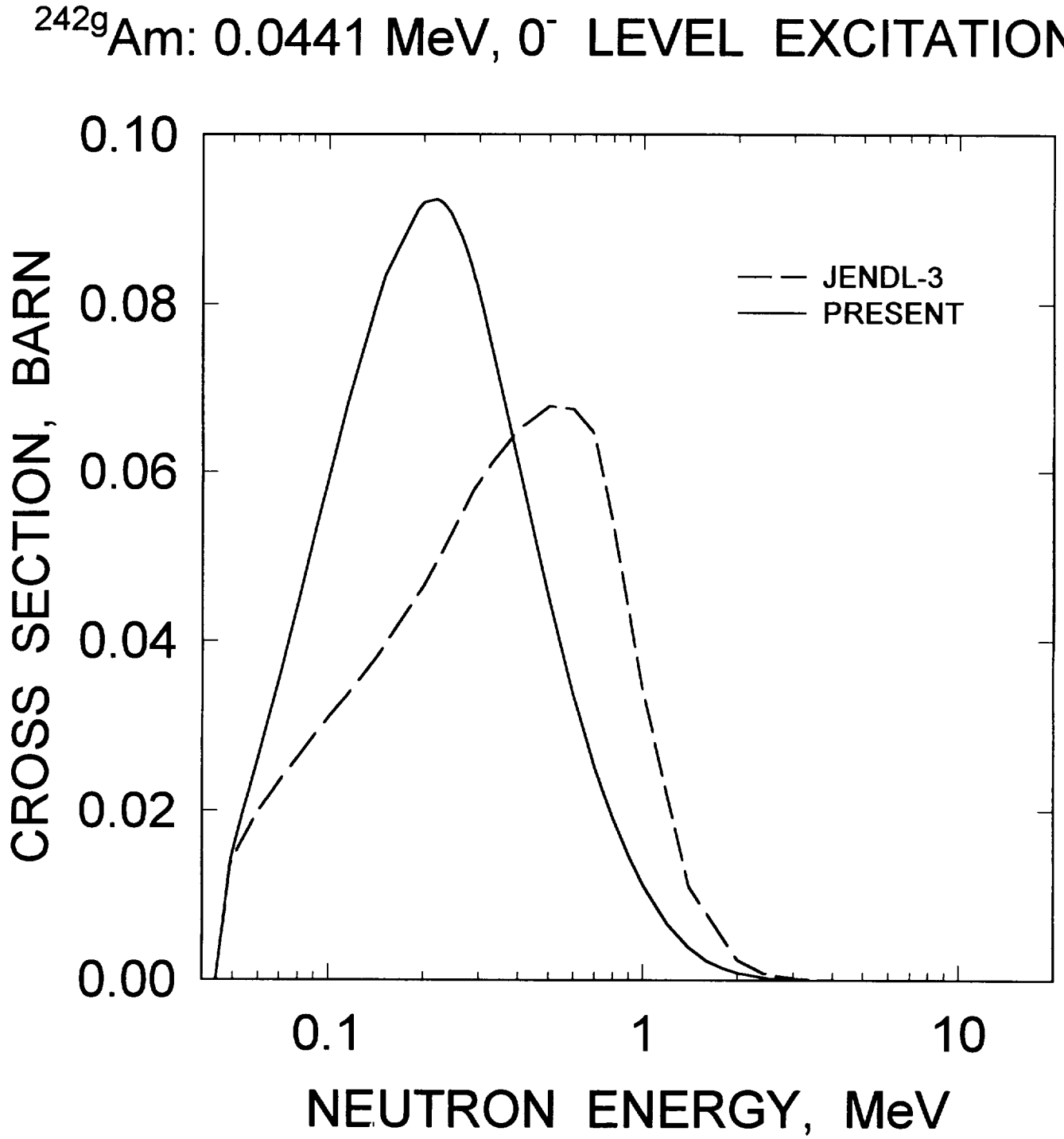
^{242g}Am: 0.0441 MeV, 0$^-$ LEVEL EXCITATION
CROSS SECTION, BARN
0.10
0.08
0.06
0.04
0.02
0.00
JENDL-3
PRESENT
0.1
1
10
NEUTRON ENERGY, MeV

FIG. 4.13

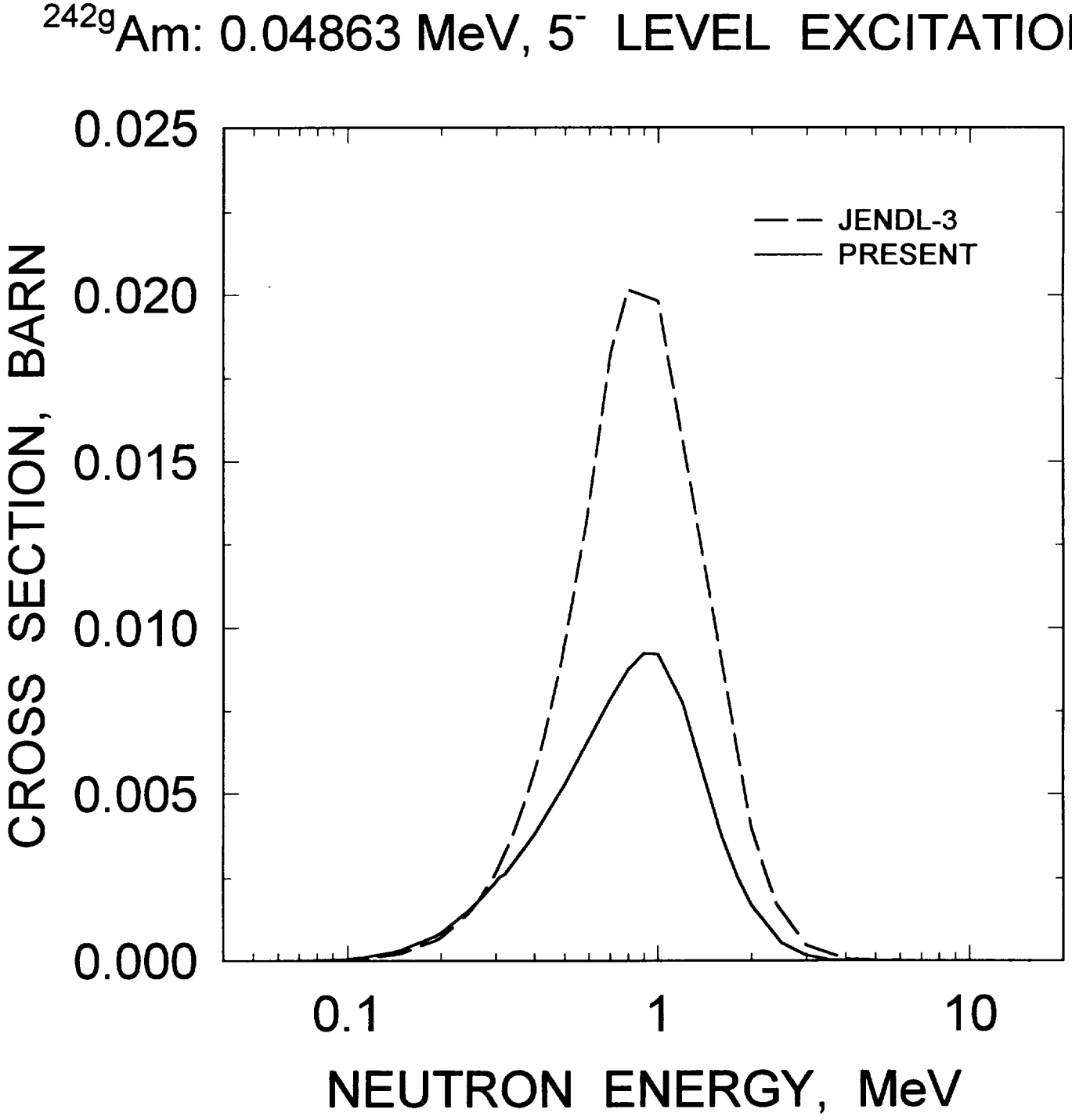
^{242g}Am: 0.04863 MeV, 5$^-$ LEVEL EXCITATION
0.025
0.020
0.015
0.010
0.005
0.000
CROSS SECTION, BARN
JENDL-3
PRESENT
0.1
1
10
NEUTRON ENERGY, MeV

FIG. 4.14

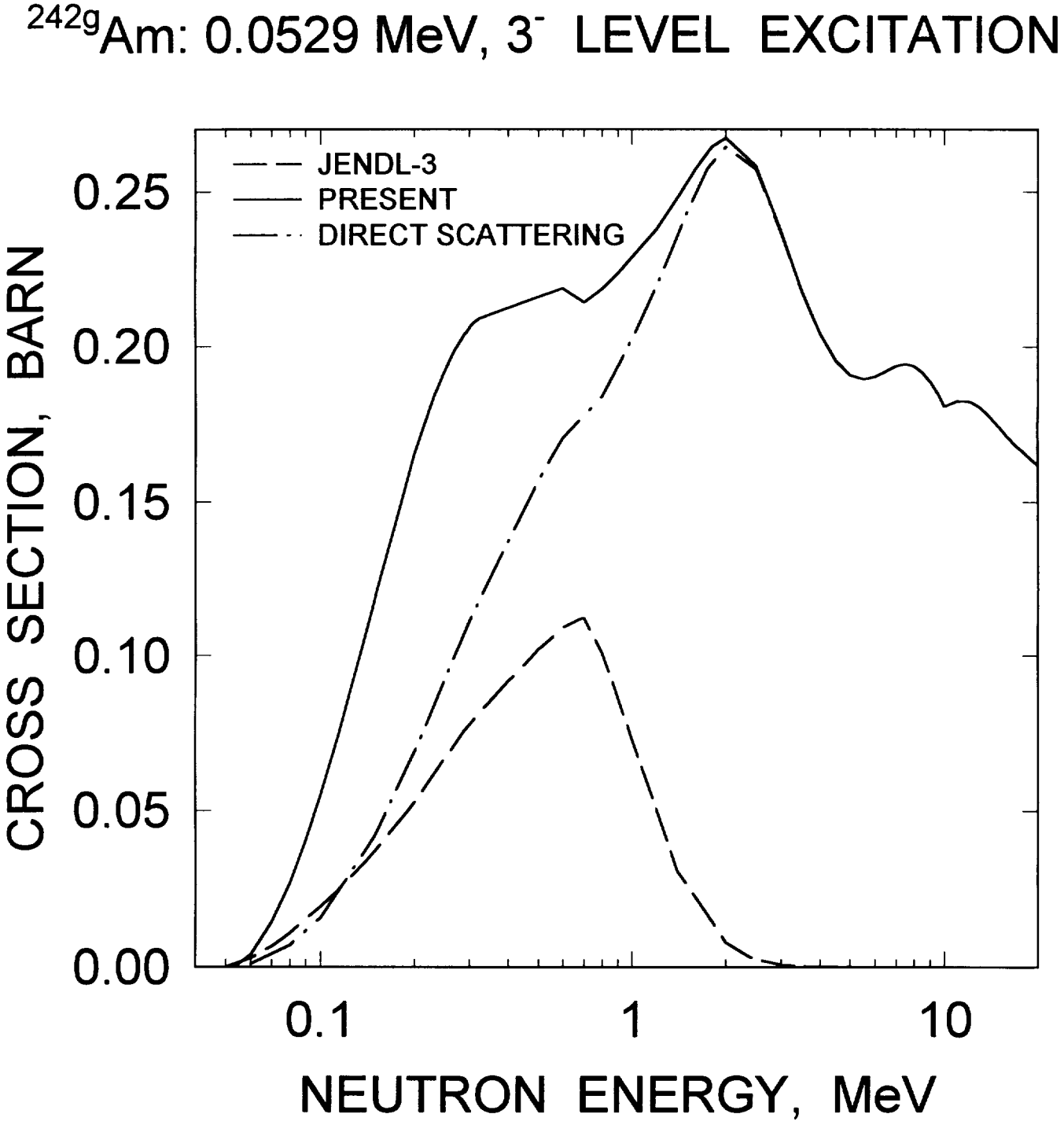
^{242g}Am: 0.0529 MeV, 3$^-$ LEVEL EXCITATION
JENDL-3
PRESENT
DIRECT SCATTERING
CROSS SECTION, BARN
0.25
0.20
0.15
0.10
0.05
0.00
0.1
1
10
NEUTRON ENERGY, MeV

FIG. 4.15

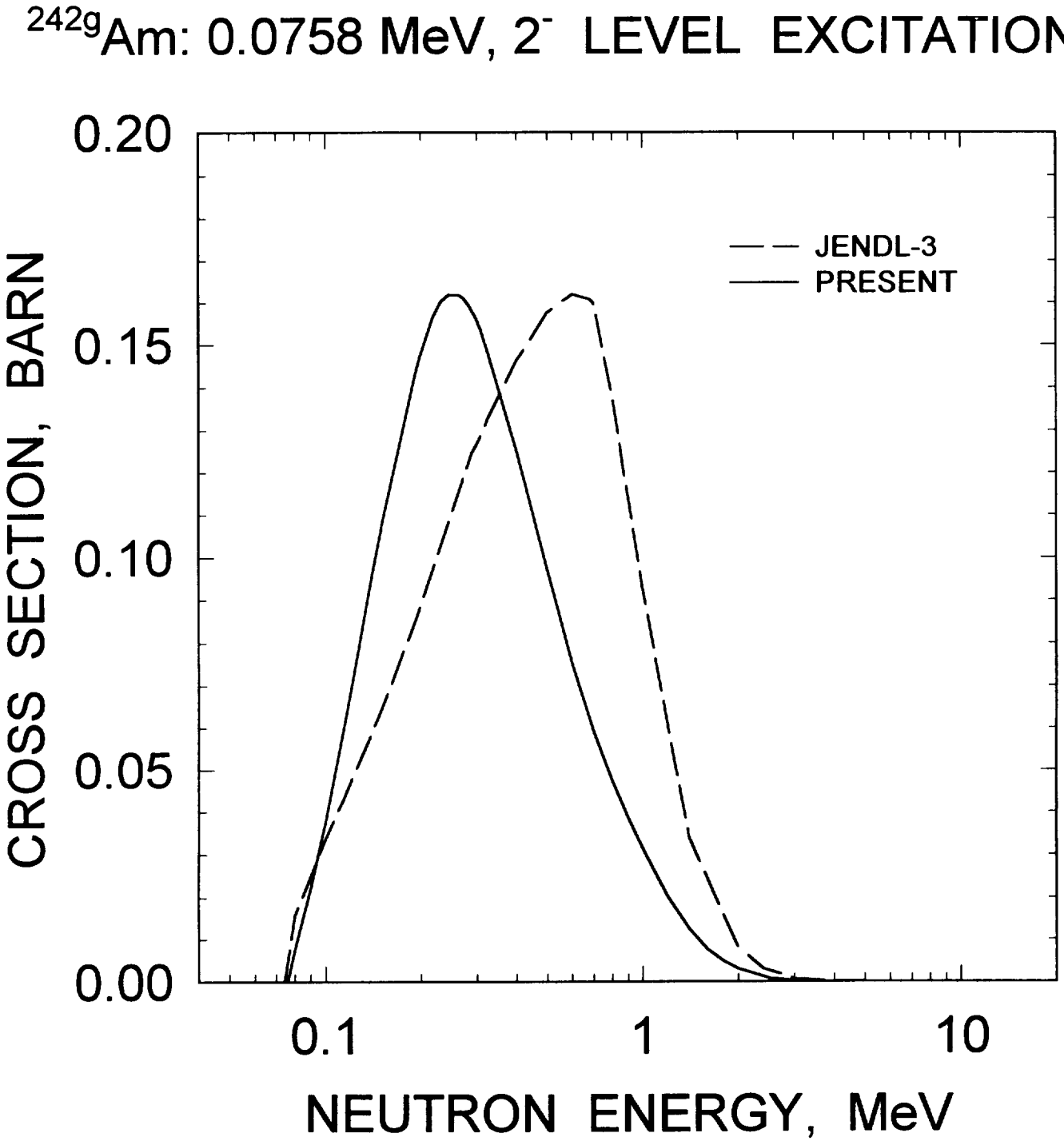
^{242g}Am: 0.0758 MeV, 2$^-$ LEVEL EXCITATION
0.20
0.15
0.10
0.05
0.00
CROSS SECTION, BARN
JENDL-3
PRESENT
0.1
1
10
NEUTRON ENERGY, MeV

FIG. 4.16

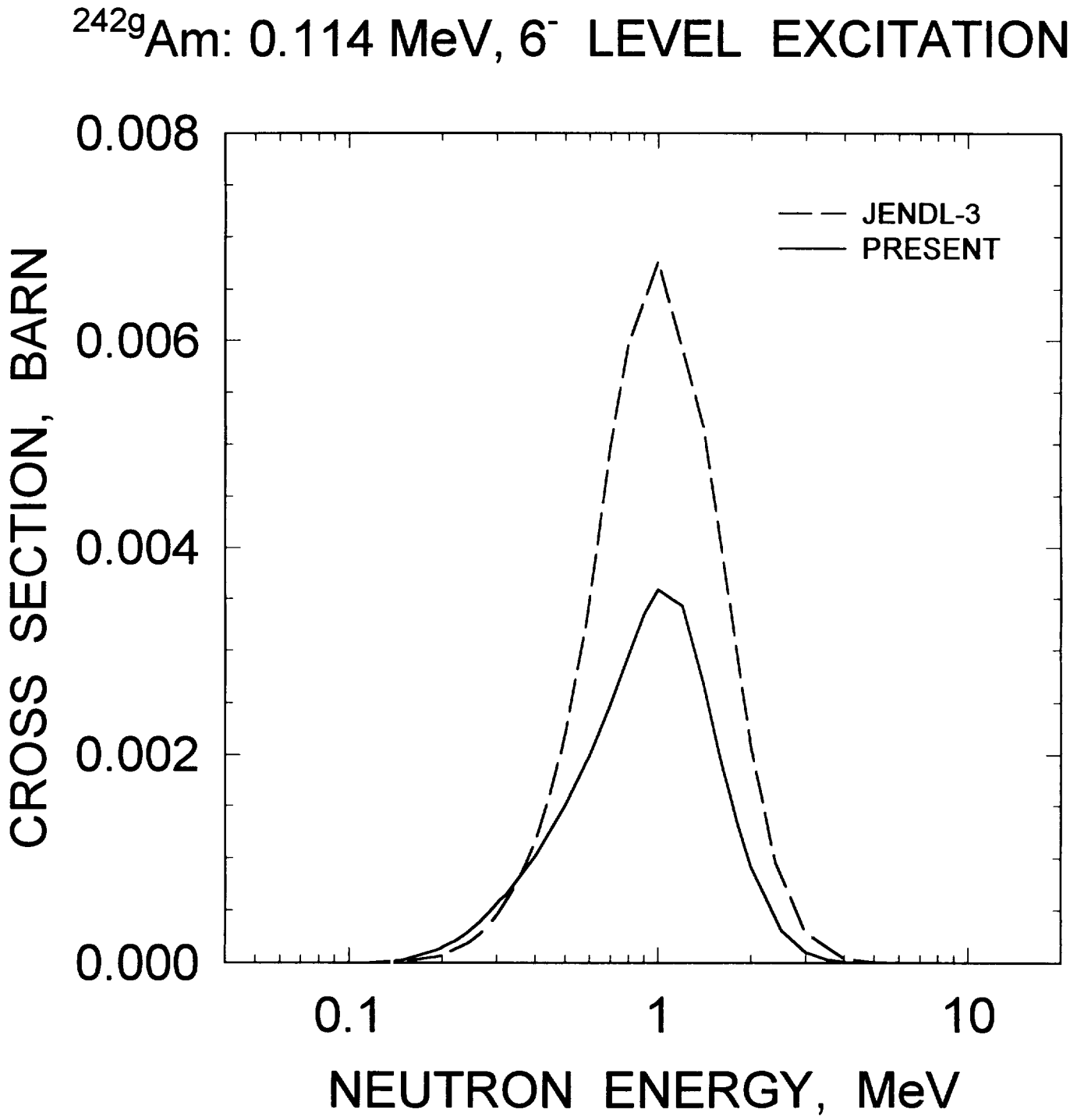
^{242g}Am: 0.114 MeV, 6$^-$ LEVEL EXCITATION
0.008
0.006
0.004
0.002
0.000
CROSS SECTION, BARN
JENDL-3
PRESENT
0.1
1
10
NEUTRON ENERGY, MeV

FIG. 4.17

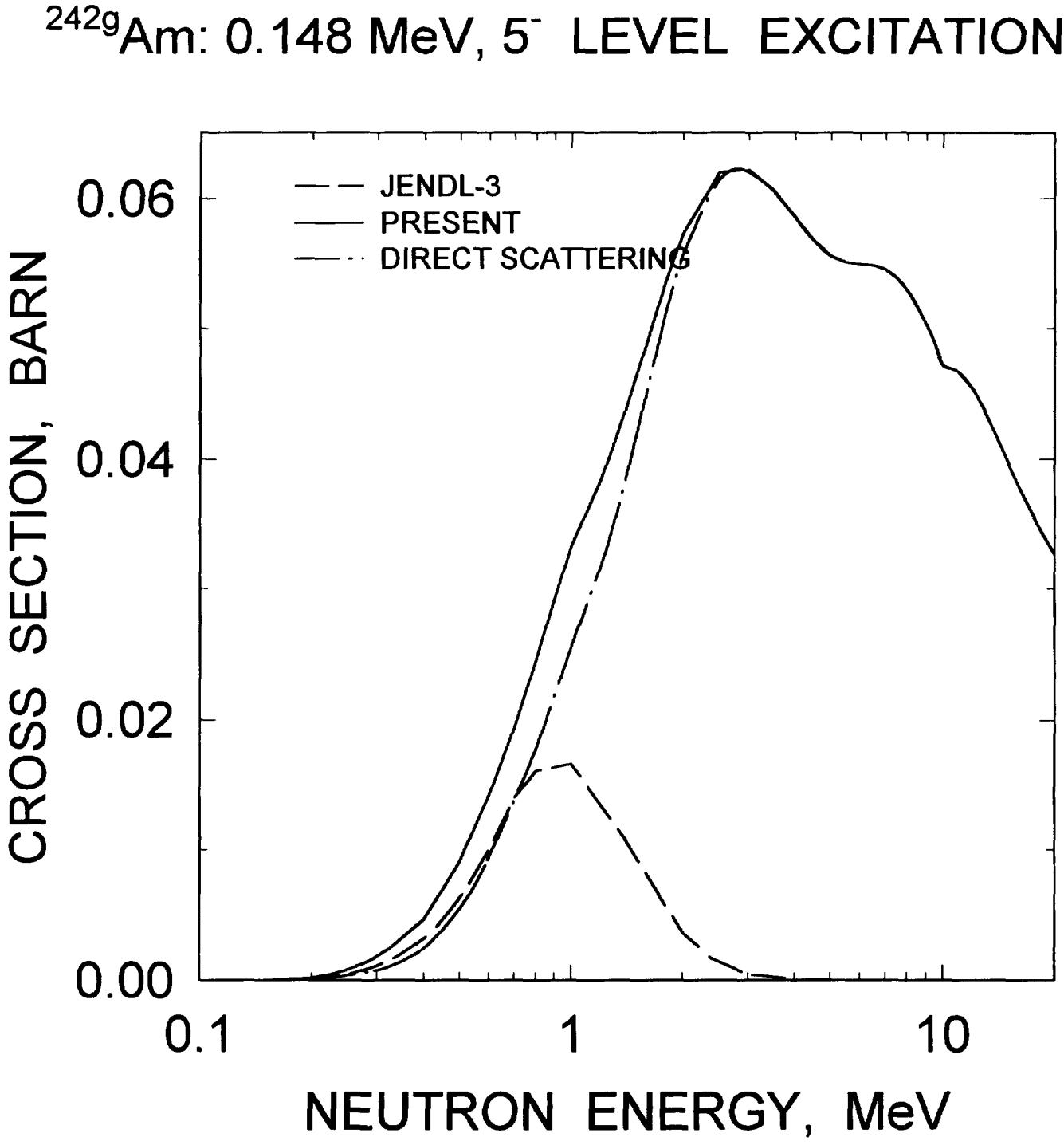
^{242g}Am: 0.148 MeV, 5$^-$ LEVEL EXCITATION
JENDL-3
PRESENT
DIRECT SCATTERING
CROSS SECTION, BARN
0.06
0.04
0.02
0.00
0.1
1
10
NEUTRON ENERGY, MeV

FIG. 4.18

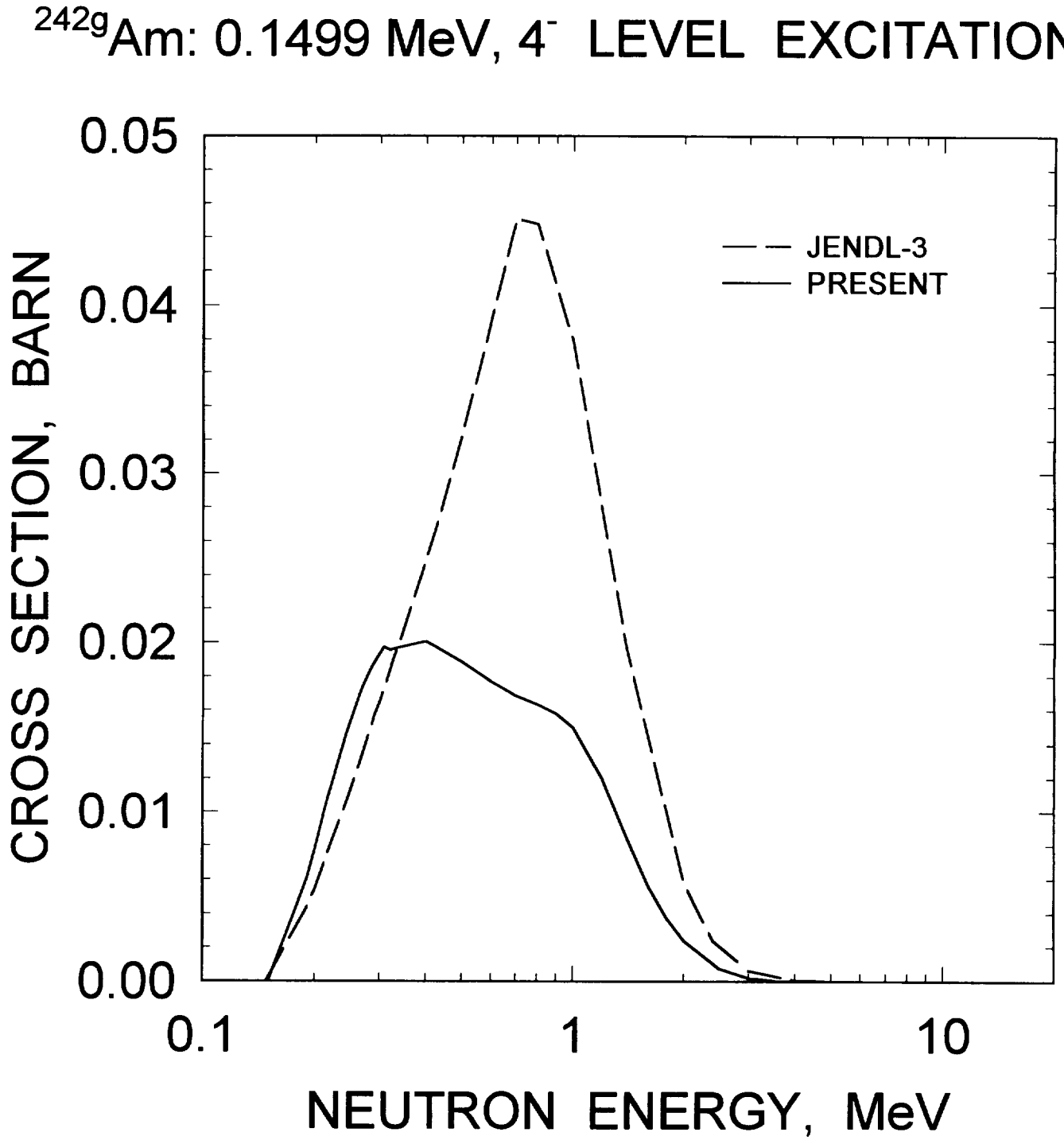
^{242g}Am: 0.1499 MeV, 4$^-$ LEVEL EXCITATION
CROSS SECTION, BARN
0.05
0.04
0.03
0.02
0.01
0.00
JENDL-3
PRESENT
0.1
1
10
NEUTRON ENERGY, MeV

FIG. 4.19

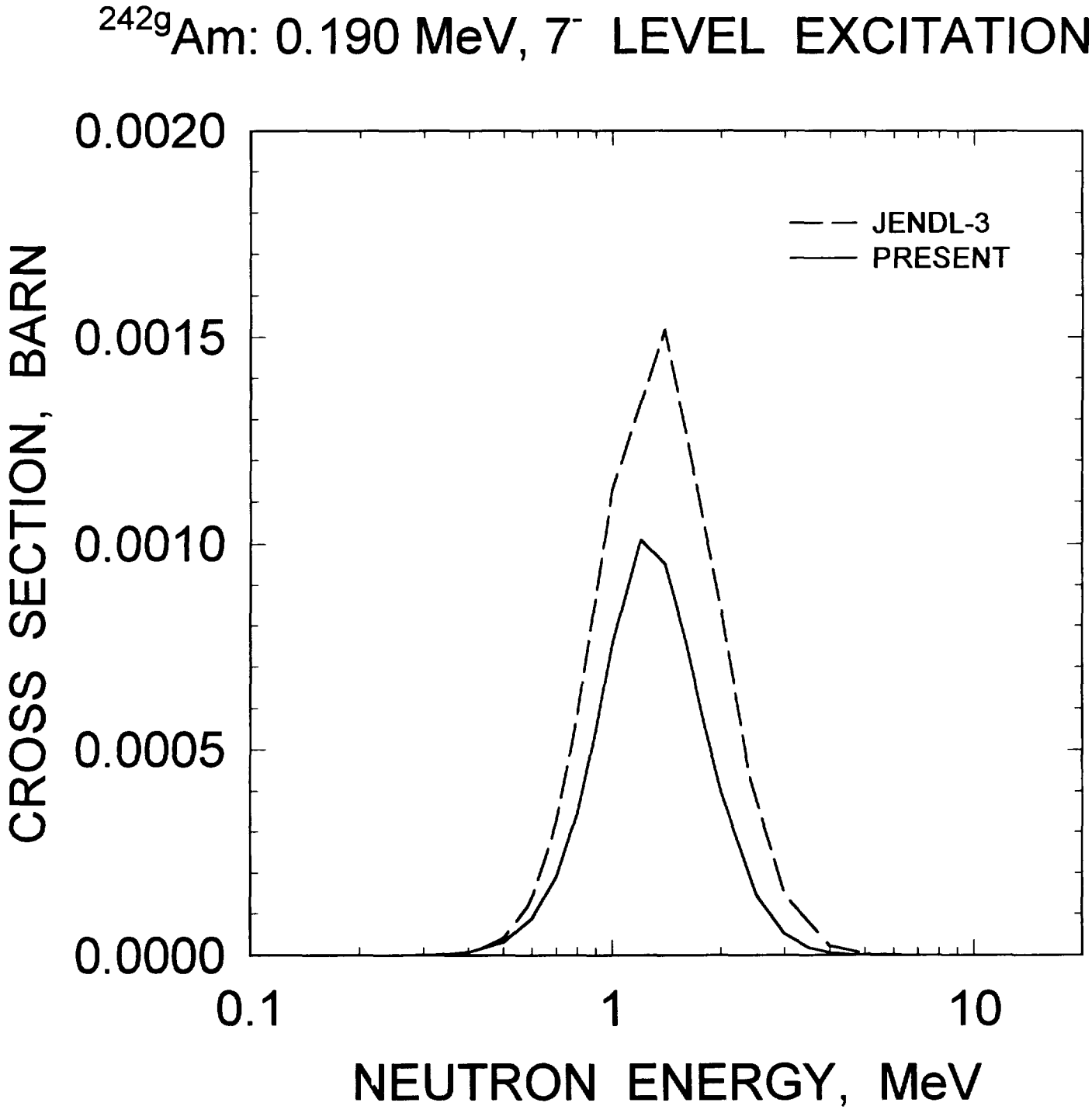
^{242g}Am: 0.190 MeV, 7$^-$ LEVEL EXCITATION
0.0020
0.0015
0.0010
0.0005
0.0000
CROSS SECTION, BARN
JENDL-3
PRESENT
0.1
1
10
NEUTRON ENERGY, MeV

FIG. 4.20

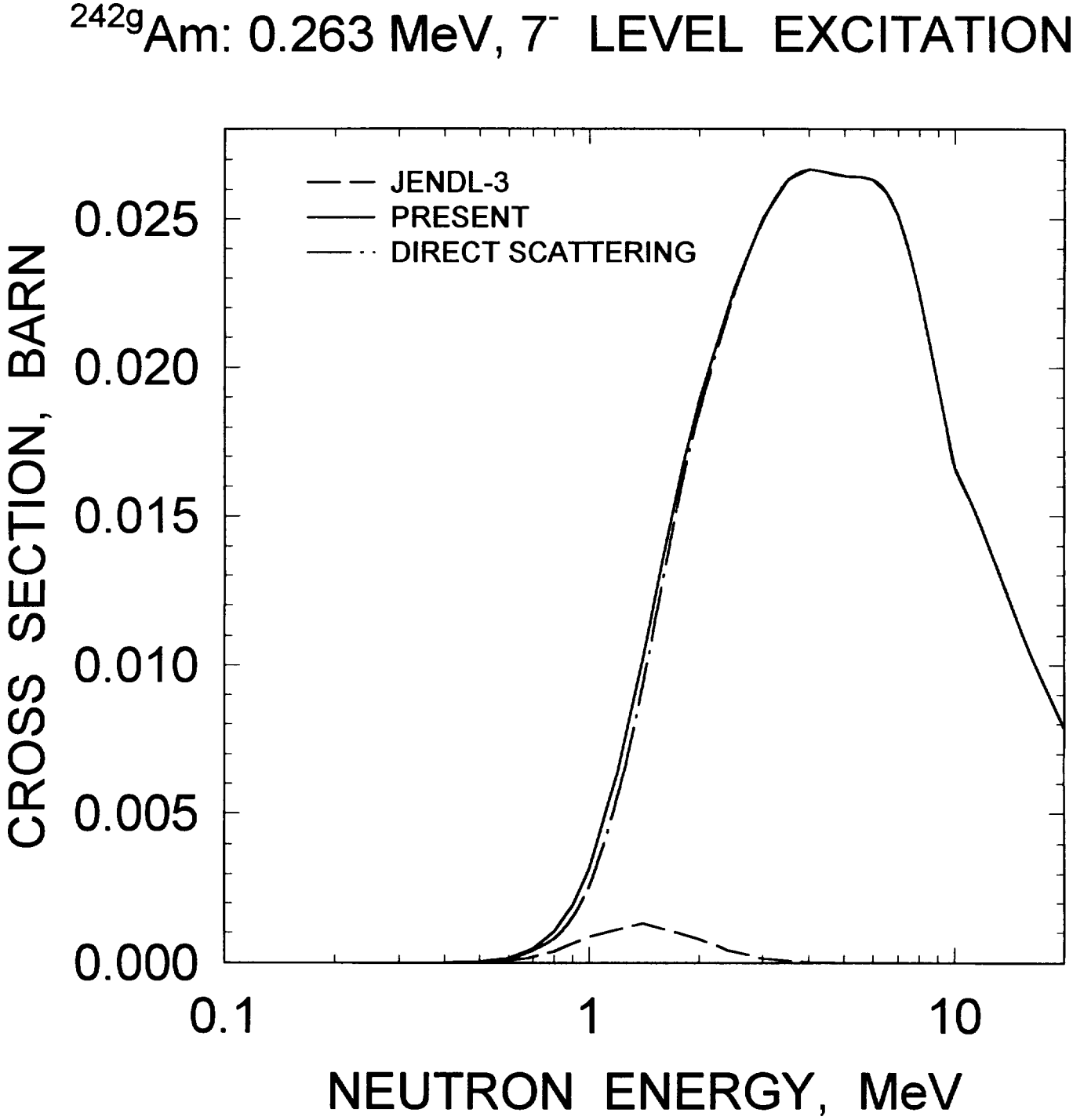
^{242g}Am: 0.263 MeV, 7$^-$ LEVEL EXCITATION
JENDL-3
PRESENT
DIRECT SCATTERING
CROSS SECTION, BARN
0.025
0.020
0.015
0.010
0.005
0.000
0.1
1
10
NEUTRON ENERGY, MeV

FIG. 4.21

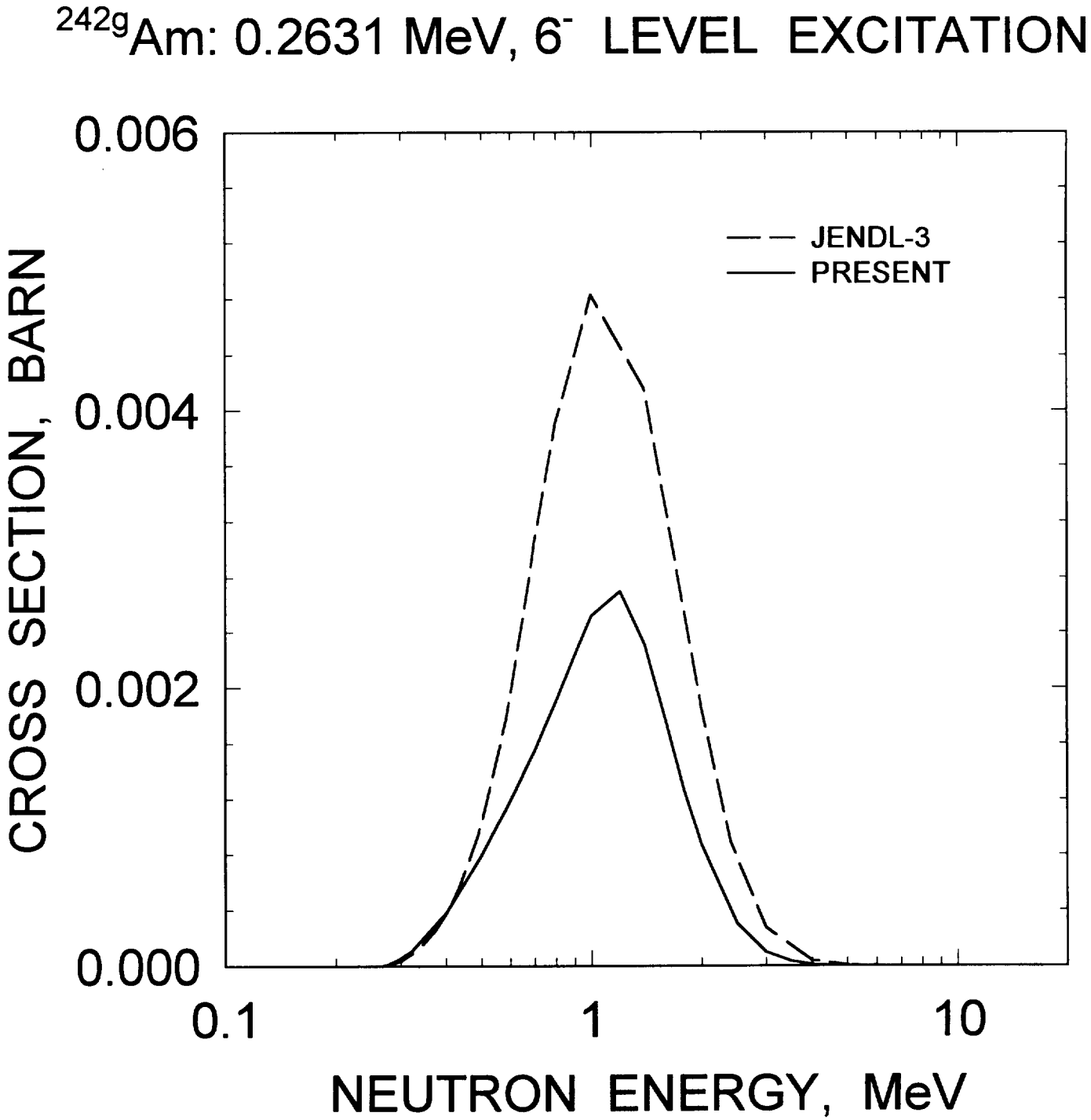
^{242g}Am: 0.2631 MeV, 6$^-$ LEVEL EXCITATION
0.006
0.004
0.002
0.000
CROSS SECTION, BARN
JENDL-3
PRESENT
0.1
1
10
NEUTRON ENERGY, MeV

FIG. 4.22

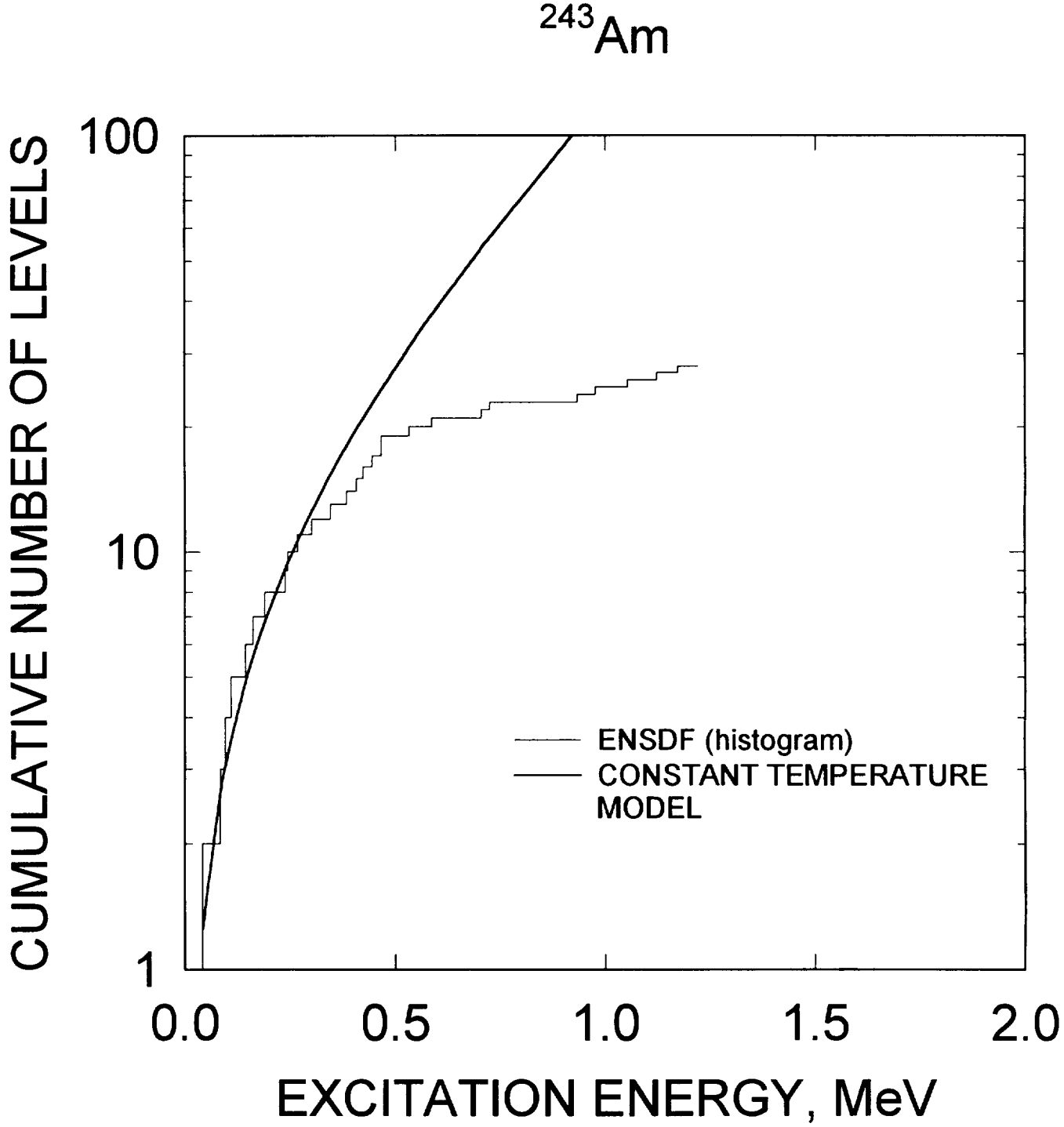
^{243}Am
CUMULATIVE NUMBER OF LEVELS
100
10
1
0.0
0.5
1.0
1.5
2.0
EXCITATION ENERGY, MeV
ENSDF (histogram)
CONSTANT TEMPERATURE MODEL

FIG. 4.23

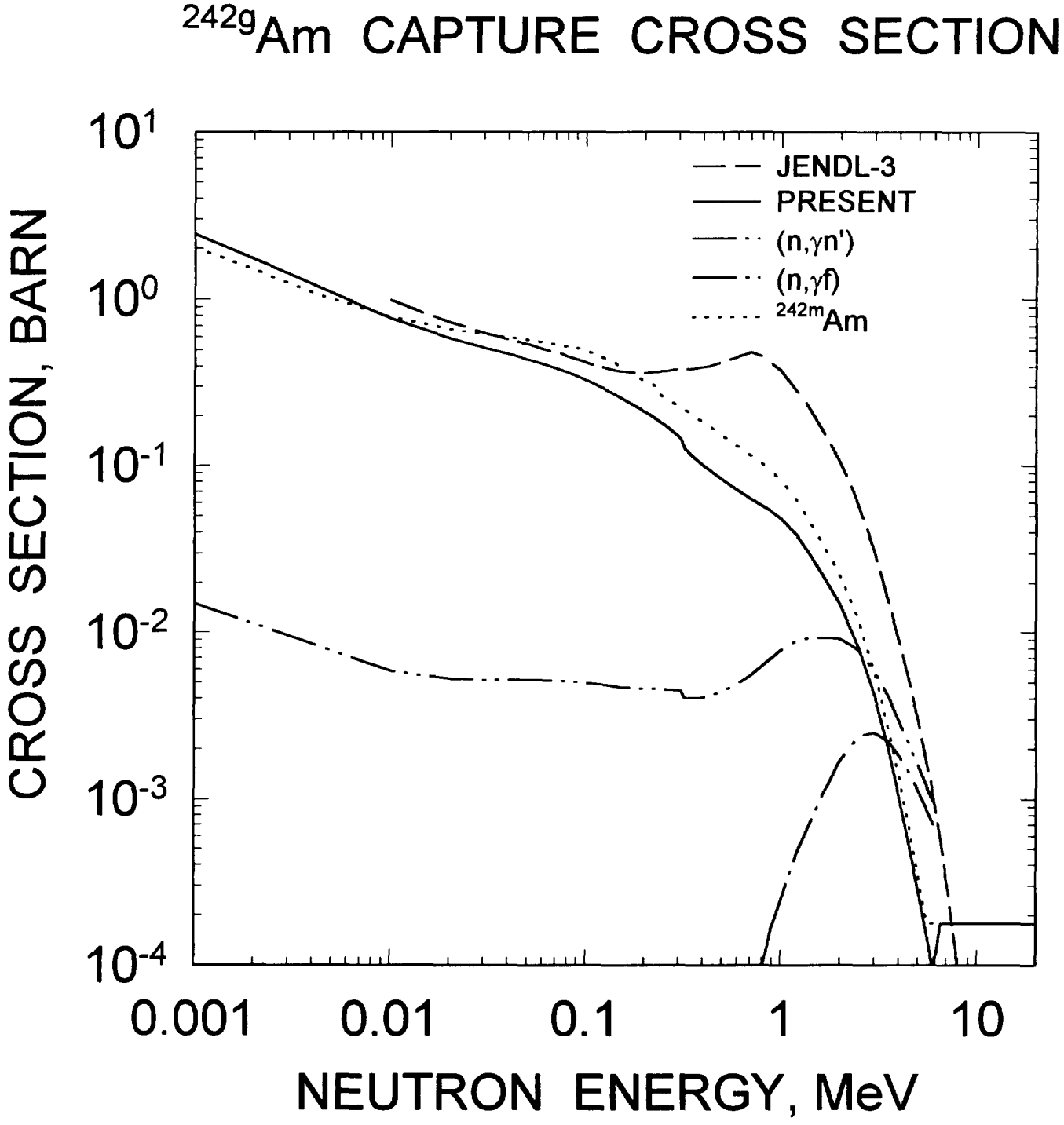
^{242g}Am CAPTURE CROSS SECTION
CROSS SECTION, BARN
10^{1}
10^{0}
10^{-1}
10^{-2}
10^{-3}
10^{-4}
0.001
0.01
0.1
1
10
NEUTRON ENERGY, MeV
JENDL-3
PRESENT
(n,γn')
(n,γf)
^{242m}Am

FIG.4.24

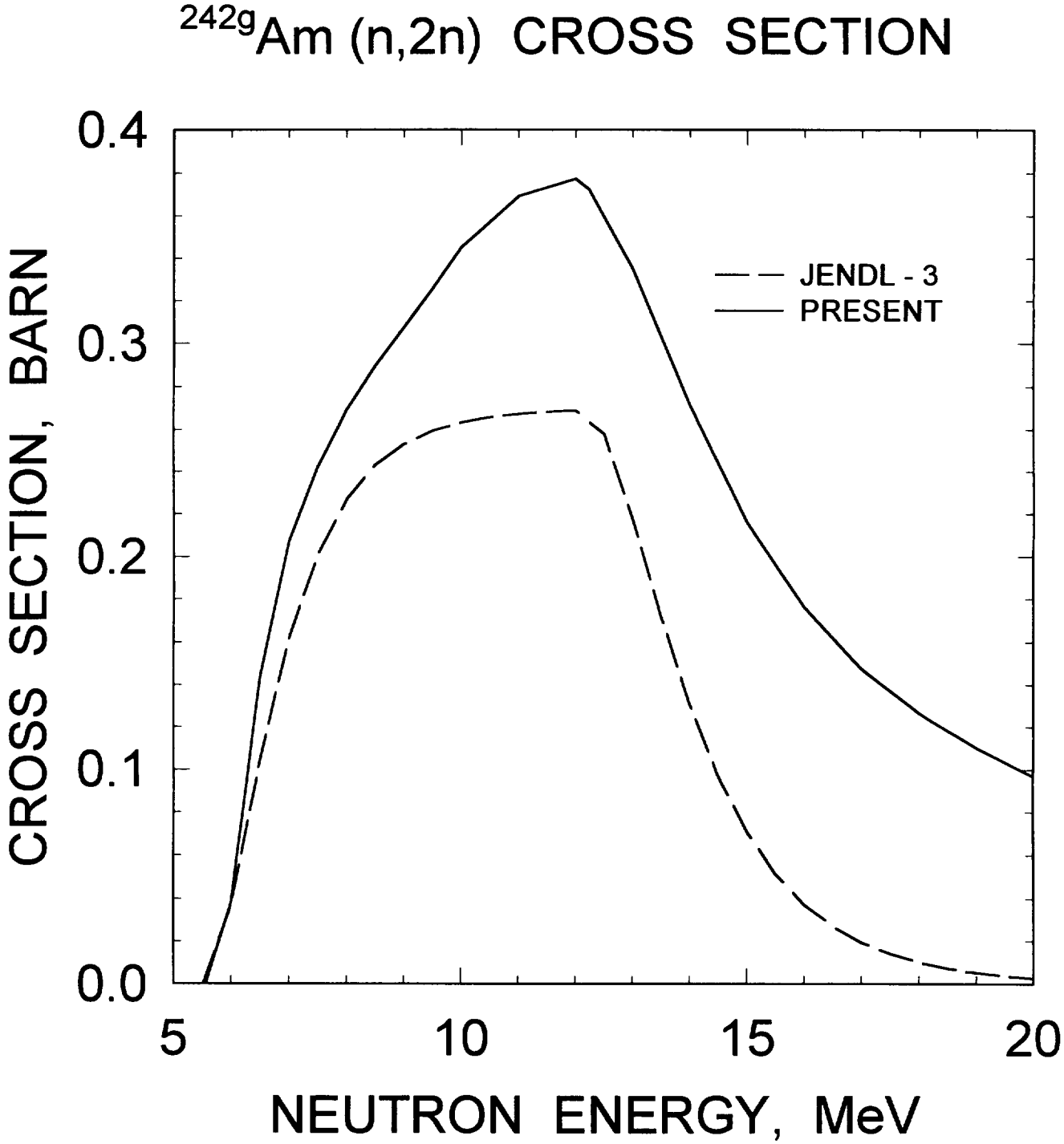
^{242g}Am (n,2n) CROSS SECTION
CROSS SECTION, BARN
0.0
0.1
0.2
0.3
0.4
5
10
15
20
NEUTRON ENERGY, MeV
JENDL - 3
PRESENT

FIG. 4.25

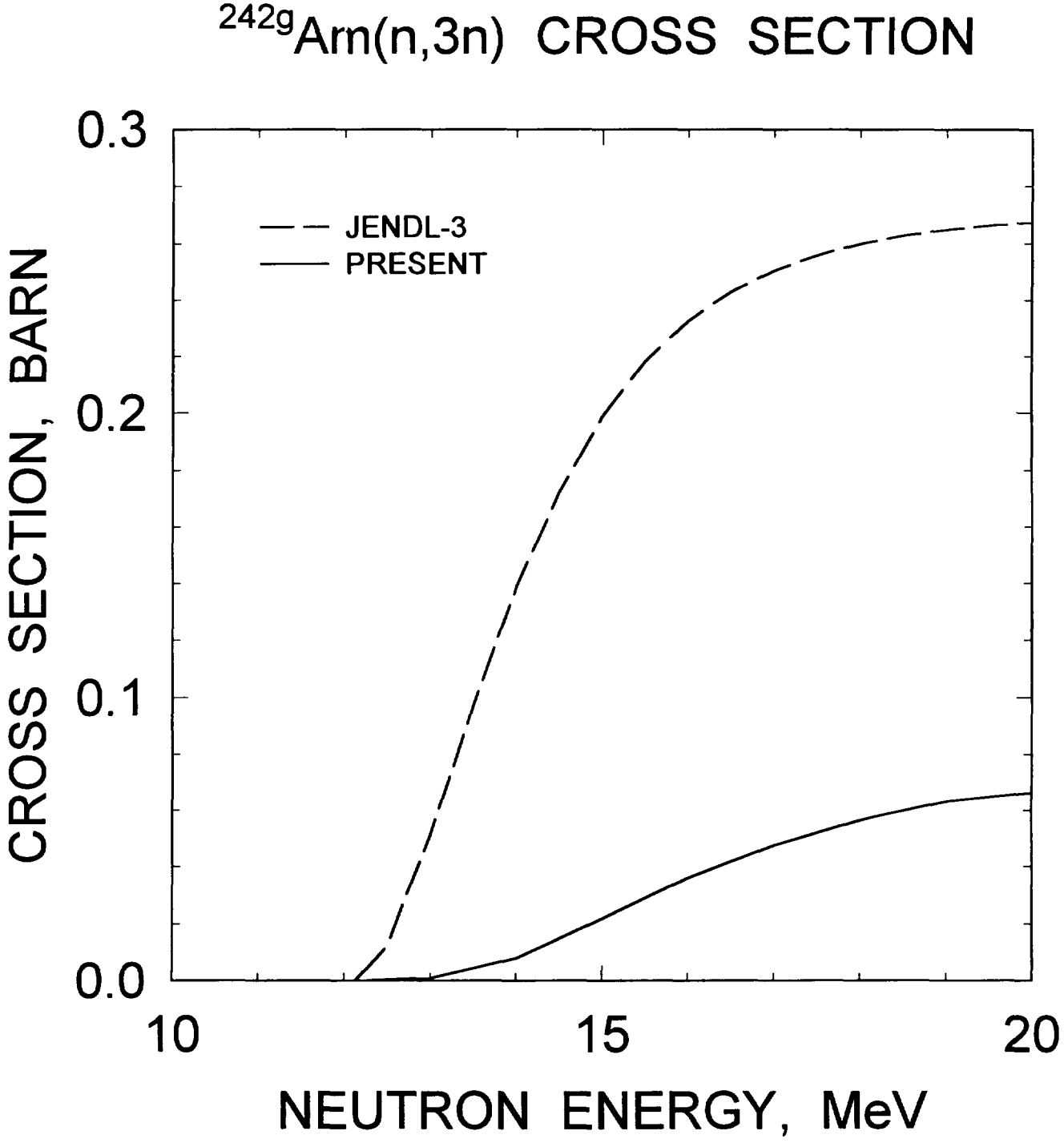
242gArn(n,3n) CROSS SECTION
JENDL-3
PRESENT
CROSS SECTION, BARN
0.3
0.2
0.1
0.0
10
15
20
NEUTRON ENERGY, MeV

FIG. 4.26

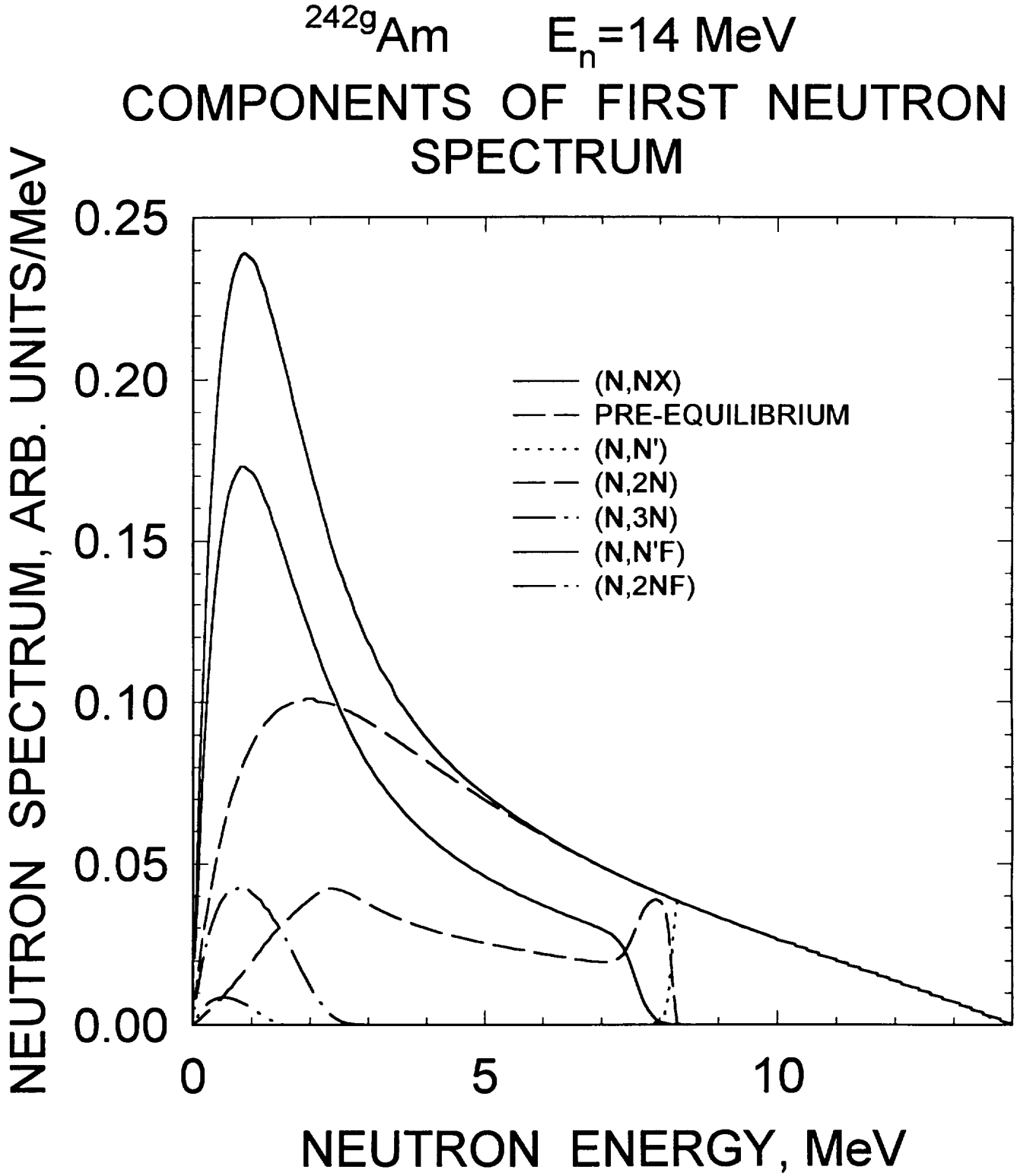
^{242g}Am E_n=14 MeV
COMPONENTS OF FIRST NEUTRON SPECTRUM
NEUTRON SPECTRUM, ARB. UNITS/MeV
0.25
0.20
0.15
0.10
0.05
0.00
0
5
10
NEUTRON ENERGY, MeV
(N,NX)
PRE-EQUILIBRIUM
(N,N')
(N,2N)
(N,3N)
(N,N'F)
(N,2NF)

FIG.5.1

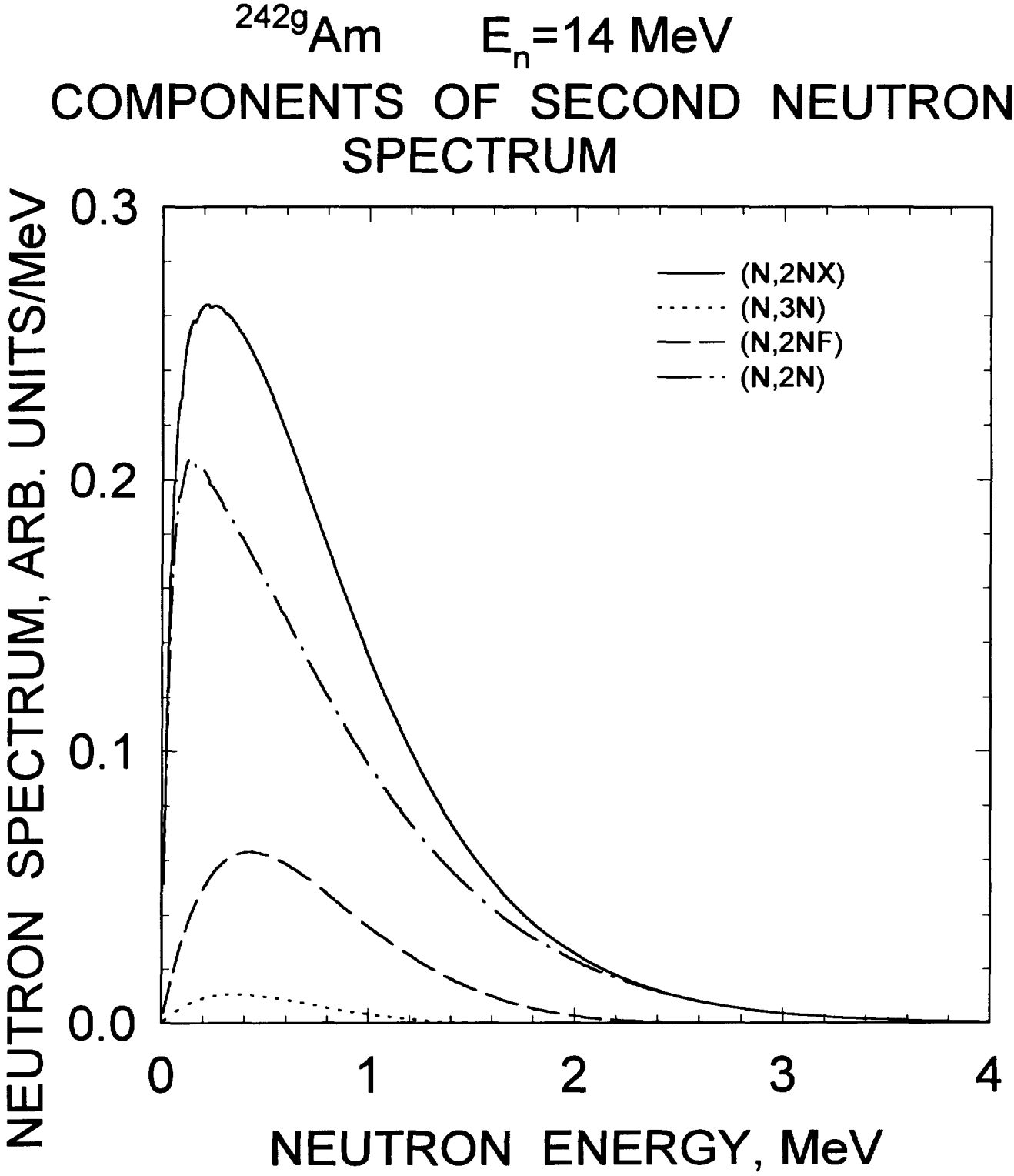
^{242g}Am E_n=14 MeV
COMPONENTS OF SECOND NEUTRON SPECTRUM
NEUTRON SPECTRUM, ARB. UNITS/MeV
0.3
0.2
0.1
0.0
0
1
2
3
4
NEUTRON ENERGY, MeV
(N,2NX)
(N,3N)
(N,2NF)
(N,2N)

FIG.5.2

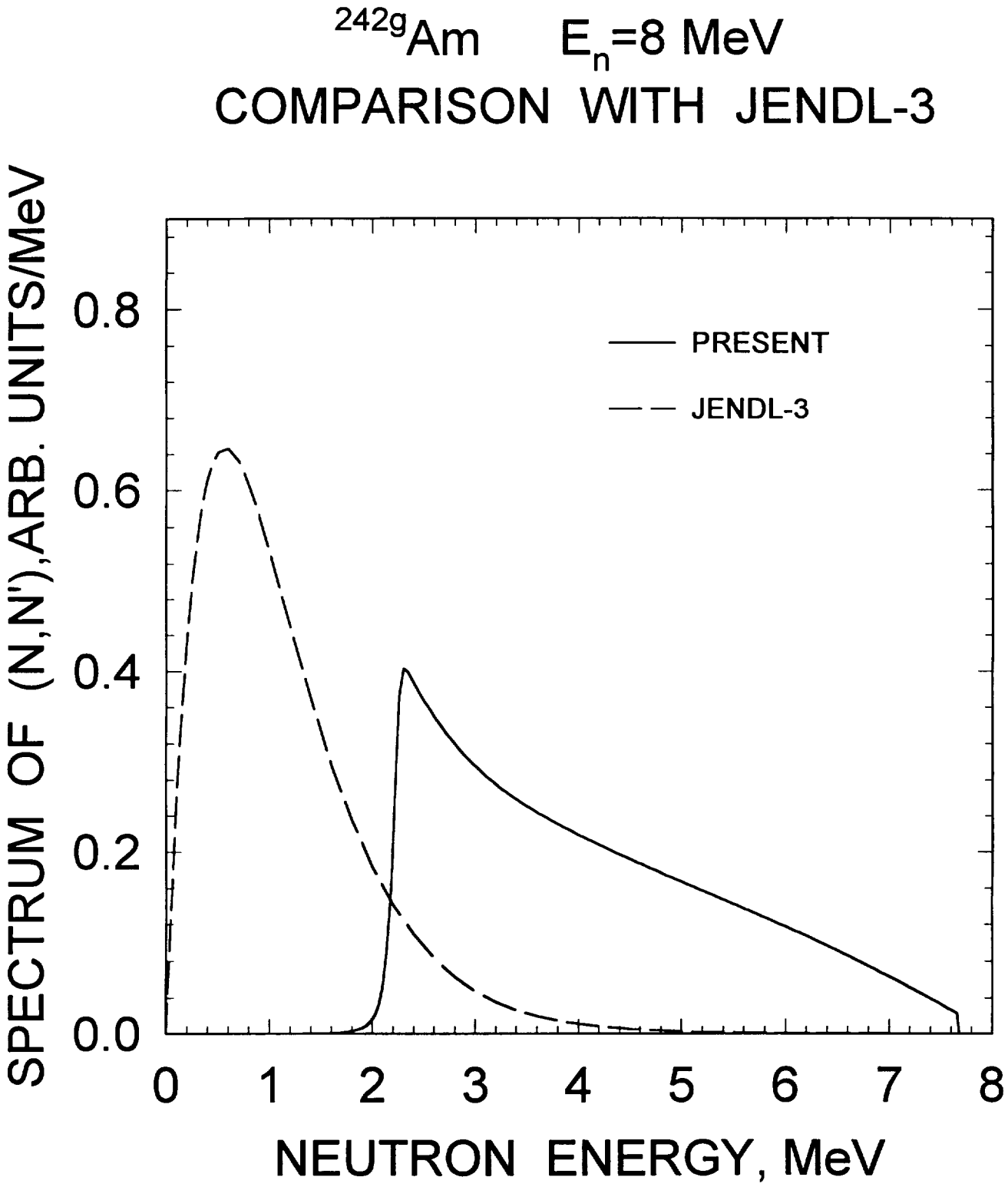
^{242g}Am E_n=8 MeV
COMPARISON WITH JENDL-3
SPECTRUM OF (N,N'),ARB. UNITS/MeV
0.0
0.2
0.4
0.6
0.8
PRESENT
JENDL-3
0
1
2
3
4
5
6
7
8
NEUTRON ENERGY, MeV

FIG.5.3

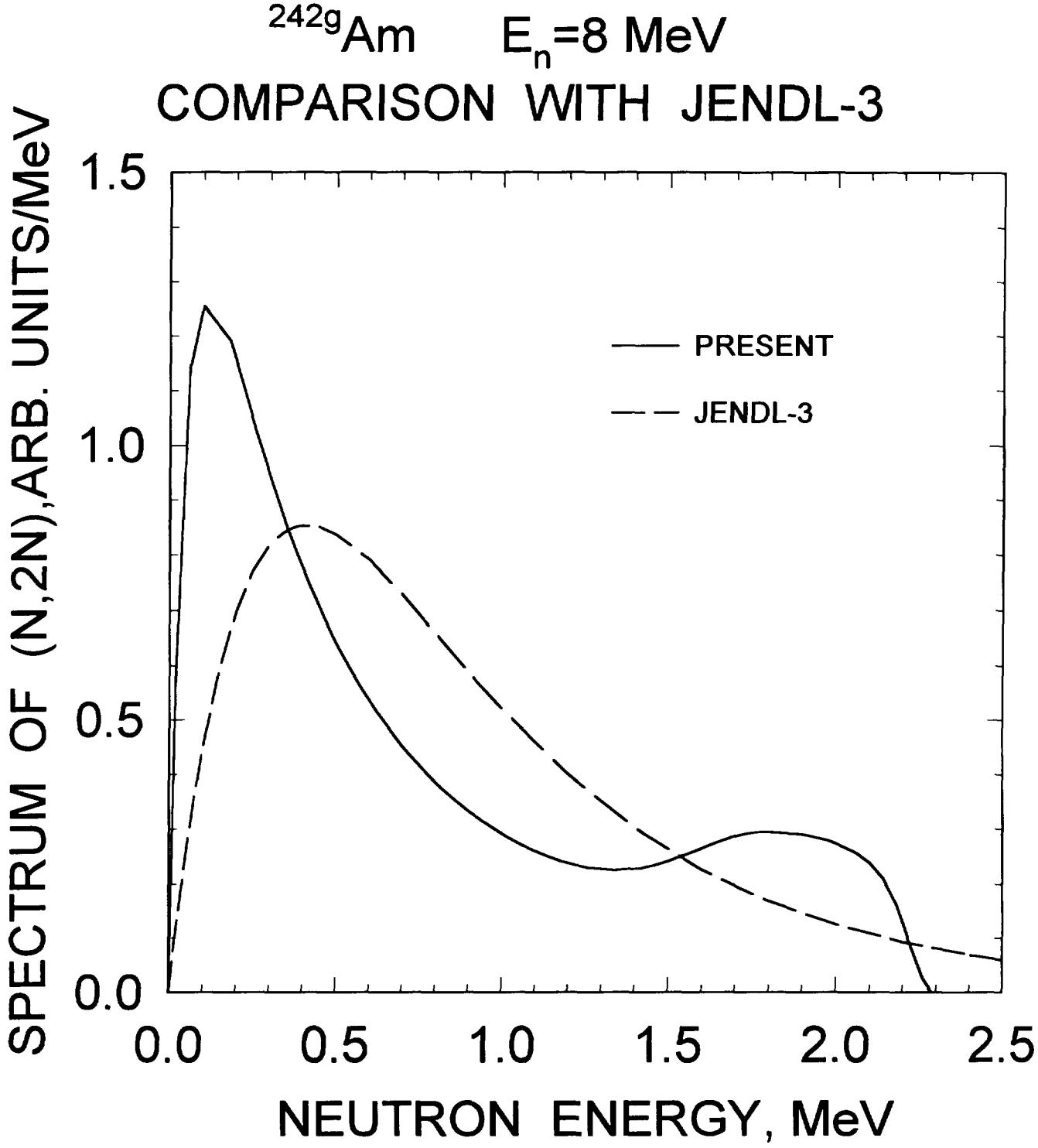
^{242g}Am E_n=8 MeV
COMPARISON WITH JENDL-3
SPECTRUM OF (N,2N),ARB. UNITS/MeV
1.5
1.0
0.5
0.0
PRESENT
JENDL-3
0.0
0.5
1.0
1.5
2.0
2.5
NEUTRON ENERGY, MeV

FIG.5.4

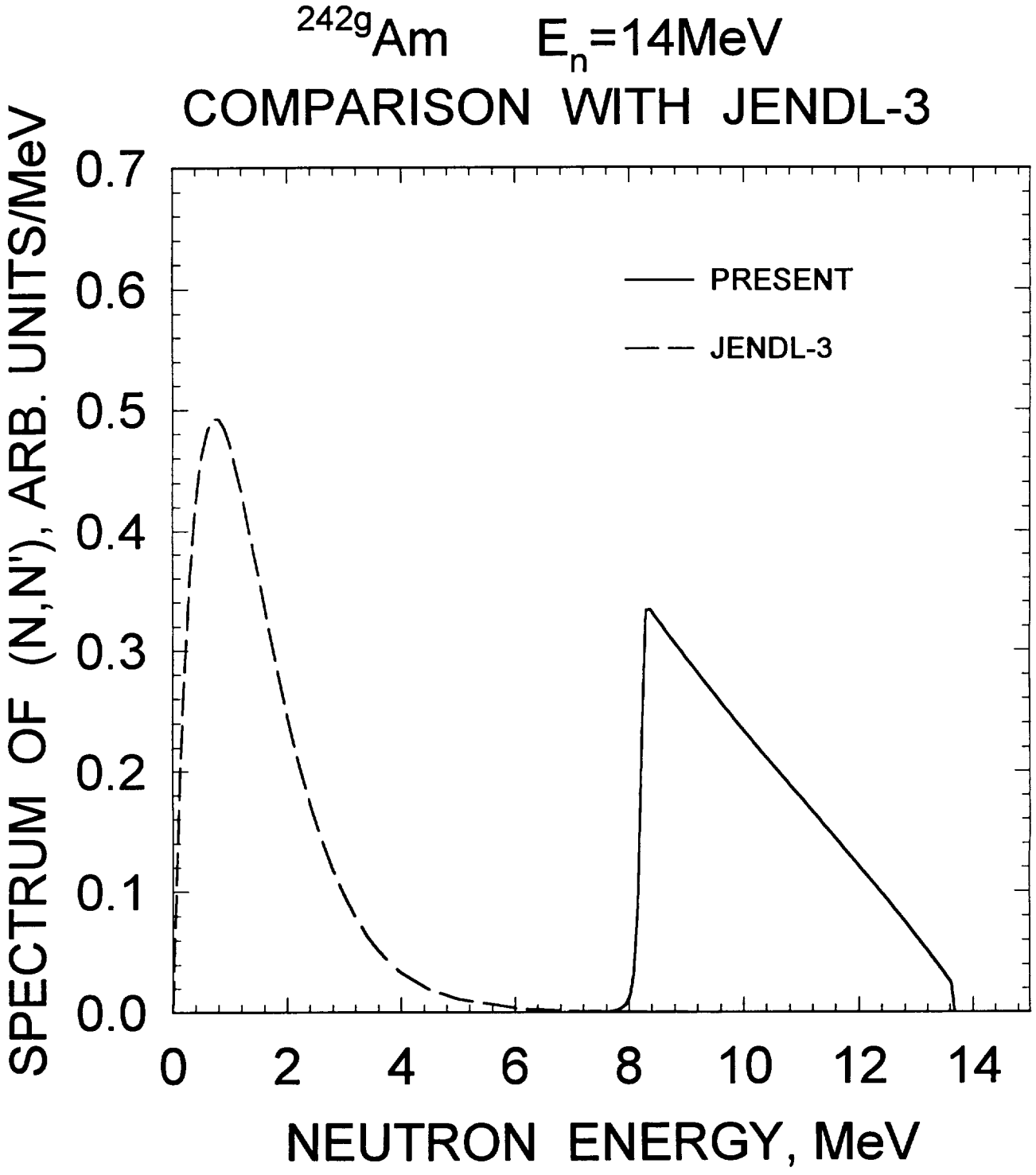
^{242g}Am E_n=14MeV
COMPARISON WITH JENDL-3
SPECTRUM OF (N,N'), ARB. UNITS/MeV
0.7
0.6
0.5
0.4
0.3
0.2
0.1
0.0
PRESENT
JENDL-3
0
2
4
6
8
10
12
14
NEUTRON ENERGY, MeV

FIG.5.5

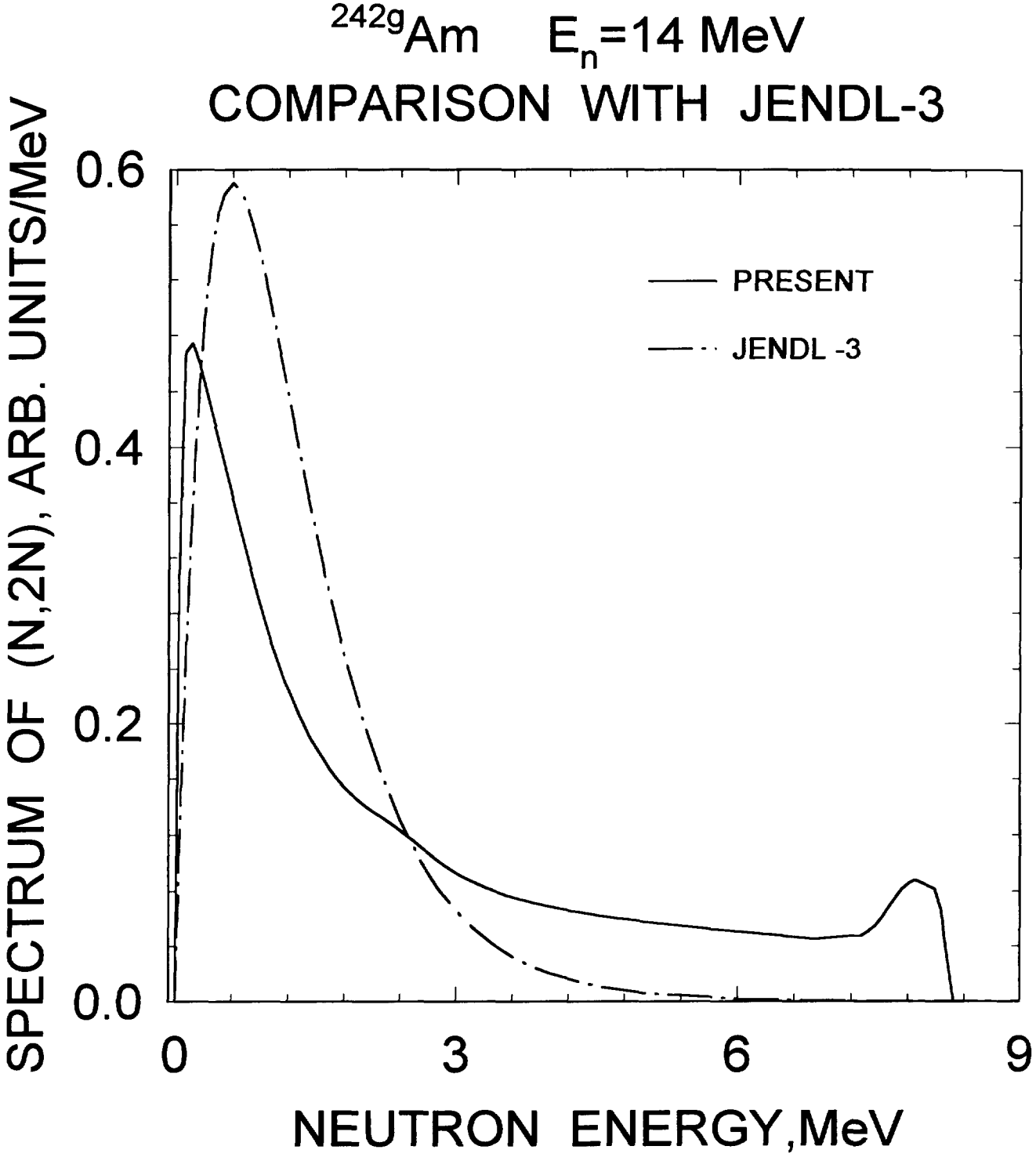
^{242g}Am E_n=14 MeV
COMPARISON WITH JENDL-3
SPECTRUM OF (N,2N), ARB. UNITS/MeV
0.6
0.4
0.2
0.0
0
3
6
9
NEUTRON ENERGY,MeV
PRESENT
JENDL -3

FIG.5.6

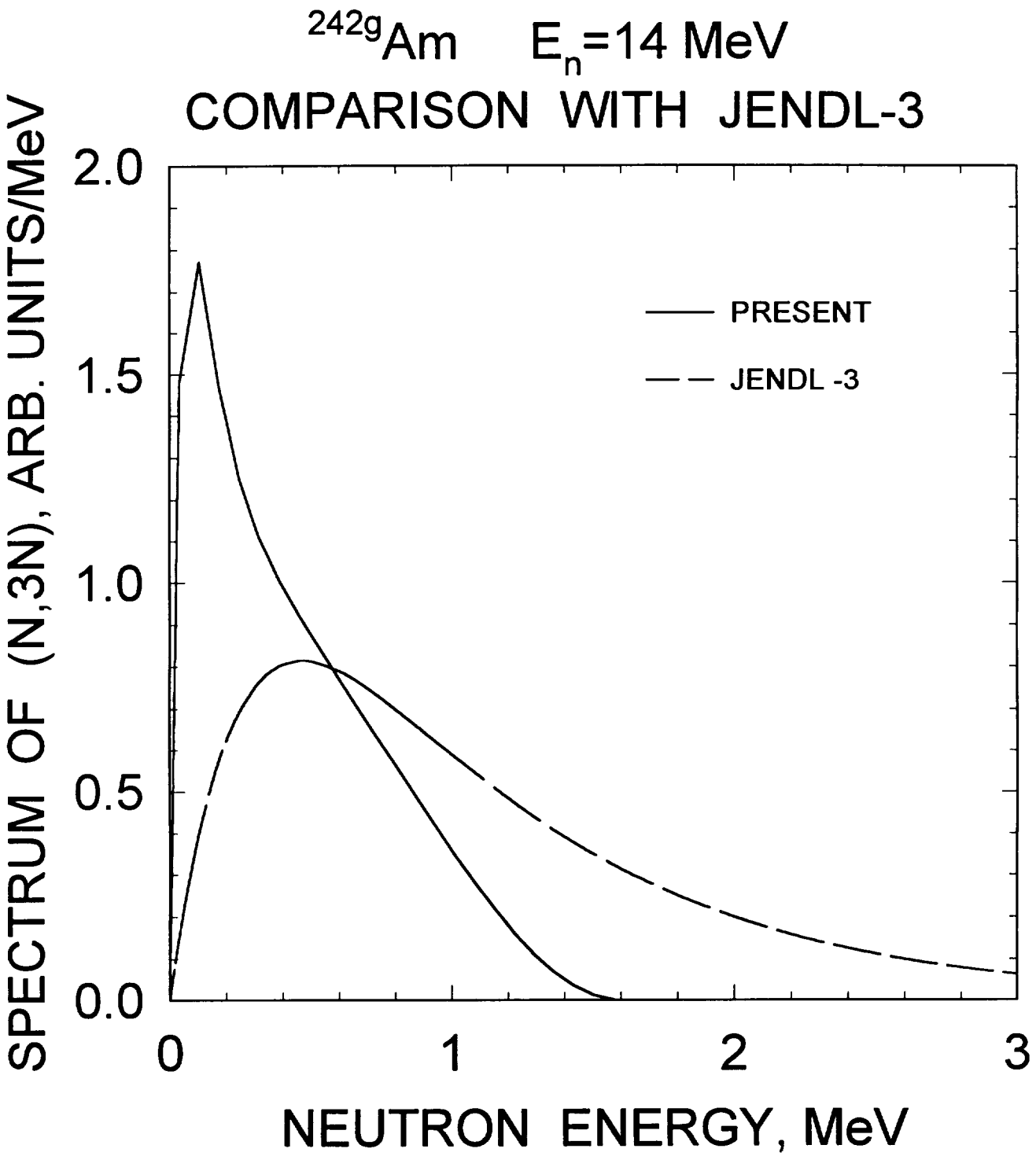
^{242g}Am E_n=14 MeV
COMPARISON WITH JENDL-3
SPECTRUM OF (N,3N), ARB. UNITS/MeV
2.0
1.5
1.0
0.5
0.0
0
1
2
3
NEUTRON ENERGY, MeV
PRESENT
JENDL -3

FIG.5.7

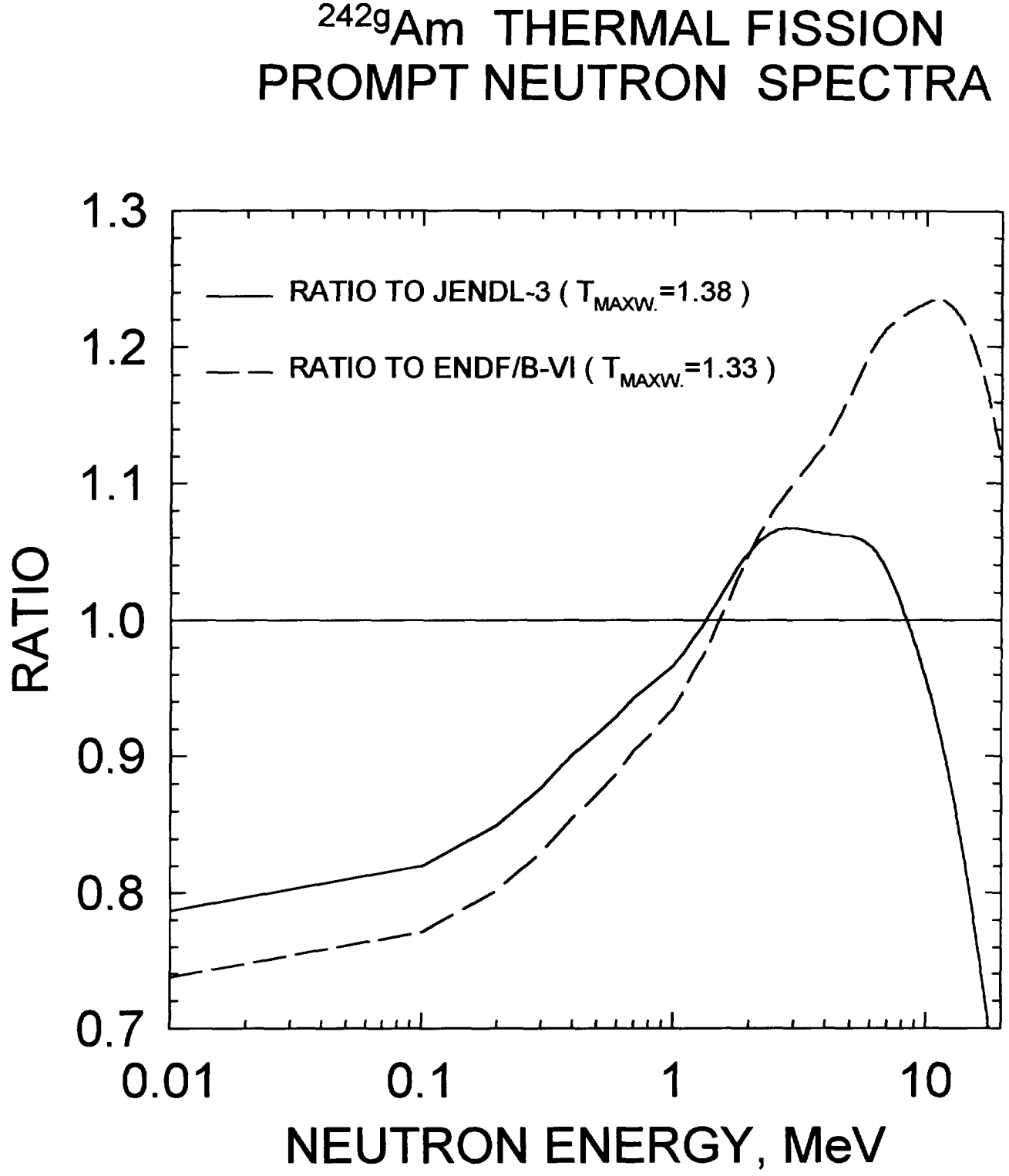
^{242g}Am THERMAL FISSION
PROMPT NEUTRON SPECTRA
RATIO TO JENDL-3 ($T_{MAXW.}$=1.38)
RATIO TO ENDF/B-VI ($T_{MAXW.}$=1.33)
RATIO
1.3
1.2
1.1
1.0
0.9
0.8
0.7
0.01
0.1
1
10
NEUTRON ENERGY, MeV

FIG.5.8

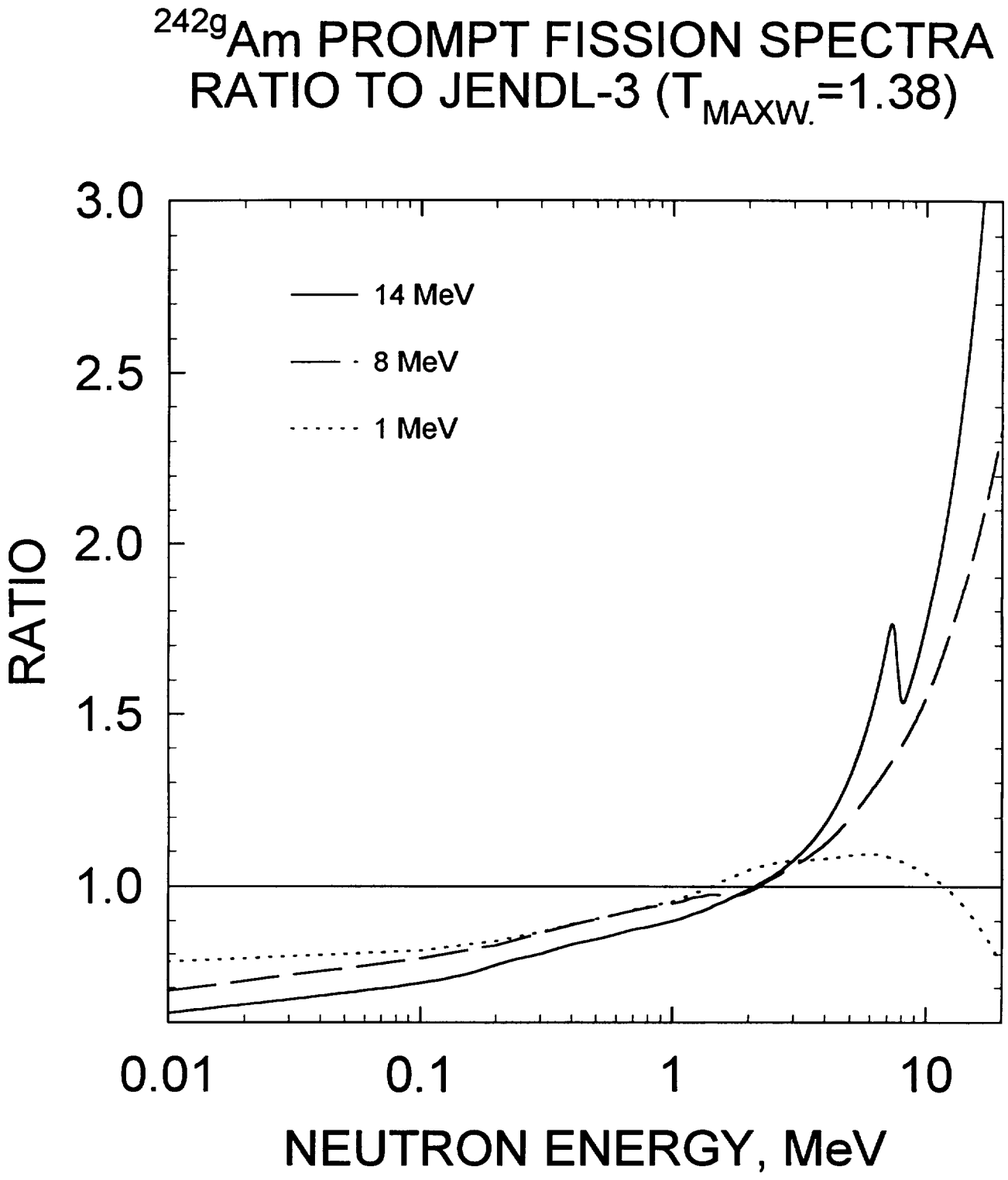
^{242g}Am PROMPT FISSION SPECTRA
RATIO TO JENDL-3 ($T_{MAXW.}$=1.38)
3.0
2.5
2.0
1.5
1.0
RATIO
14 MeV
8 MeV
1 MeV
0.01
0.1
1
10
NEUTRON ENERGY, MeV

FIG. 5.9

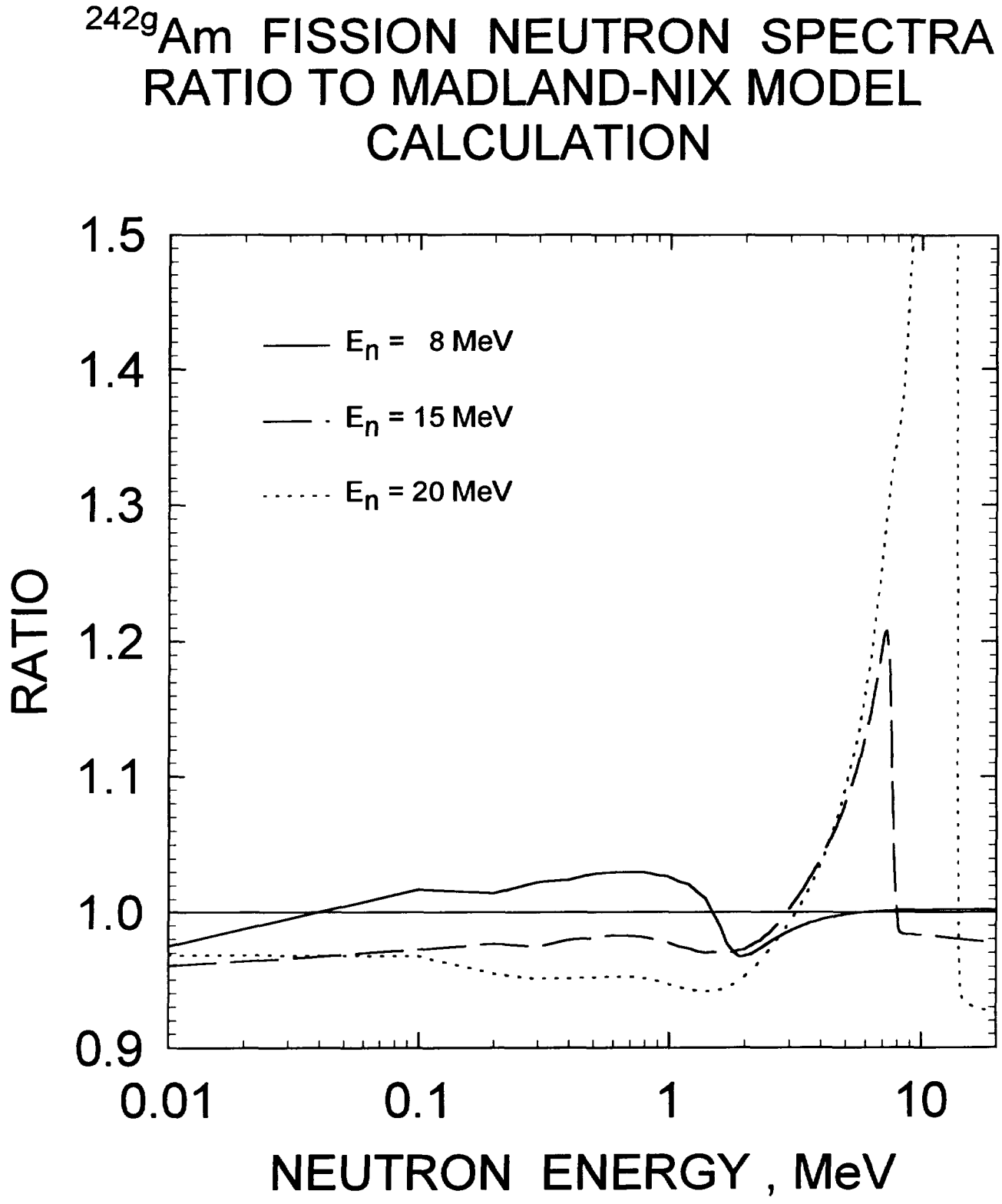
^{242g}Am FISSION NEUTRON SPECTRA
RATIO TO MADLAND-NIX MODEL
CALCULATION
1.5
1.4
1.3
1.2
1.1
1.0
0.9
RATIO
E_n = 8 MeV
E_n = 15 MeV
E_n = 20 MeV
0.01
0.1
1
10
NEUTRON ENERGY , MeV

FIG.5.10

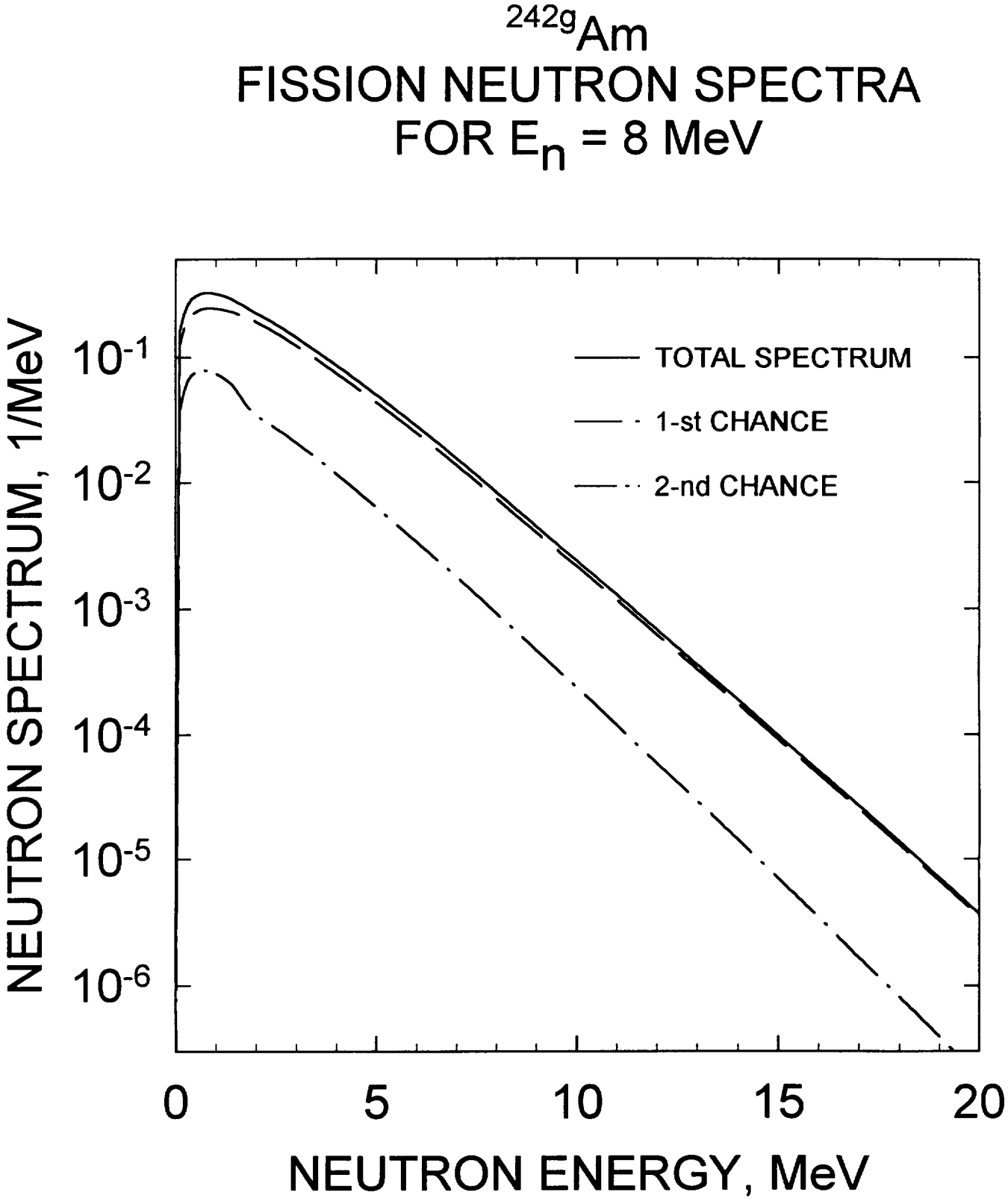
^{242g}Am
FISSION NEUTRON SPECTRA
FOR E_n = 8 MeV
NEUTRON SPECTRUM, 1/MeV
10^{-1}
10^{-2}
10^{-3}
10^{-4}
10^{-5}
10^{-6}
TOTAL SPECTRUM
1-st CHANCE
2-nd CHANCE
0
5
10
15
20
NEUTRON ENERGY, MeV

FIG.5.11

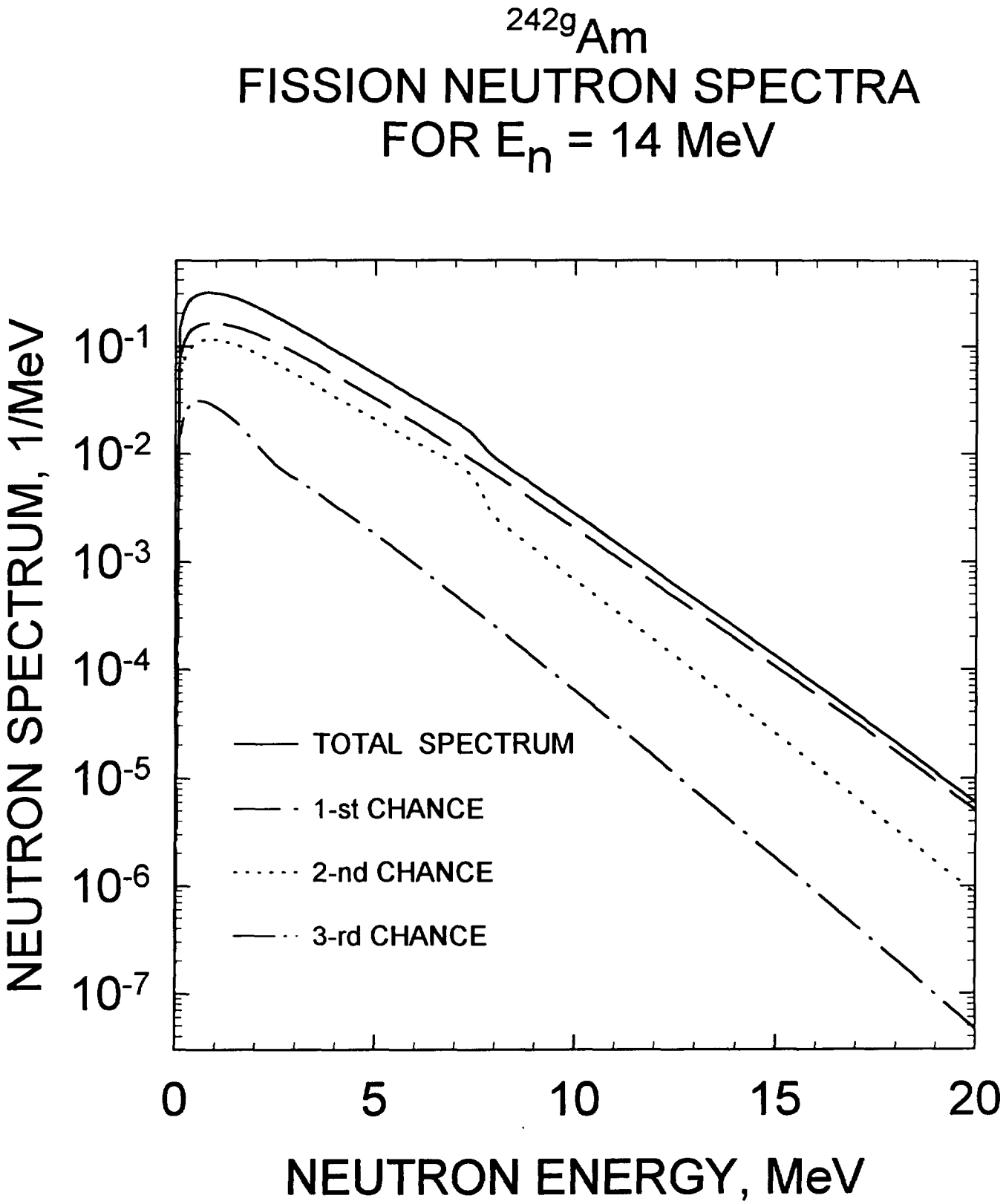
^{242g}Am
FISSION NEUTRON SPECTRA
FOR E_n = 14 MeV
NEUTRON SPECTRUM, 1/MeV
10^{-1}
10^{-2}
10^{-3}
10^{-4}
10^{-5}
10^{-6}
10^{-7}
TOTAL SPECTRUM
1-st CHANCE
2-nd CHANCE
3-rd CHANCE
0
5
10
15
20
NEUTRON ENERGY, MeV

FIG.5.12

^{242g}Am PROMPT NEUTRON MULTIPLICITY

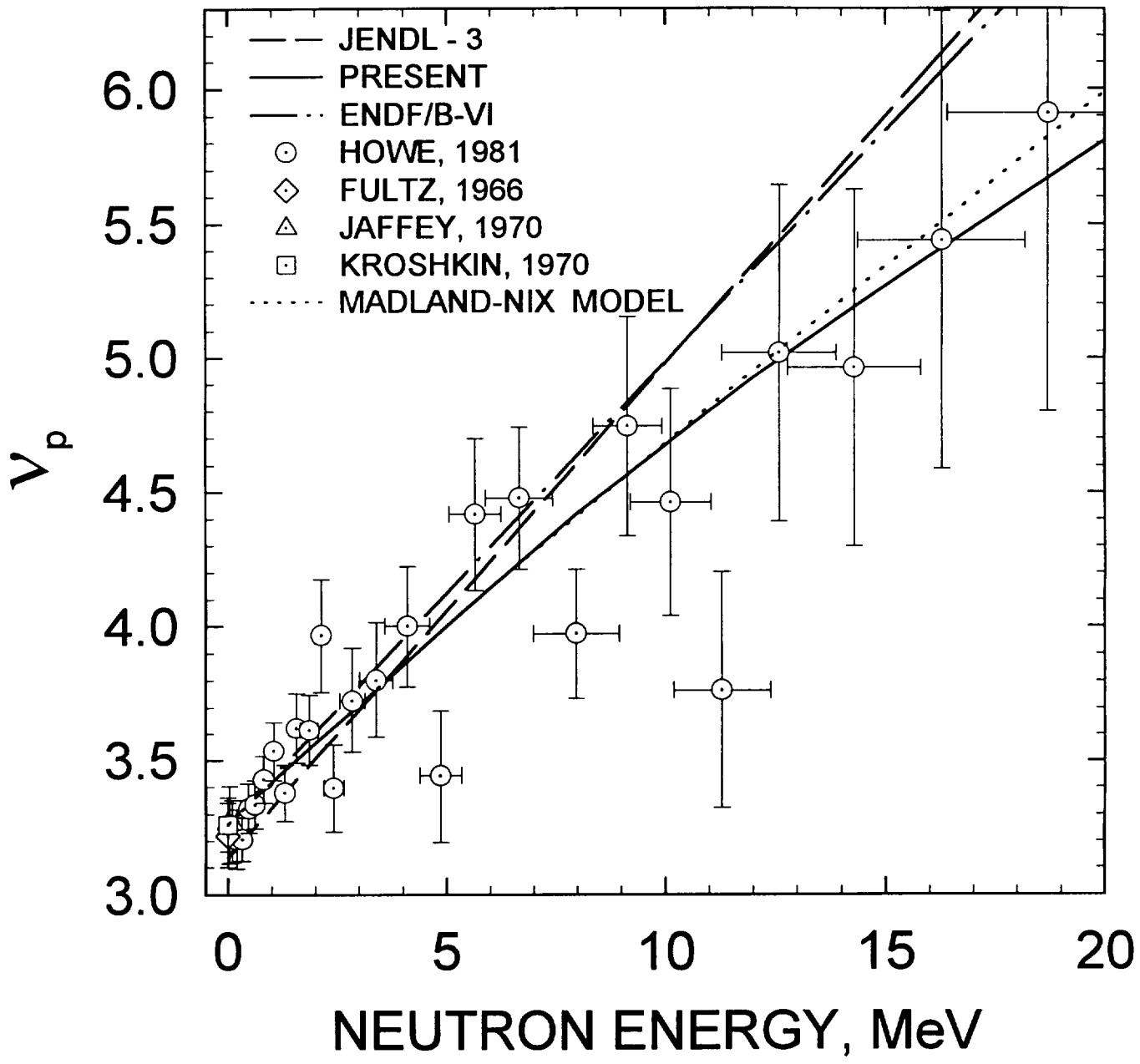

FIG.6.1

MS. MAGRIN AVEDIKIAN
INIS ROOM: A2418
INTERNATIONAL ATOMIC ENERGY
AGENCY
P.O. BOX 100
A-1400 VIENNA
AUSTRIA

Nuclear Data Section
International Atomic Energy Agency
P.O. Box 100
A-1400 Vienna
Austria

e-mail: services@iaeand.iaea.or.at
fax: (43-1)20607
cable: INATOM VIENNA
telex: 1-12645 atom a
telephone: (43-1)2060-21710

online: TELNET or FTP: iaeand.iaea.or.at
username: IAEANDS for interactive Nuclear Data Information System
username: ANONYMOUS for FTP file transfer
For users with Web-browsers: http://www-nds.iaea.or.at